6-17-2019

Chemosensors Based on Higher Energy Gap Control of Fluorescence in Conjugated Polymers

Chun-Han Wang
Louisiana State University and Agricultural and Mechanical College

CHEMOSENSORS BASED ON HIGHER ENERGY GAP CONTROL OF FLUORESCENCE IN CONJUGATED POLYMERS

A Dissertation

Submitted to the Graduate Faculty of the
Louisiana State University and
Agricultural and Mechanical College
in partial fulfillment of the
requirements for the degree of
Doctor of Philosophy

in

The Department of Chemistry

by
Chun-Han Wang
B.S., National Sun Yat-Sen University, Taiwan, 2006
M.S., National Taiwan Normal University, Taiwan, 2009
August 2019

In memory of

Lin, Huang Fu-Mei

1938- 2018

AKNOWLEDGMENTS

I would like to acknowledge Professor Evgueni E. Nesterov for his continuous guidance, advice, and support. His deep and commanding knowledge of science along with mindfulness in research inspired me to strive for excellence. Additional to this, Professor Nesterov often shared his cleverness and common sense with me, pushing me to becoming a better person.

A special thanks to my committee, Drs. David Spivak, Semin Lee, and George Judy for their education and encouragement.

To my past and present group members: Carlos Chavez, Sourav Chatterjee, Sang Gil Youm, Chien-Hung Chiang, Peter Kei, Gerard Ducharme, Fetemeh Khamespanah. Thanks for all your support in these years and it's my honor to work with you at LSU.

To my parents and my sister who live in Taiwan, your unconditional love and support guided me to overcome enormous difficulties during these years.

Most importantly, I would like to thank my wife Ying-Chieh Lai as a constant source of encouragement and love. Without your understanding and support, I would not be able to achieve the same level of success in my PhD career. Also, I sincerely appreciate you for giving me endless joy by bringing our daughter Emma Fei-Ning Wang into our life.

TABLE OF CONTENTS

ABBREVIATIONS AND ACRONYMS

CP	Conjugated Polymer
Cys	Cysteine
DCB	Dichlorobenzene
DCM	Dichloromethane
DFT	Density Functional Theory
DIPA	Diisopropylamine
DMF	*N,N*-dimethylformamide
DMSO	Dimethylsulfoxide
DNA	Deoxyribonucleic Acid
dppp	1,3-bis(diphenylphosphino)propane
ET	Energy Transfer
FRET	Fluorescence Resonance Energy Transfer
F	Fluorescence Intensity
GPC	Gel-permeation Chromatography
GSH	Glutathione
Hcy	Homocysteine
HEPES	(4-(2-hydroxyethyl)-1-piperazineethanesulfonic acid)
HOMO	Highest Occupied Molecular Orbital
ICT	Intramolecular Charge Transfer
PET	Photoinduced Electron Transfer
KCTP	Kumada Catalyst-Transfer Polycondensation
LUMO	Lowest Unoccupied Molecular Orbital
MeOH	Methanol

MS	Mass Spectroscopy
NMR	Nuclear Magnetic Resonance
NP	Nanoparticle
OFET	Organic Field Effect Transistor
OLED	Organic Light-emitting Diode
OPV	Organic Photovotaic
P3HT	Poly(3-hexylthiophene)
PA	Polyallene
PAc	Polyacetylene
PAE	Poly(arylene ethynylene)
PANI	Polyaniline
PAV	Poly(arylene vinylene)
PBS	Phosphate-Buffered Silane
PDI	Polydispersity Index
PEDOT	Poly(3,4-ethylenedioxythiophene)
Ph	Phenyl
PFO	Polyfluorene
PMMA	Poly(methyl-methacrylate)
PPE	Poly(*para*-phenylene ethenylene)
Ppm	Parts-per-million
PPP	Poly(*para*-phenylene)
PPV	Poly(*para*-phenylene vinylene)
PPy	Polypyrrole

PT	Polythiophene
PTA	Polytetradecyloxyallene
SANS	Small-angle Neutron Scattering TEM Transmission Electron Microscopy
TEG	Triethylene Glycol
TGA	Thermogravimetric Analysis
THF	Tetrahydrofuran
UV-Vis	Ultraviolet-visible

ABSTRACT

Conjugated polymers (CPs) have been widely investigated for their remarkably high sensitivity towards various chemical detection applications. CPs can exhibit effective transduction of certain analyte binding events through changes in fluorescence. These changes include amplified fluorescence quenching ("*turn-off* mechanism") or an appearance of a fluorescent emission ("*turn-on* mechanism"). Whereas *turn-off* sensors can be readily designed and are widely used, amplifying *turn-on* sensors, from a practical standpoint, are more convenient to use but are more challenging to design.

This dissertation primarily focuses on the development and study of conjugated polymer based amplifying *turn-on* fluorescence chemosensors utilizing the novel “higher energy gap” control concept as well as further investigation of the scope of applicability and generality of this concept. The higher energy gap control paradigm that relies on relatively minor changes in the electronic nature of the receptor site upon its reaction with analytes could offer a general and universal approach towards using conjugated polymers as a platform for the design of amplifying *turn-on* fluorescent chemosensors. To expand the practical applicability of the higher energy gap paradigm, singlet oxygen and cysteine were chosen as target analytes as they are important biochemical and industrial analytical targets.

The last chapter of this dissertation involves the design of a novel nanoscale hybrid system consisting of silica core and fluorescent triblock copolymer shell which is prepared via surface-initiated Kumada catalyst transfer polymerization. Although this project is not directly related to the “higher energy gap” concept, these studies can help in better understanding the fundamental mechanisms behind the design of chemo- and biosensors.

CHAPTER 1. CONJUGATED POLYMERS AS FLUORESCENT CHEMOSENSING MATERIALS: AN INTRODUCTION

1.1 Introduction to Conjugated Polymers

Conjugated polymers are organic macromolecules which consist of alternating double- and single-bonds and its π-bonding structure allows for electronic delocalization along the backbone. This extensive orbital delocalization corresponds to the conjugation length and is responsible for the unique photophysical and electronic properties that have attracted widespread research attention in the past three decades. The cornerstone discovery in the field of conjugated polymers was that of iodine-doped polyacetylene (PAc) which was published in 1977 by Heeger, MacDiarmid, and Shirakawa. Upon exposing polyacetylene thin films to iodine vapor, they found that the conductivity of PAc increased nine orders of magnitude to almost the metal-like range.[1] This discovery opened the door for the field of organic conductive polymers and was recognized by the Nobel Prize in chemistry in 2000.[2-4] Since that pioneering study, scientists expanded the research scope to many conjugated polymers such as poly(3-alkylthiophene) (PT), poly(*para*-phenylene) (PPP), poly(*para*-phenylene vinylene) (PPV), poly(*para*-phenylene ethynylene) (PPE), polypyrrole (PPy), polyaniline (PANI), poly(3,4-ethylenedioxythiophene) (PEDOT), and polydioctylfluorene (PFO) that are shown in Figure 1.1.[5] These conjugated polymers benefit from extensive orbital delocalization along their CP backbone which lowers the HOMO-LUMO energy gap and is responsible for their semiconducting features. The low cost, flexible substrates compatibility, solution processability, and tunable electrical and optical properties have enabled popularity of these materials in a variety of applications including organic light-emitting diodes (OLEDs),[6] organic field-effect transistors

(OFETs),[7] organic batteries,[8] organic photovoltaic cells (OPVs),[9] and chemical and biological sensory materials.[10-14]

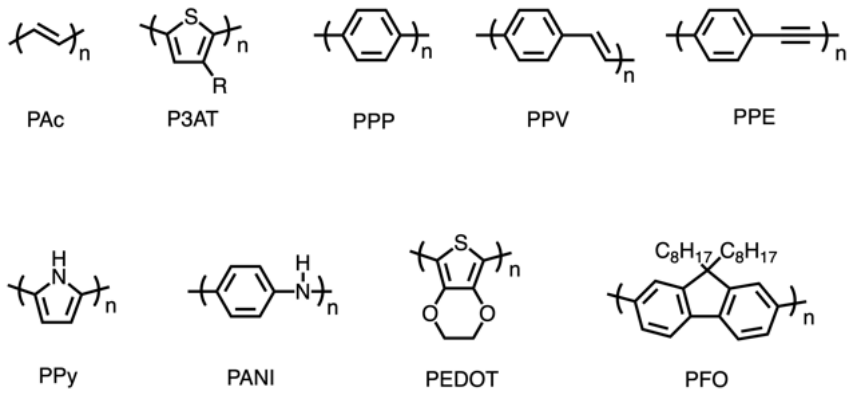

Figure 1.1. Representative examples of commonly used conjugated polymers for organic materials applications.

1.2 Mechanisms of Energy Transfer

The mechanisms of excitation energy transfer, or exciton migration, in conjugated polymers have been long discussed[15-16] to understand the fundamental principles of how excitons transport in/between CP chains and to gain better knowledge to design functional practical CPs devices. The two well-recognized mechanisms of energy transfer are: (1) Förster (through-space)[17] and (2) Dexter (through-bond) energy transfer[18] (Figure 1.2). The Förster mechanism is a radiationless transition occurring through Coulombic interactions between electronic transition dipoles on the donor and acceptor moieties. This dipole-induced dipole interaction occurs through space and thus does not require the direct orbital overlap which is significant in the Dexter energy transfer. Because of the electrostatic dipole-induced dipole interaction, Förster transfer can operate in a relatively long range (up to 100 Å). On the other hand, the Dexter mechanism, also known as an electron exchange mechanism, requires the direct wavefunction overlap and therefore the donor and acceptor should be in closer proximity than in the Förster energy transfer. The exchange mechanism is closely related to the distance and molecular orbital

interactions between the donor and acceptor. This essentially forces the donor and acceptor units to be electronically conjugated *via* π-bonds in organic molecules and it usually happens within the distance of less than 10 Å.

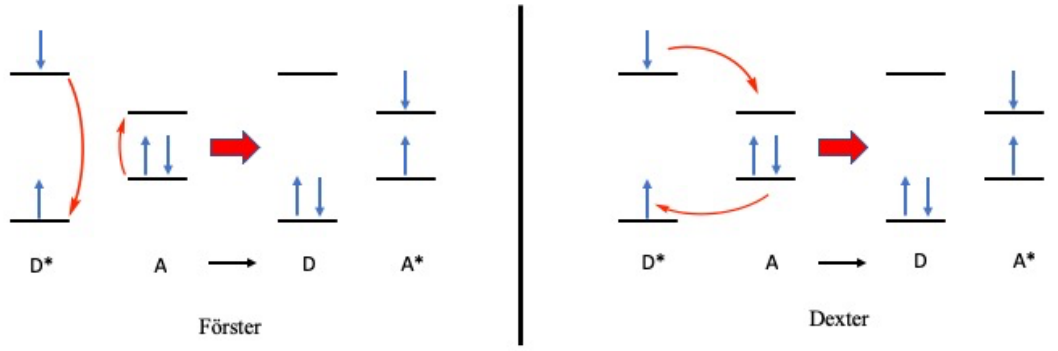

Figure 1.2. Schematic diagrams of Förster (left) and Dexter (right) energy transfer mechanisms

In general, the energy transfer can happen both through-space (Förster) and through-bond (Dexter), but it highly depends on a specific system and the environment where the CPs are. For example, in a dilute solution system, where polymer chains are more isolated, the energy transfer happens mainly along the backbone (one-dimensional) which means Dexter energy transfer is a significant contributor. While in thin films (solid state), the exciton migration would happen as a three-dimensional process since it is a more compact and dense system, and the combination of Dexter and Förster energy transfer pathways would be observed (Figure 1.3).[19] Although it is still debatable as to what mechanism is the major contributor to the energy transfer in conjugated polymers due to the difficulty of quantitative measurements of energy transfer within an isolated polymer chain or between the chains, it has been widely accepted that energy transfer in CPs is primarily attributed to Förster energy transfer via dipole-induced dipole interactions of chromophores.[20, 21] To better understand this idea, the nature of CPs should be taken

into account. An exciton, a bound state of an electron and a hole which are attracted to each other by the electrostatic Coulombic force, can transport along the isolated CP backbone (through-bond) which should be planar and completely delocalized theoretically. However, in a real system, CPs are intrinsically disordered materials which contain structural defects such as kinking, coiling, and twisting, suppressing the efficiency of energy transfer by the Dexter mechanism (Figure 1.4).[22]

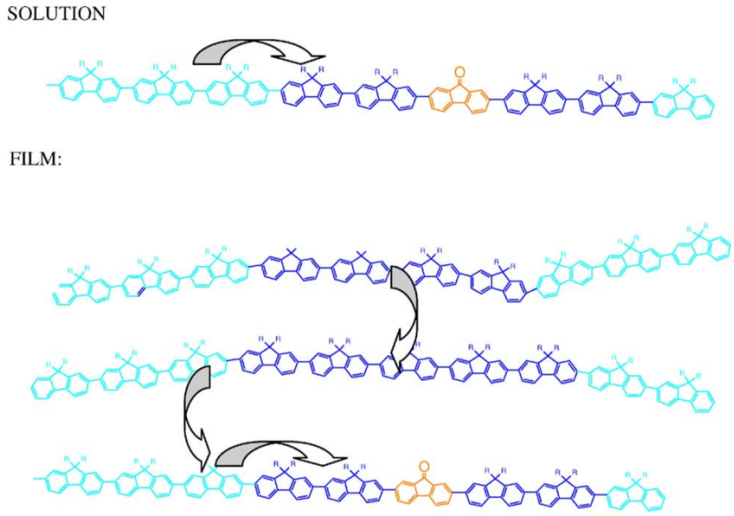

Figure 1.3. Schematic drawing for the singlet exciton on-chain and singlet exciton interchain migration process in a polyfluorene containing a fluorenone unit for the molecule in solution and in a solid-state film. Reproduced with permission from Ref. 19. Copyright © 2009 Elsevier.

Schwartz and co-workers have shown the evidence that interchain energy transfer is much faster than intrachain energy transfer by isolating PPV chains into pores of an extended silica matrix.[23] With isolated PPV chains, they could measure the exciton diffusion using polarized luminescence spectroscopy along the chain while inhibiting interchain interaction. They have found that exciton diffusion is a slow process in intrachain energy migration due to weak dipole coupling along the backbone, ranging in rate from tens to hundreds of picoseconds. Meanwhile, interchain energy migration was

found to be faster, with the rate from one to tens of picoseconds. This dominance of interchain interactions can also be supported through fluorescence spectroscopy where the spectrum shows a red-shifted emission as a result of delocalization between segments, which lowers the energy relative to the isolated chain exciton.[24]

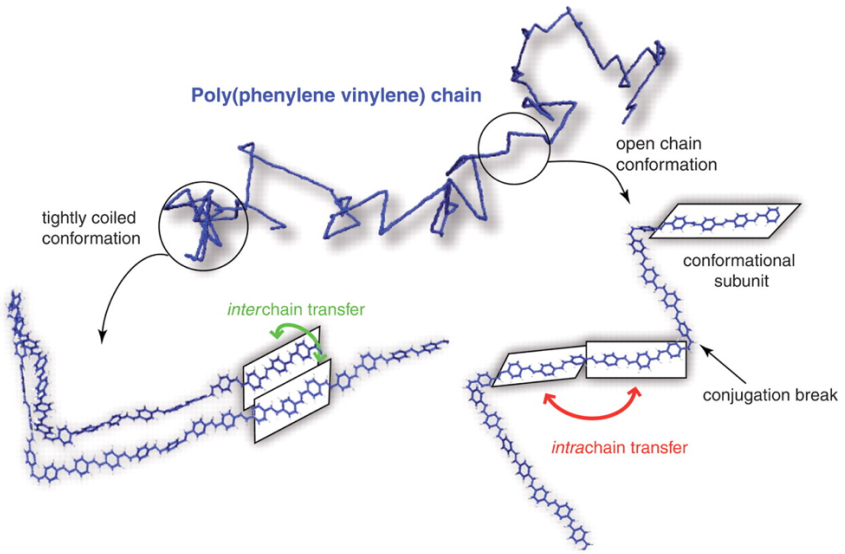

Figure 1.4. Example of single-chain conformation of a poly(phenylene vinylene) conjugated polymer, referred to as the defect cylinder conformation. Conformational disorder produces a chain of linked chromophores (or conformational subunits) outlined conceptually by the boxes. The intramolecular excitation energy transfer (migration along the backbone) is the predominant mechanism when the polymer chain assumes an open, extended conformation, typical for solutions in good solvents such as chloroform; on the other hand, intermolecular interactions (hopping between segments in close proximity) are dominant for tightly coiled configurations, typically found in polymer nanoparticles, or thin films. Reproduced with permission from Ref. 22. Copyright © 2009 The American Association for the Advancement of Science.

Because the intramolecular energy transfer via orbital overlap (Dexter mechanism) must overcome structural defects, it is considered less efficient than both intramolecular and intermolecular through-space exciton migration (Förster mechanism). While it is believed that interchain energy transfer is dominant in conjugated polymers in condensed state, Swager and co-workers have demonstrated that intramolecular energy transfer is

actually playing an important role during excitation of conjugated polymers in anisotropic Langmuir-Blodgett films of monolayered-PPE.[25, 26] The major contribution of intramolecular energy transfer by the through-bond mechanism was further confirmed in chain-extended conformations in nematic liquid crystals which allows to enhance the conjugation length while limiting the amount of intermolecular interactions (Figure 1.5). [27] Via installing lower-energy fluorophores which act as acceptors at the ends of the polymer chain, energy migration can be monitored intramolecularly by site-selective emission of the fluorescent terminal groups when dissolved in nematic liquid crystal media. The fluorescent emission from the terminal fluorophores indicates the efficiency and importance of intrachain energy migration as it could be inhibited via decrease of conjugation length caused by increasing the temperature to a point of the nematic-isotropic transition resulting in switching to a dominant emission from PPE backbone.

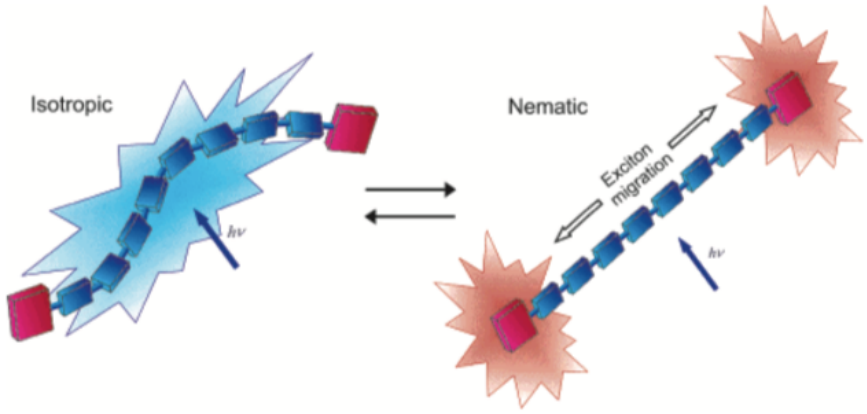

Figure 1.5. Simplified representation of conjugated polymer PPE in isotropic and liquid crystalline solutions. In isotropic solution, the conformational disorder in the polymer backbone prevents efficient intramolecular exciton migration, thus resulting in predominant emission from the PPE backbone. In nematic liquid crystalline solution, the increased electronic conjugation in the straightened and planarized polymer chains is higher, which leads to the enhanced intramolecular migration toward the terminal groups with a concomitant increase in the termini's emission. Reproduced with permission from Ref. 27. Copyright 2005 American Chemical Society.

It can be confidently said that both Förster and Dexter mechanisms contribute significantly to energy transfer in conjugated polymers. Förster mechanism dominates in more compact and dense systems such as solid state films due to the close interchain distances, whereas Dexter mechanism plays a significant role in more dilute systems where energy transfer happens predominantly as an intramolecular process along the backbone of isolated polymer chains.

1.3 Signal Amplification: *Turn-off* vs. *Turn-on* Response

Conjugated polymers demonstrate a remarkably high sensitivity in a variety of chemical sensing applications.[14] These polymeric materials were shown to be superior to small-molecule based sensor systems in some trace chemical detection applications due to the polymers' intrinsic amplifying feature. In general, in a small-molecule based sensory system, the binding of a single analyte can result in a response from a single receptor. The sensitivity of this mono-receptor system depends strongly on the equilibrium constant of analyte binding. When the same receptors are wired in series (as in a conjugated polymer), the binding of a single analyte at any of the receptor sites can result in a collective response from the system (as known as the molecular wire effect) that is significantly greater than the response from the case of the mono-receptor system (Figure 1.6). This represents the amplification feature of the sensor's response for a poly-receptor system and shows the molecular wire effect which is the basis for the high sensitivity of CP based sensory systems. Swager *et al.* have reported that a conjugated polymer in the solution state can demonstrate a 65-fold enhancement in sensitivity toward paraquat compared to a mono-receptor system.[28]

Conjugated polymers can demonstrate the effective transduction of certain analyte binding events through changes in fluorescence. These changes can include fluorescence quenching ("*turn-off* mechanism") or the appearance of fluorescence emission ("*turn-on* mechanism"). Change in fluorescence intensity can be easily measured with simple optical systems, or in some cases, can be seen by bare eyes which provide a potential practical application ability for making chemo/biosensors.

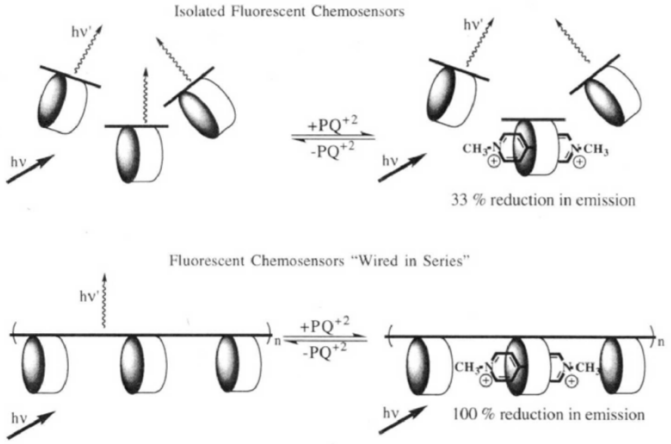

Figure 1.6. Graphical representation of mono-receptor system vs. poly-receptor system upon binding of an analyte (paraquat molecule). Reproduced with permission from Ref. 28. Copyright © 1995 American Chemical Society.

1.3.1 *Turn-off* Fluorescence Amplification

In a *turn-off* mechanism, an analyte binding interaction can result in quenching of the fluorescence of a conjugated polymer through a photo-induced electron transfer (PET) process (Figure 1.7). The absorption of a photon by conjugated polymer can generate a mobile exciton that travels along the polymer backbone, effectively sampling many different potential analyte binding sites along the chain. After some time, the excited state relaxes to the ground state by emitting a photon (fluorescence). However, if the exciton encounters a bound analyte on the polymer backbone, the excited state electron on the conduction band is brought back to the valence band via a non-radiative process by

passing through the LUMO of an electron-deficient analyte. This electron transfer process deactivates the excited state of the polymer and results in amplified fluorescence quenching.

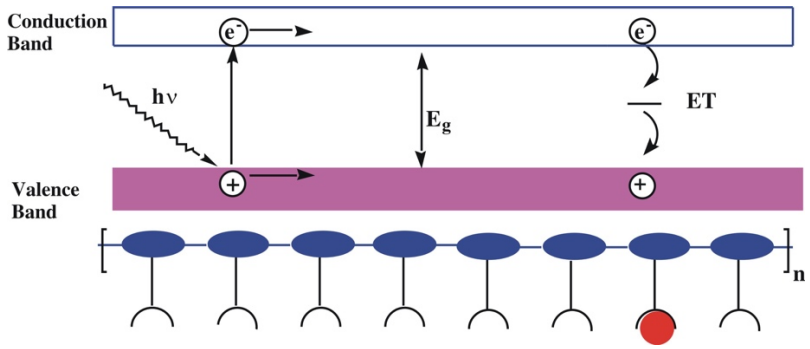

Figure 1.7. Schematic band diagram illustrating the mechanism of electron quenching via a photo-induced electron transfer (PET) process. Reproduced with permission from Ref. 10. Copyright © 2007 American Chemical Society.

Conjugated polymer sensors based on the *turn-off* mechanism are common and widely used for sensing a range of analytes. For example, Swager *et al.* have shown pentiptycene functionalized PPE as a TNT sensing material. The bulky pentiptycene units prevent the polymer chains from aggregating and create substantial cavities in the bulk of the polymer (large internal free volume) for TNT vapor to enter and bind. Once the analyte is bound, a large decrease in the fluorescent response from fluorescent PPE is observed due to energy transfer from the excited conjugated polymer to the electron-deficient TNT (Figure 1.8).[29] This polymer-based sensor benefits from the efficient interchain energy transfer (Förster type) at solid state and is at the core of widely used commercially manufactured explosive detecting devices. Nesterov *et al.* have introduced another notable example of fluorescent polymer sensor utilizing the quenching effect for sensing nitroaromatics.[30] A TNT-molecularly imprinted conjugated polymer (MICP) has been synthesized having shape-selective cavities where TNT molecules can reasonably fit. Upon exposure to the nitroaromatics vapors, the polymer shows a significant decrease

in the fluorescence intensity which indicates an efficient *turn-off* mechanism (Figure 1.9). In both cases, quenching behavior was observed due to the strong electron deficient nature of the nitroaromatic analytes.

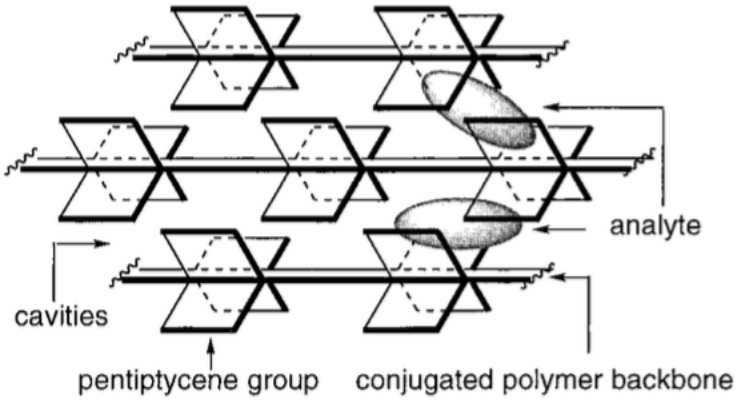

Figure 1.8. TNT-detecting high free-volume conjugated polymers. Reproduced with permission from Ref. 29. Copyright © 1998 American Chemical Society.

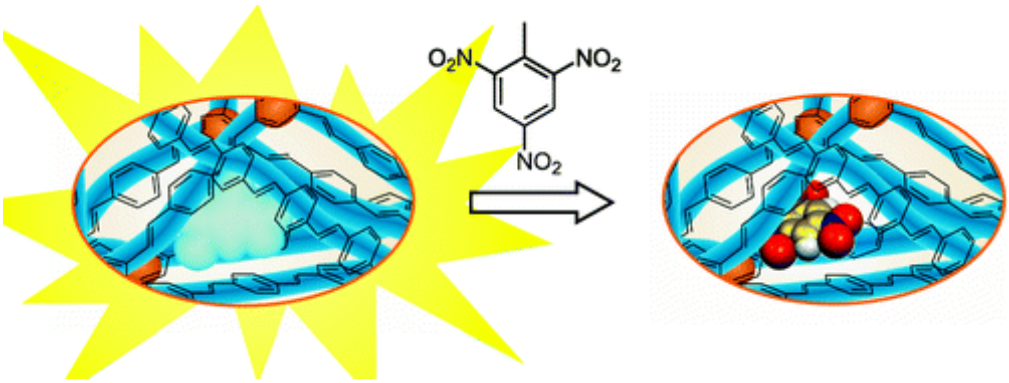

Figure 1.9. Amplifying conjugated polymer with a molecularly imprinted cavity capable of selective binding trinitrotoluene where it behaves as a quencher of the polymer fluorescence. Reproduced with permission from Ref. 30. Copyright © 2007 American Chemical Society.

In addition, Whitten *et al.* have demonstrated that the fluorescence of water-soluble polyanionic conjugated polymer [poly(2-methoxy-5-propyloxy sulfonate phenylene vinylene (MPS-PPV)] could be quenched when *N*, *N*′-dimethyl-4,4′-bipyridinium (MV^{2+}) was present in dilute solutions. This extreme case showed the MPS-PPV conjugated polymer was a million times more sensitive than its corresponding small-

molecule sensor (trans-stilbene) which perfectly illustrated the power of the wire effect for designing conjugated polymer based *turn-off* fluorescent amplifying sensors.[31]

1.3.2 *Turn-on* Fluorescence Amplification

In sharp contrast to a widely used design of conjugated polymer sensors based on fluorescence quenching (*turn-off*) mechanism, there is only a limited number of conjugated polymers sensors based on fluorescence enhancement (*turn-on*) mechanism. This is because of the difficulties in coming up with designing principles for such sensors. A commonly utilized strategy to achieve an amplified *turn-on* response is based on quencher removal, and thus is a reverse of the previously discussed *turn-off* sensing mechanism. In such cases, the fluorescence of conjugated polymers is initially suppressed due to the binding of quenchers to the conjugated polymer. In the presence of a target analyte, the CPs fluorescence restores when quenchers are removed from CPs by the analyte-quencher binding event, therefore showing a *turn-on* amplifying feature (Figure 1.10).[31-33]

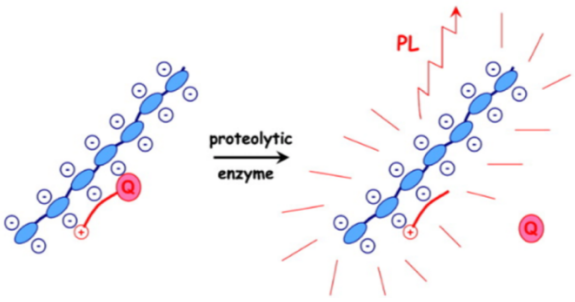

Figure 1.10. Graphical representation of a *turn-on* fluorescent response utilizing quencher removal concept. Reproduced with permission from Ref. 32. Copyright © 2004 The National Academy of Sciences.

A related scheme utilizing fluorescent resonance energy transfer (FRET) for *turn-on* sensing has been also developed.[34-36] FRET is a widely used technique in the detection of large biomolecules such as DNA and protein. A FRET based sensor is sensitive to the

distance between donor and acceptor fluorophores and it also relies on the overlap integral between donor emission and acceptor absorption, where a greater overlap results in a higher efficiency of the FRET process.

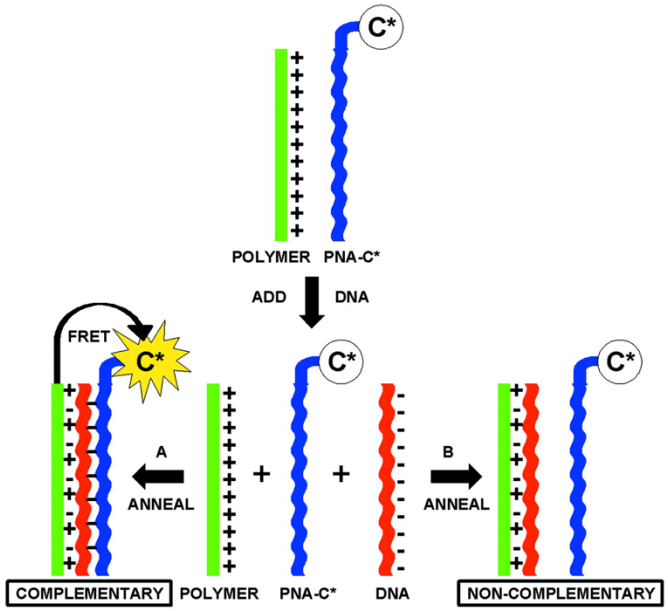

Figure 1.11. Schematic description of an amplified fluorescent detection of a complimentary ssDNA strand (red) by using FRET from CP (P-IX) (green) to fluorescein chromophore linked to a PNA reporter (blue). Addition of a complementary DNA strand results in the formation of a triplex where efficient FRET from CP to fluorescein produces an amplified fluorescent response; addition of a non-complementary DNA produces no response. Reproduced with permission from Ref. 34. Copyright © 2002 The National Academy of Sciences.

For example, Bazan and co-workers have introduced a *turn-on* amplifying sensor for DNA detection utilizing the FRET effect. A cationic conjugated poly(fluorene-*co*-phenylene) polymer, a probe peptide nucleic acid strand labeled with fluorescein (PNA-C*), and the target DNA strand have been prepared where the donor polymer and fluorescein labeled PNA acceptor are spectrally overlapped which is required for efficient FRET. When the DNA strand complementary to PNA is added, an electrostatic attraction between PNA and DNA strands brings the fluorescein on PNA close enough to the polymer for an

efficient fluorescent resonance energy transfer. The sensor displayed a 25 times amplified response on the emission intensity from fluorescein caused by FRET compared to the emission of the directly excited free fluorescein (Figure 1.11).

In sharp contrast to the examples based on a quencher removal and FRET mechanism in the designing *turn-on* amplifying sensors, Swager and co-workers have demonstrated a milestone example of an intrinsically *"turn-on"* fluorescence amplifying conjugated polymer for the detection of fluoride.[37] This conjugated polymer sensor was based on a sophisticated design with the generation of a lower energy, high quantum yield coumarin fluorophore upon cyclization caused by an analyte (fluoride anion), from a non-emissive TIPS protected alcohol functionalized group (Figure 1.12).

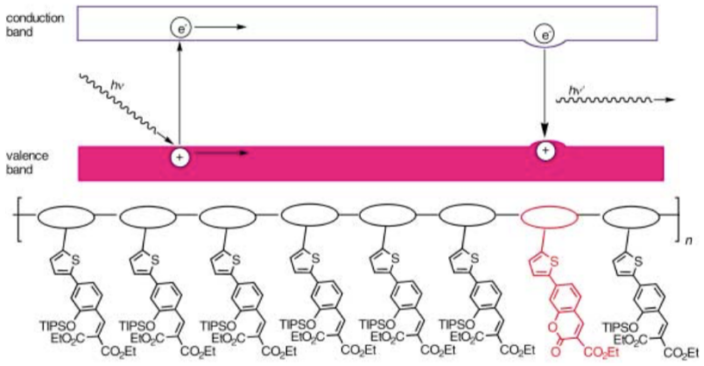

Figure 1.12. Schematic band diagram illustrating the mechanism by which a fluorescent conjugated polymer can produce an amplifying *turn-on* fluorescence chemosensory response. The horizontal dimension represents the direction along the polymer backbone shown schematically at the bottom. Excitons are created by absorption of a photon (*hv*) and then randomly migrate along the π-conjugated backbone. Fluoride-induced lactonization in the side-chain produces a trapping site with a smaller energy gap (E_g) and recombination of excitons at that site results in a new amplified emission. Reproduced with permission from Ref. 37. Copyright © 2003 Wiley-VCH.

The excitons formed upon irradiation of the polymer would migrate to the formed lower energy coumarin site resulting in the fluorescence increase. It was found that the CP based sensor was approximately 100 times more sensitive than its small-molecule analog.

This design scheme towards *turn-on* amplification based upon the creation of a lower energy gap fluorescent site is ingenious and truly remarkable, but it is severely limited by the availability of reactions since there are only a few available reactions that can generate a lower energy, high quantum yield fluorophore from a precursor unit electronically incorporated in the π-conjugated backbone upon reaction with a target analyte. This intrinsically limits the generality and application potential of this approach. Indeed, the described case of fluoride anion detection remains the only example in the literature that utilizes the mechanism mentioned above to possess a *turn-on* fluorescence amplification feature.

To overcome the narrow scope of the previous approach, Nesterov *et al.* have introduced a more practically accessible strategy which they called a "higher energy gap" control mechanism to achieve a *turn-on* amplified response (Figure 1.13).[38]

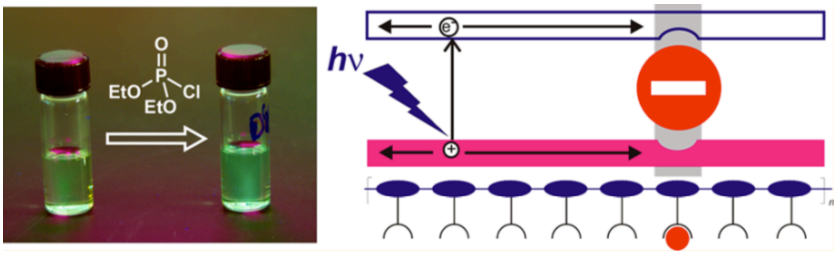

Figure 1.13. Schematic diagram illustrating the higher energy gap control of CP fluorescence: an analyte (red circle) binding creates a local higher energy gap site in the CP backbone which acts as a "roadblock" and decreases the length of the excitation/exciton migration along the π-conjugated system, resulting in the increase of fluorescent intensity of the conjugated polymer. Reproduced with permission from Ref. 38. Copyright © 2013 American Chemical Society.

In sharp contrast to the practically difficult design based on generating a lower-energy emissive fluorophore, in the new concept a reaction with an analyte creates a local higher energy gap site on the CP backbone. The higher energy gap site can act as a "roadblock" to restrict exciton migration distance. The lowering excitons migration length can

efficiently reduce the chance of excitons to be quenched by intrinsic quenching sites always present on the polymer such as structural defects (kinking, coiling, and twisting, etc.) or transient defects (triplet states, photogenerated free charge carriers, or charge-separated states, etc.),[30] hence resulting in an amplified *turn-on* fluorescence enhancement.

The first example to illustrate this higher energy gap mechanism was aimed towards detection of diethyl chlorophosphate (DCP), a commonly used mimics of organophosphorus nerve agents. The poly(*p*-phenylene vinylene) (PPV) has been chosen to be the CP backbone because of its special emissive nature and a low energy band gap ($\lambda(\text{em})_{max}$ > 500nm) to couple with naphthalene based hydroxy oxime chromophore ($\lambda(\text{em})_{max}$ 392nm) which acted as a reactive site toward DCP. With the cyclization on the hydroxy oxime site caused by DCP, the isoxazole unit would be generated that possessed a noticeably higher HOMO-LUMO gap relative to the unreacted hydroxy oxime, resulting in a *turn-on* amplifying fluorescent response. This *turn-on* amplified response was mainly related to the prevalence of intramolecular energy transfer (Dexter type) in the isolated polymer chain in a dilute solution, and the conjugated polymer based sensor showed not only 20 to 30 times higher sensitivity but also a broader analyte detection range than a corresponding small-molecule sensor. Moreover, this example introduced an important concept that can be used in the design of efficient *turn-on* amplifying sensors utilizing the “higher energy gap” control mechanism for other practically important analytes.

Recently, Nesterov and co-workers have described another example of an efficient *turn-on* amplifying fluorescent sensor based on the “higher energy gap” control

mechanism for sensing hydrogen sulfide[39] - an important industrial and biomedical analytical target. The poly(*p*-phenylene vinylene)s (PPVs) has been chosen once again as the CP backbone, and incorporated the hydrogen sulfide receptor unit which was a naphthalene based cyanine moiety. Reaction between hydrosulfide anion and the cyanine moiety creates a higher HOMO-LUMO gap site due to the effective electronic isolation of the cyanine unit from the CP backbone. This local higher energy gap site – an exciton "roadblock"- restricts the intramolecular exciton migration distance resulting in an amplified *turn-on* fluorescent response (Figure 1.14).

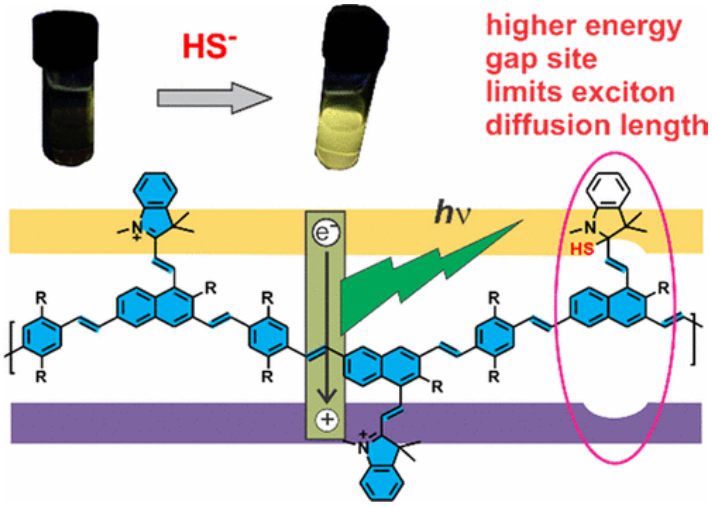

Figure 1.14. Schematic diagram illustrating the higher energy gap control of CP fluorescence: a hydrosulfide anion binding event creates a local higher energy gap site in the CP backbone which acts as a "roadblock" and decreases the length of the excitation/exciton migration along the π-conjugated system, resulting in the increase of fluorescent intensity of the conjugated polymer. The top picture shows a fluorescence enhancement that can be seen with bare eyes by photoirradiation at 365nm using a handheld UV lamp. Reproduced with permission from Ref. 39. Copyright © 2017 American Chemical Society.

The high optical gain (up to 74-fold) could easily be seen with bare eyes upon photoirradiation at 365nm using a handheld UV lamp. Beside the high sensitivity, this CP based sensor also displayed a high selectivity toward hydrosulfide anion with respect to

various competing nucleophiles (such as hydrogen peroxide, halide ion and other ions, biological thiols, etc.) which illustrates the possibilities for potential practical applications.

1.4 Research Focus

The main focus of this dissertation was further development of conjugated polymer based amplifying *turn-on* fluorescence chemosensors utilizing the higher energy gap control concept, and investigation of the scope of applicability and generality of this concept. Instead of a sophisticated design to match the energy level of donor and acceptor or relying on practically difficult complex synthetic approaches, the higher energy gap control paradigm that relies on relatively minor changes in the electronic nature of the receptor site upon its reaction with analytes could offer a general and universal approach towards using conjugated polymers as a platform for amplifying *turn-on* fluorescent chemosensor design. To expand the practical applicability of the higher energy gap paradigm, singlet oxygen was chosen as a target analyte as it is an important receptive oxygen species in photodynamic therapy (PDT) treatment where it plays an important role in destroying cancerous cells in the course of PDT treatment. On the other hand, singlet oxygen has been implicated in the genotoxicity of UV light, as well as in photodegradation of organic electronic and optoelectronic materials. Therefore, efficient detection of singlet oxygen is crucial for a number of research and practical applications. Chapter 2 describes a new conjugated polymer design consisting of a novel 1,4-disubstituted tetracene unit incorporated in a PPV backbone that was proposed for an efficient, real-time amplifying fluorescent detection of singlet oxygen.

Chapter 3 focuses on investigation of applicability and mechanistic limitations of the higher energy gap concept. In particular, it describes application of the “higher energy

gap" concept towards designing a conjugated polymer amplifying fluorescent sensor for the detection of cysteine. This CP based sensor shows the unique capacity of the "higher energy gap" paradigm where even a very small change (about 0.3 eV) in the HOMO-LUMO gap upon reaction of the receptor site with a target analyte can still produce a significant fluorescence intensity enhancement. This example also implies the potential ability for designing a broad range of chemo- or biosensors based on the "higher energy gap" concept due to its high sensitivity for even a minor energy gap change.

In chapter 4, a series of hybrid materials consisting of silica nanoscale core and fluorescent triblock copolymer shell has been developed via surface-initiated Kumada catalyst transfer polymerization. This chapter describes a "*grafting-from*" approach as applied towards the design of a fluorescent polymer shell consisting of a triblock copolymer shell on the silica core. The two blocks are poly(*p*-phenylene) (PPP) and poly(3-hexylthiophene) (P3HT) conjugated polymers and the third block is polytetradecyloxyallene (PTA). The photophysical properties, structure and morphology of this novel hybrid fluorescent system have been investigated by using optical spectroscopy, thermogravimetric analysis (TGA), transmission election microscopy (TEM) and neutron reflectometry. Although this project is not directly related to the "higher energy gap" concept described in Chapters 2 and 3, it reveals the structure-property relationships between conjugated polymer morphology and fluorescent properties, and the effect of fine morphology attenuation on photophysics of conjugated polymers. This knowledge can help in better understanding of the underlying fundamental principles behind the "higher energy gap" mechanism.

1.5 References

(1) Shirakawa, H.; Louis, E. J.; MacDiarmid, A. G.; Chiang, C. K.; Heeger, A. J. Synthesis of Electrically Conducting Organic Polymers: Halogen Derivatives of Polyacetylene, $(CH)_X$. *J. Chem. Soc. Chem. Commun.* **1977**, *16*, 578-580.

(2) Shirakawa, H. The Discovery of Polyacetylene Film: The Dawning of an Era of Conducting Polymers (Nobel Lecture). *Angew. Chem. Int. Ed.* **2001**, *40*, 2574-2580.

(3) MacDiarmid, A. G. "Synthetic Metals": A Novel Role for Organic Polymers (Nobel Lecture). *Angew. Chem. Int. Ed.* **2001**, *40*, 2581-2590.

(4) Heeger, A. J. Semiconducting and Metallic Polymers: The Fourth Generation of Polymeric Materials (Nobel Lecture). *Angew. Chem. Int. Ed.* **2001**, *40*, 2591-2611.

(5) *Conjugated Polymers: A Practical Guide to Synthesis*; Müllen, K., Reynolds, J. R., Masuda, T., Eds.; RSC polymer chemistry series; RSC Publishing: Cambridge, 2014.

(6) Perepichka, I. F.; Perepichka, D. F.; Meng, H.; Wudl, F. Light-Emitting Polythiophenes. *Adv. Mater.* **2005**, *17*, 2281-2305.

(7) Sirringhaus, H. 25th Anniversary Article: Organic Field-Effect Transistors: The Path Beyond Amorphous Silicon. *Adv. Mater.* **2014**, *26*, 1319-1335.

(8) Schubert, U. S. Polymer-Based Organic Batteries *Chem. Rev.* **2016**, *116*, 9438-9484.

(9) Cheng, Y.-J.; Yang, S.-H.; Hsu, C.-S. Synthesis of Conjugated Polymers for Organic Solar Cell Applications. *Chem. Rev.* **2009**, *109*, 5868-5923.

(10) Thomas, S. W.; Joly, G. D.; Swager, T. M. Chemical Sensors Based on Amplifying Fluorescent Conjugated Polymers. *Chem. Rev.* **2007**, *107*, 1339–1386.

(11) Rochat, S.; Swager, T. M. Conjugated Amplifying Polymers for Optical Sensing Applications. *ACS Appl. Mater. Interfaces* **2013**, *5*, 4488-4502.

(12) McQuade, D. T.; Pullen, A. E.; Swager, T. M. Conjugated Polymer-Based Chemical Sensors. *Chem. Rev.* **2000**, *100*, 2537–2574.

(13) Bunz, U. H. F.; Seehafer, K.; Bender, M.; Porz, M. Poly(Aryleneethynylene)s (PAE) as Paradigmatic Sensor Cores. *Chem. Soc. Rev.* **2015**, *44*, 4322-4336.

(14) Swager, T. M. The Molecular Wire Approach to Sensory Signal Amplification. *Acc. Chem. Res.* **1998**, *31*, 201–207.

(15) Bredas, J.-L; Beljonne, D.; Coropceanu, V.; Cornil, J. Charge-Transfer and Energy-Transfer Processes in -Conjugated Oligomers and Polymers: A Molecular Picture. *Chem. Rev.* **2004**, *104*, 4971-5004

(16) Scholes, G D.; Rumbles, G. Excitons in Nanoscale System. *Nat. Mater*. **2006**, *5*, 683-696

(17) Förster, T. Zwischenmolekulare Energiewanderung und Fluoreszenz. *Ann. Phys.* **1948**, *437*, 55–75.

(18) Dexter, D. L. A Theory of Sensitized Luminescence in Solids. *J. Chem. Phys.* **1953**, *21*, 836– 850.

(19) List, E. J. W.; Leising, G. Excitation energy migration assisted processes in conjugated polymers. *Synthetic Metals* **2004**, *141*, 211-218.

(20) Beljonne, D.; Pourtois, G.; Silva, C.; Hennebicq, E.; Hertz, L. M.; Friend, R. H.; Scholes, G. D.; Setayesh, S.; Mullen, K.; Bredas, J. L. Interchain vs. intrachain energy transfer in acceptor-capped conjugated polymers. *Proc. Natl. Acad. Sci. U.S.A.* **2002**, *99*, 10982-10987

(21) Wang, C. F.; White, J. D.; Lim, T. L.; Hsu, J. H.; yang, S. C.; Fann, W. S.; Peng, K. Y.; Chen, S. Illustration of exciton migration in rodlike luminescent conjugated polymers by single-molecule spectroscopy. A. *Phys. Rev. B* **2003**, *67*, 035202

(22) Collini, E.; Scholes, G. D. Coherent Intrachain Energy Migration in a Conjugated Polymer at Room Temperature. *Science* **2009**, *323*, 369–373.

(23) Nguyen, T.; Wu, J.; Doan, V.; Schwartz, B. J.; Tolbert, S. H. Control of Energy Transfer in Oriented Conjugated Polymer-Mesoporous Silica Composites. *Science* **2000**, *288*, 652–656.

(24) Nguyen, T.; Schwartz, B. J. Conjugated Polymer Aggregates in Solution: Control of Interchain Interactions. *J. Chem. Phys.* **1999**, *110*, 4068-4078

(25) Levitsky, I. A.; Kim, J.; Swager, T. M. Energy Migration in a Poly(Phenylene Ethynylene): Determination of Interpolymer Transport in Anisotropic Langmuir−Blodgett Films. *J. Am. Chem. Soc.* **1999**, *121*, 1466–1472.

(26) Levitsky, I. A.; Kim, J.; Swager, T. M. Mass and Energy Transport in Conjugated Polymer Langmuir−Blodgett Films: Conductivity, Fluorescence, and UV−Vis Studies. *Macromolecules* **2001**, *34*, 2315–2319.

(27) Nesterov, E. E.; Zhu, Z.; Swager, T. M. Conjugation Enhancement of Intramolecular Exciton Migration in Poly(*p* -Phenylene Ethynylene)S. *J. Am. Chem. Soc.* **2005**, *127*, 10083–10088.

(28) Zhou, Q.; Swager, T. M. Fluorescent Chemosensors Based on Energy Migration in Conjugated Polymers: The Molecular Wire Approch to Increased Sensitivity *J. Am. Chem. Soc.* **1995**, *117*, 12593-12602.

(29) Yang, J.-S.; Swager, T. M. Fluorescent Porous Polymer Films as TNT Chmosensors: Electronic and Structural Effect. *J. Am. Chem. Soc.* **1998**, *120*, 11864-11873.

(30) Li, J.; Kendig, E. C.; Nesterov, E. E. Chemosensory Performance of Molecularly Imprinted Fluorescent Conjugated Polymer Materials. *J. Am. Chem. Soc.* **2007**, *129*, 15911-15918.

(31) Chen, L.; McBranch, D. W.; Wang, H.-L.; Helgeson, R.; Wudl, F.; Whitten, D. G. Highly Sensitive Biological and Chemical Sensors Based on Reversible Fluorescence Quenching in A Conjugated Polymer. *Proc. Natl. Acad. Sci. USA* **1999**, *96*, 12287-12292

(32) Pinto, M. R.; Schanze, K. S. Amplified Fluorescence Sensing of Protease Activity with Conjugated Polyelectrolytes. *Proc. Natl. Acad. Sci.* **2004**, *101*, 7505–7510.

(33) Wosnick, J. H.; Mello, C. M.; Swager, T. M. Synthesis and Application of Poly(Phenylene Ethynylene)s for Bioconjugation: A Conjugated Polymer-Based Fluorogenic Probe for Proteases. *J. Am. Chem. Soc.* **2005**, *127*, 3400–3405.

(34) Gaylord, B. S.; Heeger, A. J.; Bazan, G. C. DNA Detection Using Water-Soluble Conjugated Polymers and Peptide Nucleic Acid Probes. *Proc. Natl. Acad. Sci.* **2002**, *99*, 10954–10957.

(35) Traina, C. A.; Bakus, R. C.; Bazan, G. C. Design and Synthesis of Monofunctionalized, Water-Soluble Conjugated Polymers for Biosensing and Imaging Applications. *J. Am. Chem. Soc.* **2011**, *133*, 12600–12607.

(36) Ho, H. A.; Doré, K.; Boissinot, M.; Bergeron, M. G.; Tanguay, R. M.; Boudreau, D.; Leclerc, M. Direct Molecular Detection of Nucleic Acids by Fluorescence Signal Amplification. *J. Am. Chem. Soc.* **2005**, *127*, 12673–12676.

(37) Kim, T.-H.; Swager, T. M. A Fluorescent Self-Amplifying Wavelength-Responsive Sensory Polymer for Fluoride Ions. *Angew. Chem. Int. Ed.* **2003**, *42*, 4803–4806.

(38) Pangeni, D.; Nesterov, E. E. "Higher Energy Gap" Control in Fluorescent Conjugated Polymers: Turn-On Amplified Detection of Organophosphorous Agents. *Macromolecules* **2013**, *46*, 7266–7273.

(39) Chiang, C.-H.; Pangeni, D.; Nesterov, E. E. Higher Energy Gap Control of Fluorescence in Conjugated Polymers: *Turn-On* Amplifying Chemosensors For Hydrogen Sulfide. *Macromolecules* **2017**, *50*, 6961-6966.

CHAPTER 2. AMPLIFYING FLUORESCENT CONJUGATED POLYMER SENSOR FOR SINGLET OXYGEN DETECTION

2.1 Introduction

Conjugated polymers (CPs) make a popular choice for designing fluorescent sensors because of the intrinsic signal amplification associated with intra- and interchain photoexcitation energy (exciton) migration.[1-6] In particular, CP-based sensors deliver better detection sensitivity relative to the corresponding small-molecule sensors. A typical CP amplified fluorescent sensor utilizes exciton migration to a lower energy gap site created by analyte binding. Such a scheme is common for the detection of fluorescence-quenching electron-deficient analytes (e.g. nitroaromatic explosives) and is used in the design of *turn-off* sensors (i.e. where interaction with analyte results in amplified fluorescence quenching through a photoinduced electron transfer mechanism).[7-10] However, from a practical standpoint, *turn-on* sensors which increase fluorescent intensity upon analyte binding could be more convenient than *turn-off* sensors, but it still remains a challenge to develop and validate a general design scheme towards *turn-on* sensing which could utilize signal amplification ability of CPs. One previous scheme was based on incorporating a specially designed reactive group as part of the CP's π-electron conjugated backbone. Upon reaction with a target analyte, this group would be converted to a lower-energy fluorophore where photoexcitation energy could be funnelled to via intramolecular exciton migration, generating an amplified *turn-on* response.[11] Although promising, this scheme is severely limited by the need to use a reactive group which forms a lower-energy fluorescent chromophore upon reaction with analyte. Indeed, such analytical reactions are not very common, and they are simply not available for many practically important analytical targets.

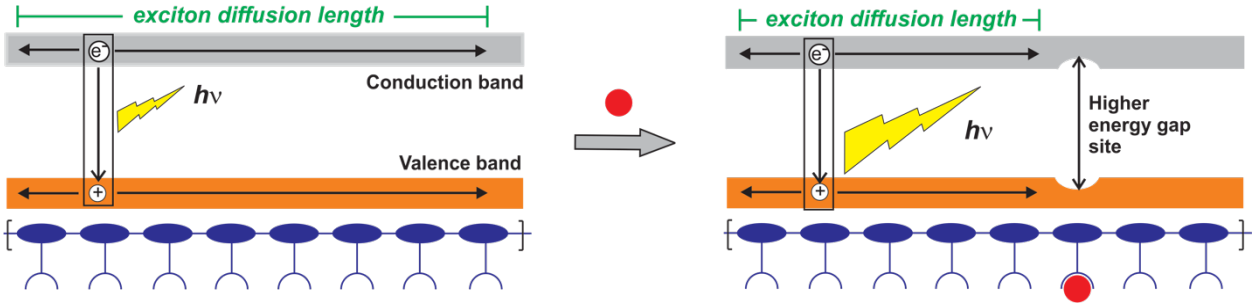

Figure 2.1. General mechanism of the "higher energy gap" control of CP fluorescence: binding an analyte (red circle) to the CP receptor generates a higher energy gap site in the π-conjugated backbone which decreases the exciton diffusion length in the CP, therefore causing an increase of the intensity of fluorescent emission.

As an alternative to this approach, we recently proposed a "higher energy gap" design concept towards fluorescent *turn-on* chemosensors which is free of the limitations of the previous scheme (Figure 2.1).[12,13] Like in the previous scheme, an analyte-reactive group has to be incorporated as part of the CP π-electron backbone. The critical (and essentially only) requirement to such a group is that, upon reaction with a target analyte, it should generate a species with a higher energy (i.e. HOMO-LUMO) gap. The generated higher energy gap site in the CP backbone would act as a "roadblock" diminishing the efficiency of exciton migration (photoexcitation energy transfer) occurring via a through-bond (Dexter-type) mechanism,[14-17] thus decreasing the overall exciton migration length. The shorter exciton migration length would result in a fluorescent emission enhancement in a *turn-on* sensor. Since this phenomenon is mechanistically related to intramolecular exciton migration in the CP π-electron system, it will benefit from the same amplification phenomenon as in the case of fluorescent-quenching *turn-off* chemosensing. Importantly, in contrast to the previous approach, there is no need to generate a fluorescent chromophore unit upon the analyte reaction, which opens

up a breadth of simple and efficient potentially applicable chemical reactions available for almost any analyte of interest. In this work, we demonstrated how the "higher energy gap" concept can be used in the design of an amplifying fluorescent sensor for singlet oxygen ($^1O_2$).

Singlet oxygen is a highly reactive excited state of molecular oxygen which is responsible for photochemical oxidative damage of biological molecules and organic optoelectronic materials, and its high cytotoxicity makes $^1O_2$ an important species in photodynamic therapy treatment.[18-21] A number of small molecules and conjugated polymers that sense $^1O_2$ specifically through changes in intensity of fluorescence have been reported.[22-25] These systems contain either a small-molecule or CP chromophore connected to a $^1O_2$-responsive unit such as anthracene which can react with dienophile $^1O_2$ through a [4+2]-cycloaddition (Diels–Alder reaction), yet these sensors normally operate through a *turn-off* pathway, and none of them demonstrate signal amplification.

2.2 The Design and Synthetic Route of CP Sensor for singlet oxygen Detection

In this this section, we describe an amplifying *turn-on* fluorescent sensor **2-P1** which was designed using the "higher energy gap" concept (Scheme 2.1a). The sensor is a poly(arylene vinylene) conjugated polymer which incorporates 1,4-tetracene unit as part of the π-electron conjugated backbone. Reaction of $^1O_2$ with the tetracene unit yields an endo-peroxide moiety which features a higher HOMO-LUMO gap compared to the initial tetracene. A key design approach was to use the 1,4-bisubsituted tetracene unit for the sensor as this unit would preferentially react with $^1O_2$ at a central benzene ring and not at the ring which is part of the CP π-conjugated backbone. In the former case, the reaction with $^1O_2$ would result in increasing HOMO-LUMO gap at the reaction site without

disrupting the π-conjugation across the polymer backbone - a main condition for the "higher energy gap" principle to be operative. This preferential reactivity is driven mostly by increasing aromatic stabilization of the corresponding endo-peroxide cycloaddition products. Indeed, DFT computations (at B3LYP/6-31G* level of theory) on a truncated 1,4-bisubstituted tetracene unit indicated significantly higher (12.4-13.0 kcal/mol) stabilization of the endo-peroxides formed at the one of the central benzene rings relative to the endo-peroxide formed at the 1,4-positions (Figure 2.2).

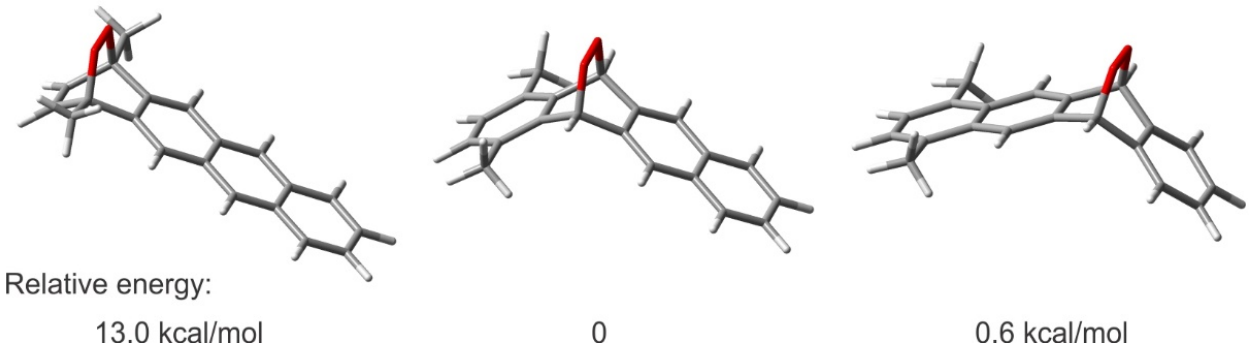

Figure 2.2. Energy difference between different endo-peroxides formed from 1,4-dimethyltetracene (calculated at B3LYP-6-31G* level of theory).

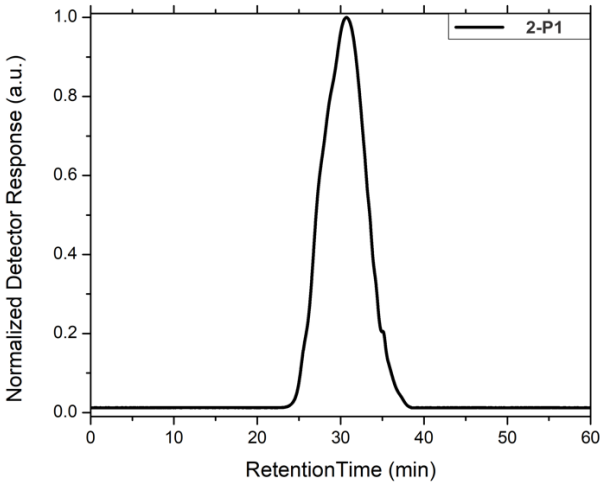

Figure 2.3. GPC elution trace for conjugated polymer **2-P1**. Experimental conditions: solvent THF, flow rate 0.7 ml/min, UV/vis absorbance detection at 450 nm.

The CP **2-P1** with number-average molecular weight M_n 11.8 kDa (as determined by GPC vs. polystyrene standards, Figure 2.3) was prepared using Suzuki polymerization of 1,4-dibromotetracene **2-1** and bis-vinylboronate monomer **2-2** (Scheme 2.1b).

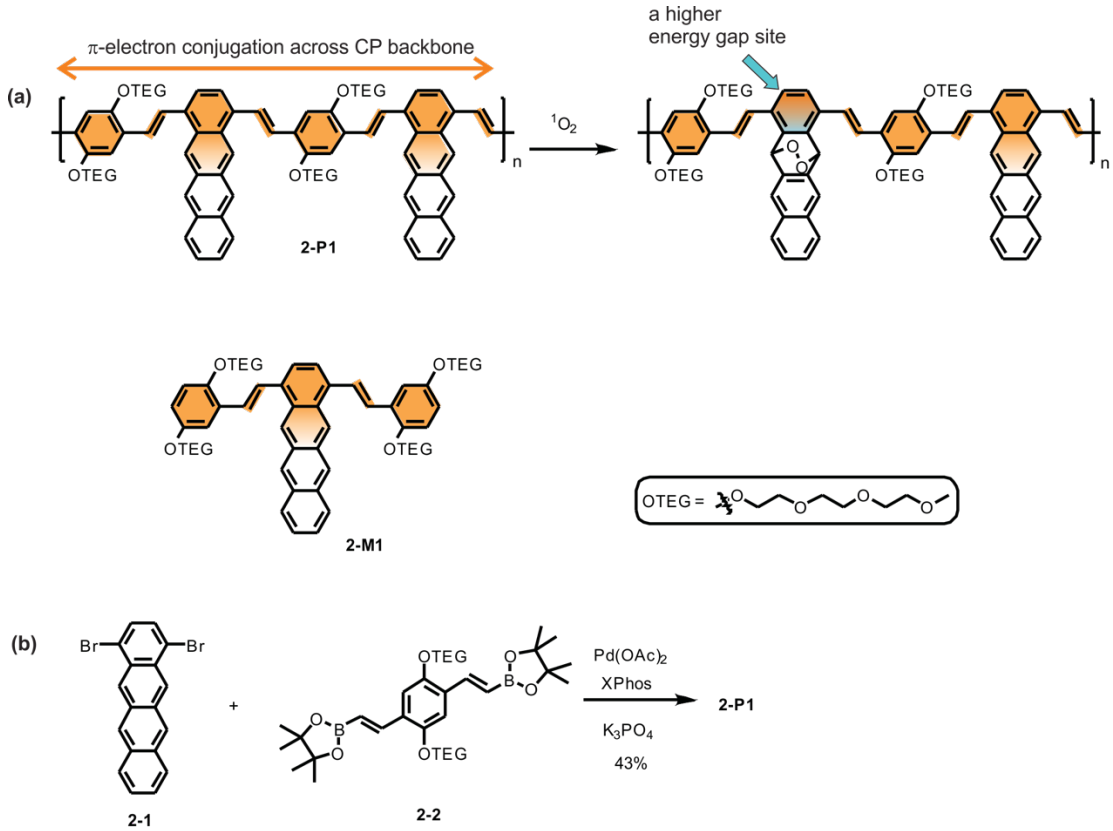

Scheme 2.1. (a) Structures of polymer sensor **2-P1** and corresponding small-molecule sensor **2-M1**, as well as the reaction with singlet oxygen $^1O_2$ to generate a higher energy gap site in the CP backbone. (b) Synthesis of polymer **2-P1**.

Preparation of 1,4-dibromotetracene has not been previously described in literature due to the difficulty of selective functionalization at the 1 and 4 positions in tetracene (since direct functionalization of tetracene through electrophilic aromatic substitution occurs at the central benzene rings). Therefore, we developed a convenient indirect method towards 1,4-dibromotetracene (Scheme 2.2). Bromination of commercially available 2,3-dimethylaniline with NBS occurred selectively and yielded 4-bromo-2,3-dimethylaniline **2-3**. Diazotization followed by Sandmeyer reaction led to 1,4-dibromo-

2,3-dimethylbenzene **2-4** which was selectively brominated at both benzylic positions to yield 1,4-dibromo-2,3-bis(dibromomethyl)benzene **2-5**. An *in situ* formation of a reactive 1,4-dibromo-5,6-bis(methylene)-1,3-cyclohexadiene intermediate and its subsequent Diels-Alder reaction with 1,4-naphthoquinone gave 1,4-dibromo-6,11-tetracenequinone **2-6**.[26,27] Reduction of **6** and subsequent dehydroxylation produced **2-1** in a total 11% yield.

In addition to CP sensor **2-P1**, we also prepared a corresponding small-molecule sensor **2-M1** to be used as a benchmark for measuring fluorescent detection amplification by **2-P1**.

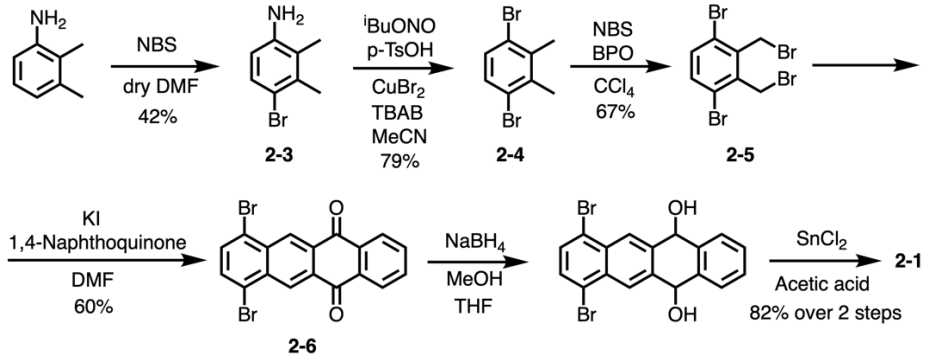

Scheme 2.2. Synthesis of 1,4-dibromotetracene **2-1**.

2.3 Photophysical Characteristics and Fluorescent Amplification

The UV-vis absorption spectrum of polymer **2-P1** showed an intense peak at 290 nm, and a broad lower-intensity shoulder spanning until 630 nm (Figure 2.4). The intense peak at 290 nm is characteristic of tetracene structure,[23-25] and was also prominent in the absorption spectra of small-molecule sensor **2-M1** as well as 1,4-dibromotetracene **2-1**. A characteristic vibronically structured tetracene absorption band between 400 and 520 nm in **1** became a featureless shoulder at around 500 nm in **2-M1**, and was not easily identifiable in **2-P1**. The small-molecule compound **2-M1** also displayed a strong absorption band with maximum at 385 nm which could be attributed to π-electron conjugation across the (arylene

vinylene) system (Scheme 2.1a). Longer π-conjugation length in CP **2-P1** resulted in a bathochromic shift of this band in the polymer's spectrum, where it also overlapped with the tetracene absorption band, producing an overall broad featureless absorption in the spectrum of **2-P1**.

The fluorescence spectrum of **2-M1** showed a broad band with maximum at 475 nm and a shoulder at 575 nm. The polymer **2-P1** spectrum displayed a significantly bathochromically shifted emission band with an overall very low intensity making **2-P1** essentially non-fluorescent.

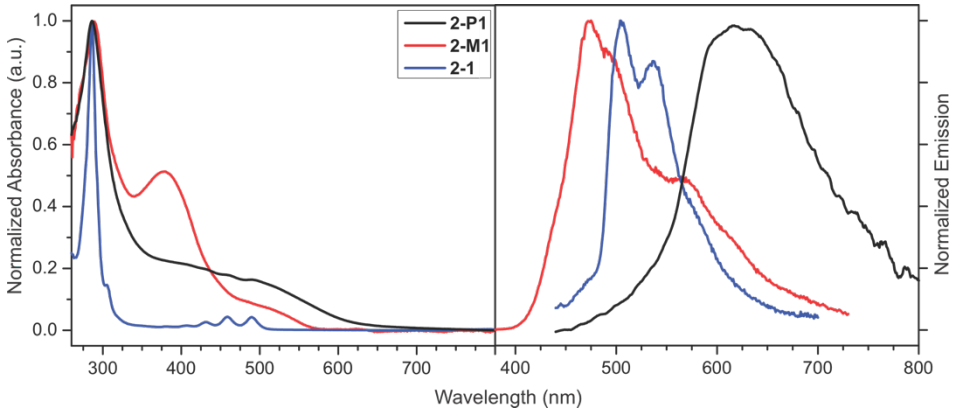

Figure 2.4. Normalized UV/vis absorption and fluorescence spectra of polymer **2-P1**, small-molecule sensor **2-M1** and 1,4-dibromotetracene **2-1** in DMSO (conc. 0.02 mg/ml).

To test chemosensing response to $^1O_2$, we used photoirradiation of the sensor solution in the presence of Rose Bengal sensitizer. In order to avoid interference of the sensitizer with UV/vis absorption and fluorescence spectroscopy experiments, we prepared Rose Bengal functionalized polystyrene beads.[28] The photoirradiation was carried out in a standard 1 cm rectangular cuvette upon stirring. When the stirring was stopped, the Rose Bengal functionalized beads would rapidly precipitate to the bottom of the cuvette, allowing performing spectroscopic measurements *in situ*, without interference from the sensitizer.

Thus, 17 μM solutions of **2-P1** or **2-M1** in DMSO were stirred with Rose Bengal functionalized beads under oxygen and irradiated using a 500 W tungsten-halogen lamp for specified time periods.

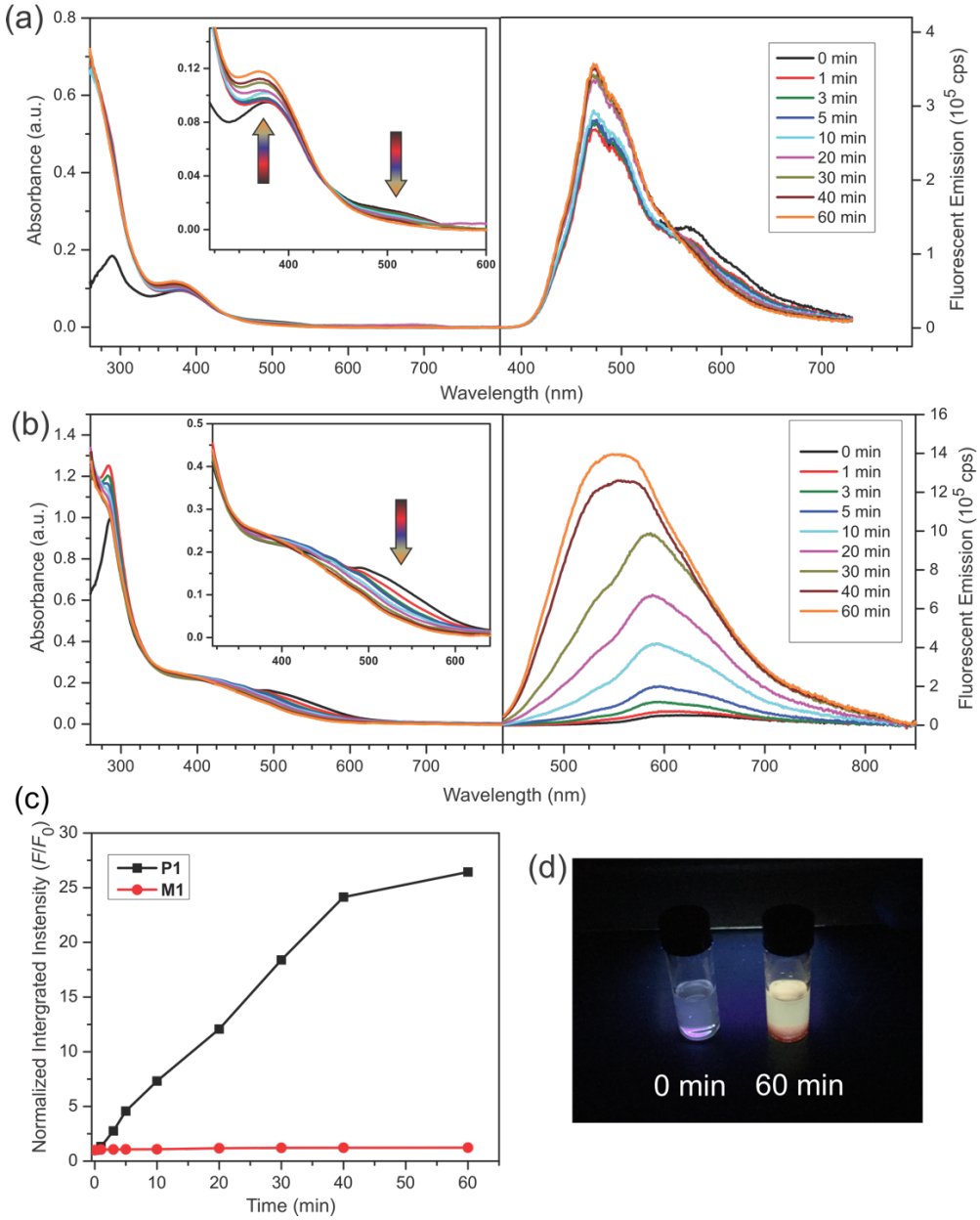

Figure 2.5. Change in absorbance and fluorescence spectra of (a) small-molecule sensor **2-M1** (10 μM solution in DMSO) and (b) polymer **2-P1** (17 μM solution in DMSO) upon exposure to $^1O_2$. (c) Change of fluorescence intensity of **2-P1** and **2-M1** upon exposure to $^1O_2$. The intensity is expressed as a ratio of integrated area of a fluorescent band at each point divided by the area of the fluorescent band before exposure to $^1O_2$. (d) Photograph of a **2-P1** solution before and after exposure to $^1O_2$ upon irradiation with a hand-held UV lamp.

In excellent agreement with the "higher energy gap" concept, the CP sensor **2-P1** exhibited a strong and near-linear increase in fluorescent intensity, with the total increase (as an integrated intensity ratio F/F_0) more than 20 times (Figure 2.5b, c, d). The control experiments (irradiation with no Rose Bengal beads sensitizer or exposure to oxygen with no photoirradiation) did not produce any significant increase in fluorescent intensity (Figure 2.6). In comparison to the polymer sensor **2-P1**, fluorescence intensity enhancement of the small-molecule sensor **2-M1** upon $^1O_2$ exposure in the same conditions was practically negligible (Figure 2.5a, c). This illustrated the significant analyte detection amplification in the *turn-on* fluorescent sensor designed using the "higher energy gap" concept.

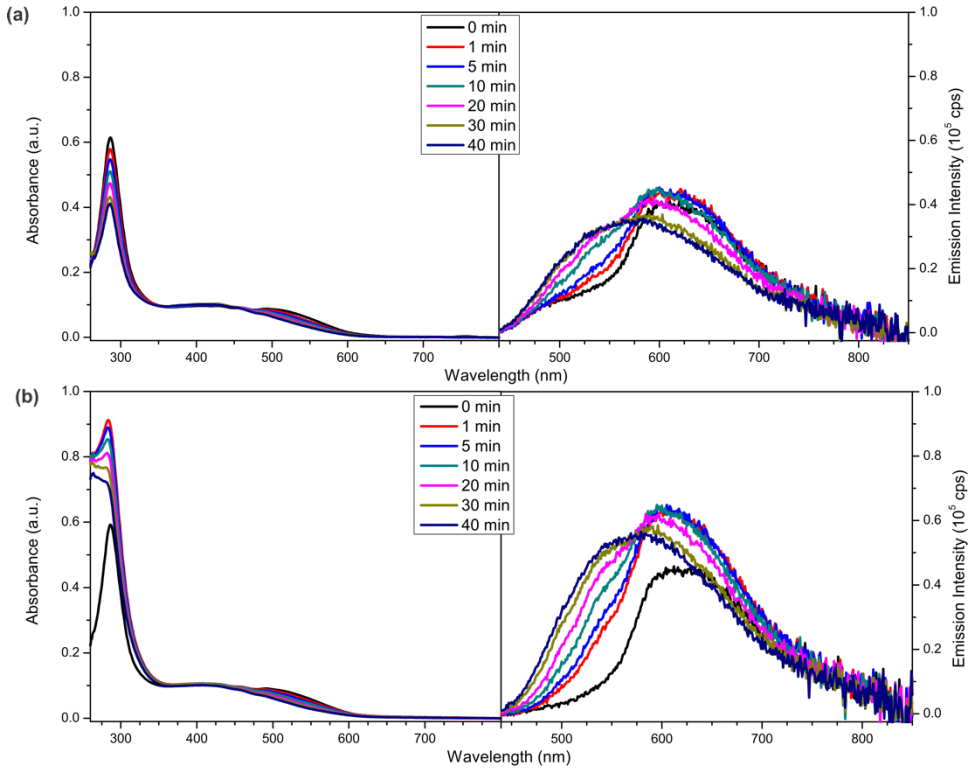

Figure 2.6. Change in UV/vis absorption (left) and fluorescence (right) spectra of a 17 μM solution of the polymer sensor **2-P1** (a) in DMSO with Rose Bengal polymer beads upon photoirradiation without oxygen and (b) in DMSO upon exposure to oxygen and photoirradiation (without Rose Bengal sensitizer).

Further analysis of the spectroscopic results and corresponding ^{1}H NMR data allowed to gain deeper insight into the $^1O_2$ sensing response. Reaction of the small-molecule sensor **2-M1** with $^1O_2$ resulted in the gradual decrease of the tetracene absorbance at 500 nm, whereas the absorption band at 385 nm (corresponding to the π-electron conjugation across the (arylene vinylene) system) persisted (and actually increased its absorbance) (Figure 2.5a). This indicated that the reaction with $^1O_2$ occurred at one of the central benzene rings of 1,4-disubstituted tetracene system, and the extended π-conjugated (arylene vinylene) system remained mostly unaffected. To determine what specific benzene ring in the 1,4-disubstituted tetracene unit the reaction with $^1O_2$ selectively occurred with, we carried out ^{1}H NMR monitoring of the reaction of **2-M1** with $^1O_2$. This reaction produced one main product showing a distinct singlet peak at 6.61 ppm (corresponding to the bridgehead protons at the dioxygen bridge in the endo-peroxide). To assign this and other ^{1}H NMR signals to a specific endo-peroxide, we carried out GIAO computational studies on a truncated analogue of **2-M1** and its corresponding endo-peroxides (Figure 2.7). The computations confirmed that the dioxygen bridge was more likely to form at the 5,12 positions of the tetracene unit, as the calculated NMR shift for the corresponding bridgehead proton was 6.72 ppm - a value close to the experimentally observed one. Other experimental chemical shifts also matched to the values calculated for this specific structure. This reactivity pattern with $^1O_2$ agreed well with the UV/vis absorption spectroscopy observations.

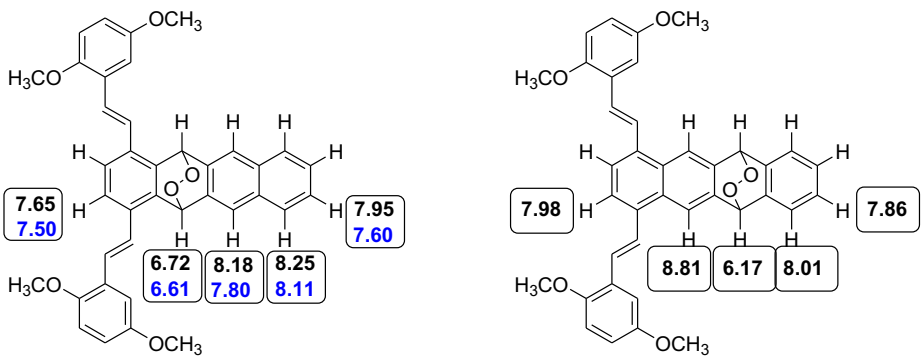

Figure 2.7. Computational prediction and experimental chemical shifts for two alternative endo-peroxides formed from small-molecule sensor **2-M1**. Calculated chemical shifts are shown in black, and experimental shifts (obtained in DMSO-D_6) are shown in blue. Computational structure was truncated by replacing OTEG substituents with OCH_3 substituents. Geometry optimizations were done at B3LYP/6-31G* level, and NMR chemical shifts were calculated on the geometry optimized structures using GIAO at HF/6-31G* level. All computations were done with CPCM solvent treatment (DMSO).

With this information, we could analyze the spectroscopic data obtained for the polymer sensor **2-P1**. The UV/vis absorption spectrum showed gradual decrease between 480 and 630 nm due to the consumption of tetracene unit through its reaction with $^1O_2$ (Figure 2.5b). At the same time, at the earlier stages of photoirradiation, there was no decrease in the absorbance (or even a slight increase) within the range of 360 - 480 nm where the π-electron conjugation in the CP backbone was the main contributor. These changes in the absorption spectra were accompanied by a dramatic intensity increase in the fluorescent emission band, but with essentially no emission wavelength shift. Thus, formation of the endo-peroxide at 5,12 positions of the tetracene unit was responsible for a HOMO-LUMO gap increase which created “roadblocks” for the excitons migrating in the CP π -conjugated backbone, and produced significant *turn-on* fluorescent response. We should also notice that longer exposure of the **2-P1** sensor to $^1O_2$ (at the later stages of photoirradiation) led to a noticeable hypsochromic shift in the

emission band and smaller intensity increase as well as absorbance decrease of the 360 - 480 nm absorption band (traces corresponding to 40 and 60 min in Figure 2.5a, b). Apparently, this was due to a secondary reaction of $^1O_2$ at the 1,4 positions of tetracene ring resulting in breakdown of the π-electron conjugation in the CP backbone.

2.4 Conclusions

In conclusion, we demonstrated how the simple "higher energy gap" concept can be used in the design of an efficient amplifying *turn-on* CP fluorescent sensor. This concept is based on hindering intramolecular exciton migration occurring via a through-bond (Dexter) mechanism when a higher energy (HOMO-LUMO) gap site is created in the polymer π-electron conjugated backbone upon reacting with a target analyte. From a fundamental standpoint, the success of this design illustrates the importance of the through-bond (Dexter-type) mechanism of intramolecular energy migration in fluorescent CPs. On practical side, the "higher energy gap" concept can be used for designing amplifying *turn-on* sensors for many other important analytes of interest.

2.5 References

(1) Swager, T. M. The Molecular Wire Approach to Sensory Signal Amplification. *Acc. Chem. Res.* **1998**, *31*, 201–207.

(2) Feng, X.; Liu, L.; Wang, S.; Zhu, D. Water-Soluble Fluorescent Conjugated Polymers and Their Interactions with Biomacromolecules for Sensitive Biosensors. *Chem. Soc. Rev.* **2010**, *39*, 2411-2419.

(3) Liu, Y.; Ogawa, K.; Schanze, K. S. Conjugated Polyelectrolytes as Fluorescent Sensors. *J. Photochem. Photobiol., C* **2009**, *10*, 173-190.

(4) McQuade, D. T.; Pullen, A. E.; Swager, T. M. Conjugated Polymer-Based Chemical Sensors. *Chem. Rev.* **2000**, *100*, 2537–2574.

(5) Thomas III, S. W.; Joly, G. D.; Swager, T. M. Chemical Sensors Based on Amplifying Fluorescent Conjugated Polymers. *Chem. Rev.* **2007**, *107*, 1339–1386.

(6) Rochat, S.; Swager, T. M. Conjugated Amplifying Polymers for Optical Sensing Applications. *ACS Appl. Mater. Interfaces* **2013**, *5*, 4488-4502.

(7) Yang, J.-S.; Swager, T. M. Fluorescent Porous Polymer Films as TNT Chmosensors: Electronic and Structural Effect. *J. Am. Chem. Soc.* **1998**, *120*, 11864-11837.

(8) Chen, L.; McBranch, D. W.; Wang, H.-L.; Helgeson, R.; Wudl, F.; Whitten, D. G. Highly Sensitive Biological and Chemical Sensors Based on Reversible Fluorescence Quenching in A Conjugated Polymer. *Proc. Natl. Acad. Sci. USA* **1999**, *96*, 12287-12292.

(9) Sun, X.; Wang, Y.; Lei, Y. Fluorescence Based Explosive Detection: From Mechanisms to Sensory Materials. *Chem. Soc. Rev.* **2015**, *44*, 8019-8061.

(10) Jiang, H.; Taranekar, P.; Reynolds, J. R.; Schanze, K. S. Conjugated Polyelectrolytes: Synthesis, Photophysics, and Applications. *Angew. Chem. Int. Ed.* **2009**, *48*, 4300-4316.

(11) Kim, T.-H.; Swager, T. M. A Fluorescent Self-Amplifying Wavelength-Responsive Sensory Polymer for Fluoride Ions. *Angew. Chem. Int. Ed.* **2003**, *42*, 4803–4806.

(12) Pangeni, D.; Nesterov, E. E. "Higher Energy Gap" Control in Fluorescent Conjugated Polymers: Turn-On Amplified Detection of Organophosphorous Agents. *Macromolecules* **2013**, *46*, 7266–7273.

(13) Chiang, C.-H.; Pangeni, D.; Nesterov, E. E. Higher Energy Gap Control of Fluorescence in Conjugated Polymers: *Turn-On* Amplifying Chemosensors For Hydrogen Sulfide. *Macromolecules* **2017**, *50*, 6961-6966.

(14) Beljonne, D.; Curutchet, C.; Scholes, G. D.; Silbey, R. J. Beyond Förster Resonance Energy Transfer in Biological and Nanoscale Systems. *J. Phys. Chem. B* **2009**, *113*, 6583-6599.

(15) Wang, C. F.; White, J. D.; Lim, T. L.; Hsu, J. H.; yang, S. C.; Fann, W. S.; Peng, K. Y.; Chen, S. Illustration of exciton migration in rodlike luminescent conjugated polymers by single-molecule spectroscopy. *A. Phys. Rev. B* **2003**, *67*, 035202.

(16) Van Averbeke, B.; Beljonne, D.; Hennebicq, E. Energy Transport along Conjugated Polymer Chains: Through-Space or Through-Bond? *Adv. Funct. Mater.* **2008**, *18*, 492-198.

(17) Nesterov, E. E.; Zhu, Z.; Swager, T. M. Conjugation Enhancement of Intramolecular Exciton Migration in Poly(*p* -Phenylene Ethynylene)S. *J. Am. Chem. Soc.* **2005**, *127*, 10083–10088.

(18) DeRosa, M. C.; Crutchley, R. J. Photosensitized Singlet Oxygen and Its Applications. *Coord. Chem. Rev.* **2002**, *233-234*, 351-371.

(19) Agostinis, P.; Berg, K.; Cengel, K. A.; Foster, T. H.; Girotti, A. W.; Gollnick, S. A.; Hahn, S. M.; Hamblin, M. R.; Juzeniene, A.; Kessel, D.; Korbelik, M.; Moan, J.; Mroz, P.; Nowis, D.; Piette, J.; Wilson, B. C.; Golab, J. Photodynamic Therapy of Cancer: An Update. *CA Cancer J. Clin.* **2011**, *61*, 250-281.

(20) Dolmans, D. E. J. G. J.; Fukumura, D.; Jain, R. K. Photodynamic Therapy for Cancer. *Nat. Rev. Cancer* **2003**, *3*, 380-387.

(21) Scurlock, R. D., Wang, B., Ogilby, P. R.; Sheats, J. R.; Clough, R. L. Singlet Oxygen as a Reactive Intermediate in the Photodegradation of an Electroluminescent Polymer. *J. Am. Chem. Soc.* **1995**, *117*, 10194-10202.

(22) You, Y. Chemical Tools for The Generation and Detection of Singlet Oxygen. *Org. Biomol. Chem.* **2018**, *16*, 4044-4060.

(23) Zhang, J.; Sarrafpour, S.; Pawle, R. H., Thomas III, S. W. Acene-Linked Conjugated Polymers with Ratiometric Fluorescent Response to $^1O_2$. *Chem. Commun.* **2011**, *47*, 3445-3447.

(24) Altinok, E.; Smith, Z. C.; Thomas III, S. W. Two-Dimensional, Acene-Containing Conjugated Polymers That Show Ratiometric Fluorescent Response to Singlet Oxygen. *Macromolecules* **2015**, *48*, 6825-6831.

(25) Frausto, F.; Thomas III, S. W. Tuning the Key Properties of Singlet Oxygen-Responsive Acene-Doped Conjugated Polymer Nanoparticles. *ChemPhotoChem* **2018**, *2*, 632-639.

(26) M. P. Cava, A. A. Deana, K. Muth, Condensed Cyclobutane Aromatic Compounds. VIII. The Mechanism of Formation of 1,2-Dibromobenzocyclobutene; A New Diels-Alder Synthesis. *J. Am. Chem. Soc.,* **1959**, *81*, 6458-6460.

(27) Plunkett, K. N.; Godula, K.; Nuckolls, C.; Tremblay, N.; Whalley, A. C.; Xiao, S. Expeditious Synthesis of Contorted Hexabenzocoronenes. *Org. Lett.,* **2009**, *11*, 2225-2228.

(28) Taylor, R. P.; Vatz, J. B. Polymer-based sensitizers for photooxidations. *J. Am. Chem. Soc.* **1973**, *95*, 5820-5822.

CHAPTER 3. "HIGHER ENERGY GAP" CONTROL IN THE DESIGN OF A *TURN-ON* AMPLIFYING FLUORESCENT CONJUGATED POLYMER SENSOR FOR CYSTEINE DETECTION

3.1 Introduction

Conjugated polymers (CPs) have attracted much attention for use as materials in the design of chemo- and biosensors due to their intrinsic signal amplification feature. This amplification feature stems from the efficient photoexcitation energy transfer in the electronically delocalized backbone and provides the better sensitivity in comparison to small molecule fluorescent sensors.[1] Besides of the amplification feature, the convenient optical detection, readily tunable spectroscopic and electronic properties, and ease of device fabrication make CPs a promising class of materials for developing sensory devices. CP sensors rely on two main mechanisms of energy transfer which are exchange (through-bond, or "Dexter" mechanism)[2,3] and dipole – induced dipole (through-space or "Förster" mechanism)[4,5] exciton migration to achieve an amplified fluorescence response for a wide variety of analytes ranging from metal ions,[6,7] chemical hazards,[8,9] and biomolecules.[10,11] The most common strategy utilizing an amplified fluorescent response is based on fluorescence quenching (*"turn-off"*) mechanism.[12-16] The fluorescence of CP sensors can be quenched via photoinduced electron transfer (PET) process when, for example, electron deficient analytes bind to the receptor on CP backbone, hence showing a *turn-off* response. Although CP-based fluorescent *turn-off* sensors are generally easy to design for some essential analytical targets, the challenge still remains in designing fluorescence enhancement (*turn-on*) sensors since this mode of detection has a better practical application potential. To achieve the *turn-on* fluorescent response, quencher removal is a general concept that is utilized for the design of CP censors. In such system, the fluorescence is initially suppressed by the quencher attached to CPs, and the fluorescence intensity of CPs will recover when quencher is removed from CP backbones due to the quencher-analyte binding event.[17-19] A related

strategy based on fluorescent resonance energy transfer (FRET) phenomenon has been developed that showing fluorescence enhancement with high sensitivity toward non-quenching analytes such as DNA and proteins.[20-22] Although FRET based CP sensors have demonstrated the effective and efficient *turn-on* fluorescent response, the complexity of their design principle which relies on spectral overlap between energy donors and acceptors intrinsically limits application of this approach.

An alternative approach to achieve an amplified *turn-on* fluorescent response is based on a sophisticated design employing formation of a lower-energy, high quantum yield fluorophore after the cyclization promoted by a target analyte (e. g. fluoride ion) leading from a non-emissive analyte-specific receptor which is electronically attached on the CP backbone.[23] The newly-formed low-energy gap strongly fluorescent site acts as a trap for excitons resulting in the increase of fluorescent intensity originating from this fluorophore. This CP sensor showed an approximately 100-times higher sensitivity for fluoride ion detection relative to its small-molecule analog. While this example demonstrated an efficient, albeit somewhat sophisticated concept to accomplish a CP-based *turn-on* amplifying chemosensor, the low availability of efficient reactions of practically important analytical targets that could generate a high quantum yield, low-energy gap fluorophore makes this case the only example utilizing this concept.

Since previous approaches towards *turn-on* fluorescent conjugated polymer sensors are problematic due to the need for excessively sophisticated design in terms of energy level matching and synthetic difficulty, finding a more practically feasible strategy to achieve an amplified *turn-on* fluorescent response using CPs for chemo/biosensing remains highly important. Recently, our group proposed the “higher energy gap” control concept as a general and universal approach in designing *turn-on* amplifying fluorescent

conjugated polymer sensors. In sharp contrast to sophisticated previous approaches, the "higher energy gap" paradigm relies on relatively minor changes in the electronic structure of the receptor side upon interaction (reaction) with a target analyte that would be sufficient to trigger an efficient *turn-on* amplified fluorescent response. In such a scheme, any reaction that can create a local higher energy (HOMO-LUMO) gap site on the CP backbone upon a reaction between receptor and analyte can be utilized in this concept. The site with an increased energy gap acts as a "roadblock" to restrict exciton migration distance. Lowering exciton migration length can efficiently reduce the chance for excitons to get quenched by intrinsically present structural or transient defects,[24,25] hence resulting in overall fluorescence enhancement. To demonstrate the practical utility of the higher energy gap paradigm, previously PPV-based sensors have been designed for the detection of organophosphorus nerve agent mimic diethyl chlorophosphite,[26] hydrogen sulfide,[27] and singlet oxygen. In this project, we decided to apply the "higher energy gap" control concept towards the detection of an important amino acid *L*-cysteine.

Although classified as a nonessential amino acid, *L*-cysteine indeed plays an important role in vital physiological functions.[28,29] An abnormal low level of cysteine was found to be related to edema, slowed growth, hair depigmentation, liver damage, muscle and fat loss, and skin lesions.[30] Thus, rapid and efficient detection of physiologically relevant concentrations of cysteine both *in vitro* and *in vivo* has attracted much attention. There are several existing methods to measure cysteine levels such as fluorescent detection,[31] Fourier transform infrared (FTIR) spectroscopy,[32] high performance liquid chromatography (HPLC),[33] and electrochemical analysis,[34] but these methods require high instrument expenses, long sample preparation and/or data collecting time, and

destruction of samples that all limit their practical utility. Recently, a number of fluorescent chemosensors for the detection of cysteine based on its strong nucleophilicity and heavy metal ions affinity have been developed.[35-39] Among various potential reactions between cysteine and functionalized receptor molecules, the rapid formation of thiazolidine from aldehyde in the presence of cysteine offers the best promise for monitoring the concentration of cysteine in aqueous solutions. Indeed, several probes which incorporated reactive aldehyde functional group for the detection of cysteine have been described in the literature as showing ratiometric response.[40-42] Although these previous examples demonstrated the efficient detection ability toward cysteine, none of exhibited an amplified *turn-on* fluorescent response. In the following sections, we introduce a novel design of the amplifying *turn-on* fluorescent CP sensor utilizing the "higher energy gap" concept for cysteine detection.

3.2 The Design and Synthetic Route of CP Sensor for Cysteine Detection

To develop an amplifying *turn-on* conjugated polymer sensor utilizing the "higher energy gap" mechanism for cysteine detection, poly(*p*-phenylene vinylene) backbone was chosen as the suitable low energy gap conjugated polymer scaffold. Similar scaffold was previously successfully applied towards the design of amplifying sensors for several important biological analytes.[26,27] Among a variety of organic reactions which can target cysteine, we selected naphthaldehyde moiety as the cysteine receptor where the aldehyde group can efficiently react with cysteine to form a thiazolidine. In addition to the relatively simple and straightforward synthetic design, the formation of thiazolidine was expected to alter the local energy gap of the chromophore without affecting the overall conjugation in the polymer backbone. Preliminary DFT computational study (at the

B3LYP/6-31G(d) level of theory) indicated that the thiazolidine formation would increase the HOMO-LUMO gap of the receptor chromophore from 3.52 to 3.80 eV (Figure 3.1). With such a small energy gap change (0.28 eV) that was computationally predicted, , it was interesting to test whether such a minor increase of HOMO-LUMO gap would be sufficient to effectively restrict intramolecular exciton migration and result in the amplified *turn-on* fluorescent response based on the "higher energy gap" mechanism.

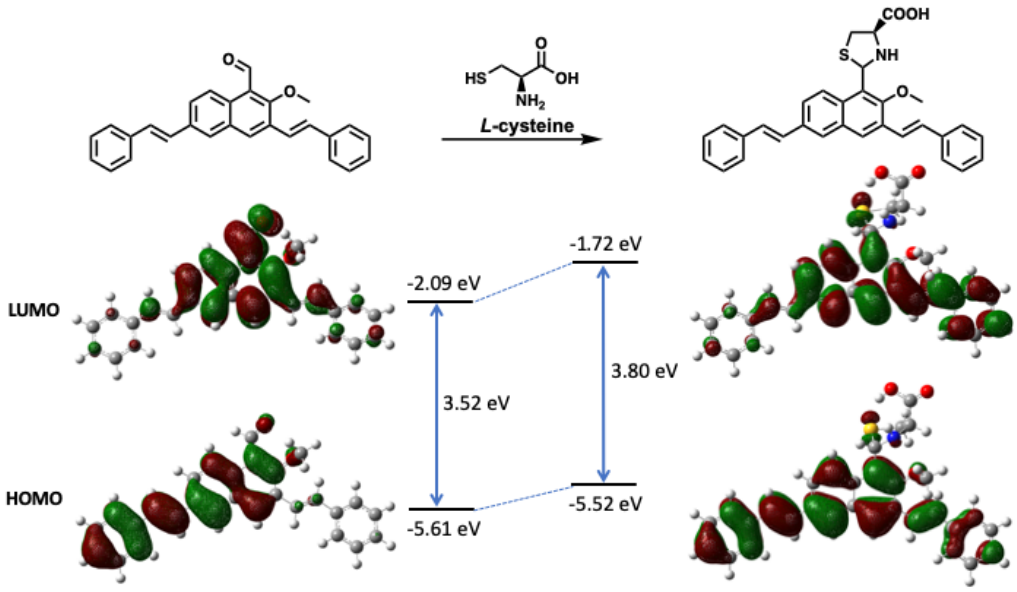

Figure 3.1. DFT computational studies (at B3LYP/6-31G(d) level) of the HOMO-LUMO gap change in the naphthaldehyde receptor upon reaction with cysteine. The molecule was truncated for better computational efficiency. The computed distribution of HOMO and LUMO of the initial receptor indicate complete electronic delocalization over the entire molecule. Reaction with cysteine effectively converted initial aldehyde into thiazolidine causing the energy gap increase of the π-conjugated system from 3.52 to 3.80 eV.

The synthetic design to approach the CP-based sensor for cysteine detection was similar to the synthetic route for the design of singlet oxygen sensor (discussed in the previous chapter). Instead of using tri(ethylene glycol) monomethyl ether (TEG) group (used in the singlet oxygen sensor design) which provided only limited aqueous solubility not sufficient to perform analytical measurements in aqueous media such as in phosphate-buffered saline (PBS) solution, we decided to use 1,6-dibromohexane as the

solubilizing group to synthesize compound **3-S3** under the same reaction conditions as described in the literature.[27] The subsequent Suzuki polymerization of **3-S3** and **3-S4**[26] utilizing $Pd(OAc)_2$, XPhos and K_3PO_4 as the base was carried out in a toluene-water 5/1 mixture to form polymer **3-P1**, which could be readily purified by precipitation from acetone and ether to give the product in a moderate yield (60%), with number average molecular weight M_n 19.34 kDa (GPC, vs. polystyrene standards). The subsequent S_N2 reaction with trimethylamine in H_2O-THF mixture converted polymer **3-P1** to a water-soluble polymer **3-P2**.[43] Polymer **3-P2** was then purified by dialysis in nanopure water for 3 days (using a dialysis membrane with an 8 kDa cutoff).

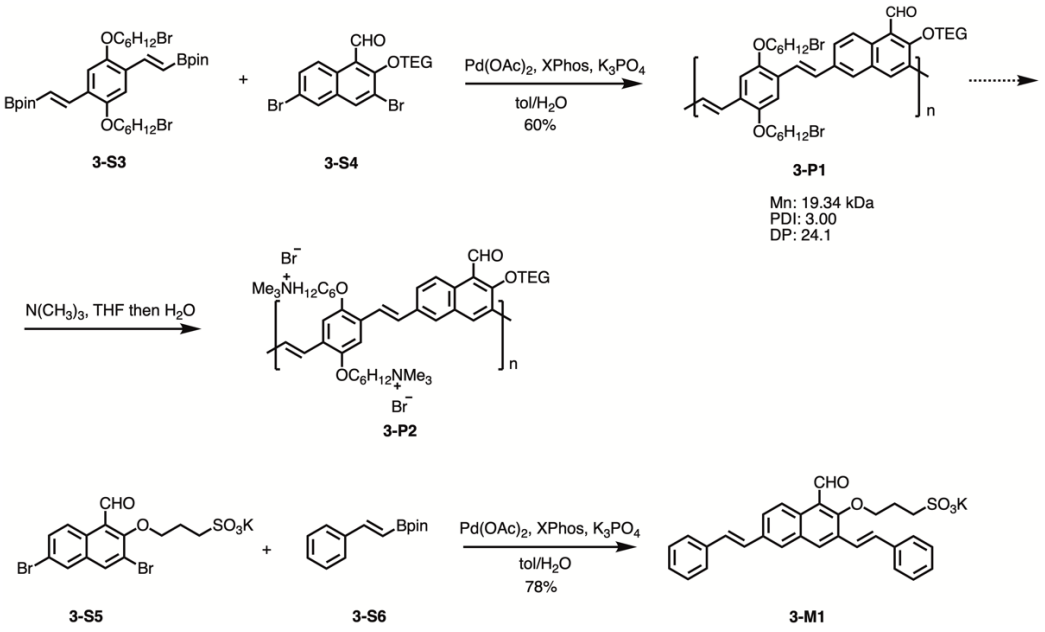

Scheme 3.1. Synthetic route towards conjugated polymers **3-P2** cysteine detection and the corresponding small-molecule sensor **3-M1**.

In addition, a small molecule reference was needed to compare the effect of fluorescent amplification in the longer π-conjugated system compared to a much shorter one. To synthesize a water-soluble small molecule sensor, water-soluble potassium sulfonate salt **3-S5** was prepared by the alkylation of 3,6-dibromo-2-hydroxy-1-

naphthaldehyde[26] with 1,3-propansultone under basic conditions in a 2-butanone - ethanol 1/1 mixture. **3-S5** was then coupled with **3-S6**[27] in a Suzuki coupling reaction to afford crude **3-M1** which was then purified by rinsing with CH_2Cl_2 and THF followed by recrystallization from H_2O-EtOH 1/9 to give the pure **3-M1** as a light greenish solid in 78% yield.

3.3 Photophysical Characterization and Cysteine-Sensing Performance

UV-vis and fluorescence spectroscopy studies were carried out on the polymer sensor **3-P2** and small molecule reference **3-M1** to characterize their photophysical properties. All the studies were performed using solutions in 1X PBS in Nanopure water, and the reactions with cysteine were allowed to run at 50 ºC for 1 hour to reach the equilibrium. The UV-vis absorption spectrum of the polymer sensor **3-P2** showed a featureless band characteristic of typical poly(phenylene vinylene) polymers. The small molecule **3-M1** showed a major absorption band at 316 nm with a low-intensity shoulder at around 400 nm. The higher-energy band can be assigned to a naphthalene-centered chromophore and the latter band was attributed to a lower-energy chromophore resulting from the extended π-electron delocalization. In addition, the UV-vis absorption spectra provided the evidence that **3-P2** possessed a longer extended π-election delocalization distance than the small molecule **3-M1** by exhibiting a significant bathochromic shift of 95 nm of the absorbance intensity maximum (λ_{max} 411 nm for **3-P2** vs λ_{max} 316 nm for **3-M1**). Upon comparison of the fluorescence spectra of the polymer sensor **3-P2** and small molecule analog **3-M1** (excited at 390 nm), **3-P2** demonstrated a noticeable bathochromic shift which could also be attributed to a longer π-electron delocalization in the polymer (λ_{max} 537 nm for **3-P2** vs λ_{max} 495 nm for **3-M1**) (Figure 3.2).

The comparative studies of the cysteine-sensing performance of **3-P2** and **3-M1** revealed the effect of signal amplification in the conjugated polymer sensor. Upon addition of cysteine, the 37.5 μM solution of the small-molecule reference **3-M1** showed a moderate gradual decrease in fluorescence intensity, and insignificant changes in UV-vis absorption spectra, even upon addition of a large excess of cysteine. The fluorescence intensity decrease (*turn-off* response) could probably be explained by the heavy atom effect from sulfur upon formation of the thiazolidine moiety. Additionally, this could be attributed to the lower solubility of the thiazolidine derivative in the aqueous conditions, causing some material precipitating from the solution. Indeed, we observed precipitation of an insoluble solid from the measured samples after some time.

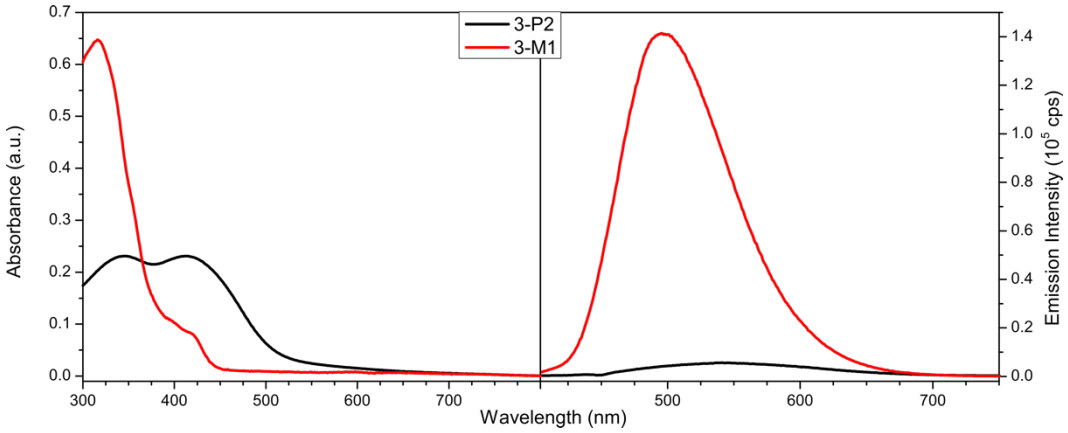

Figure 3.2. Absorption (left) and fluorescence (right) spectra of a 40μM solution of CP sensor **3-P2** and a 37.5μM solution of small-molecule reference **3-M1** in aqueous PBS.

In contrast, a similar concentration (40μM) of the polymer sensor **3-P2** solution showed a significant enhancement in fluorescence that was observed upon addition of cysteine within a range of a hundred nanomolar to a few millimolar concentrations. The insignificant changes in UV-vis absorption spectra indicated only a minor change in the electronic structure of the π-conjugated scaffold of **3-P2** upon aldehyde to thiazolidine conversion which agreed well with the concept of the “higher energy gap” mechanism

(Figure 3.3). The dramatically enhanced response of the polymer-based sensor towards cysteine can be clearly seen in Figure 3.4 where **3-P2** showed an up to 33-fold amplification in the detection of a much lower concentration of cysteine as compared to the small-molecule sensor reference **3-M1**.

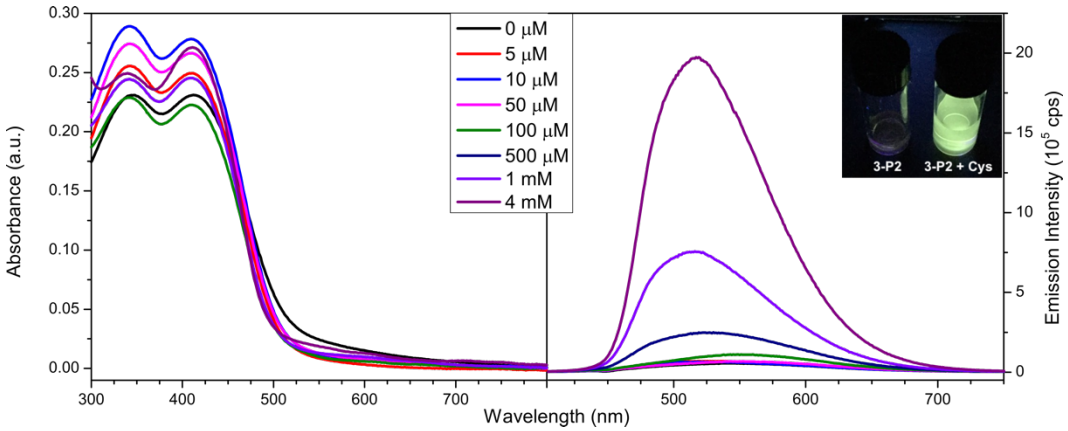

Figure 3.3. Change in absorption (left) and fluorescence (right) spectra of a 40 μM solution of **3-P2** in 1X PBS upon addition of increasing concentration of cysteine (the spectra were acquired in 1 h after cysteine addition). The inset shows a photograph of the solution before and after addition of a 4 mM concentration of cysteine upon irradiation with a hand-held UV lamp.

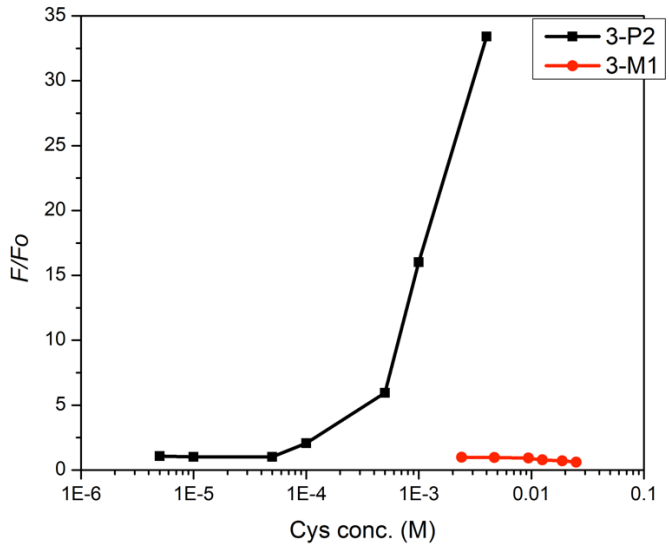

Figure 3.4. Change in integrated fluorescence intensity of a 1X PBS solution of polymer **3-P2**, and small-molecule reference **3-M1** upon addition of increasing concentrations of cysteine. The intensity is expressed as a ratio of integrated area of a fluorescence band at each cysteine concentration divided by the area of the fluorescent band in the absence of analyte (F/F_0).

For the practical applications of the sensor polymer **3-P2**, it should display not only high sensitivity but also high selectivity toward the target analyte. The fluorescent response of **3-P2** to various potentially competing nucleophiles is shown in Figure 3.5. These analytes include a model for reactive oxygen species (H_2O_2), common thiols (*L*-methionine (Met), 2-mercaptoethanol (2-Me), glutathione (GSH)), and amino acids (*L*-glutamine (Gln), *L*-serine (Ser), *L*-glycine (Gly), *L*-glutamic acid (Glu)). Among reactions of **3-P2** with all the nucleophiles motioned above, only cysteine caused a significant fluorescent response. Therefore, **3-P2** demonstrated both the amplified fluorescent response sensitivity as compared to the small-molecule analog and a high selectivity toward target analyte that could make it an excellent sensor for cysteine detection.

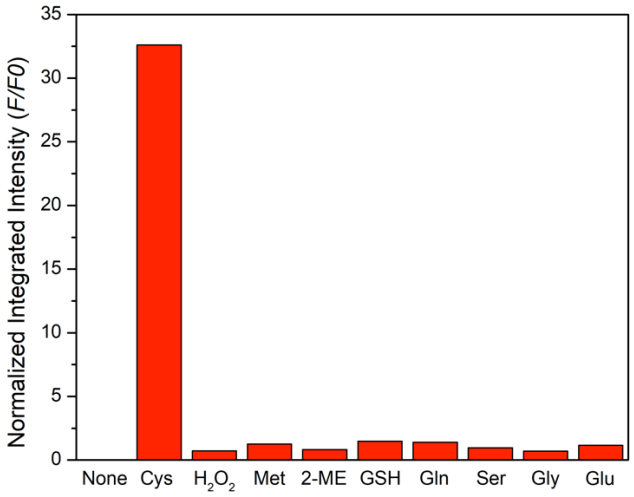

Figure 3.5. Normalized integrated fluorescence intensity (as a ratio of integrated areas of fluorescent bands after and before addition of the analyte) of a 40 μM solution of polymer **3-P2** in 1X PBS upon addition of various analytes.

3.4 Conclusions

We have developed a PPV-based conjugated polymer functionalized with the electronically coupled naphthaldehyde receptor as an amplifying fluorescent sensor for

cysteine detection which utilizes the “higher energy gap” concept. The “higher energy gap” mechanism hinges on reducing exciton migration length in a conjugated polymer backbone by creating a local higher energy gap site upon reaction with an analyte. In this study, reaction of naphthaldehyde receptor electronically connected to the π-electron system of on the polymer sensor **3-P2** with cysteine causes only a small increase (0.28eV) of the HOMO-LUMO gap by the formation of thiazolidine moiety. Despite this minor energy gap increase, the polymer sensor exhibited substantial amplified fluorescent *turn-on* response with up to a 33-fold amplification in fluorescence intensity. The minor change in UV/vis absorption spectra and the significant increase of fluorescent intensity were in excellent agreement with the “higher energy gap” paradigm. This work, from the practical point of view, shows the potential for the design of highly efficient amplifying *turn-on* fluorescent sensors based on the novel “higher energy gap” control concept since even a relatively small change in HOMO-LUMO gap can cause a substantial amplified fluorescent response. This will enable simple design of the *turn-on* sensors for a broad range of important chemical and biological analytes.

3.5 References

(1) Zhou, Q.; Swager, T. M. Fluorescent Chemosensors Based on Energy Migration in Conjugated Polymers: The Molecular Wire Approch to Increased Sensitivity *J. Am. Chem. Soc.* **1995**, *117*, 12593-12602.

(2) Levitsky, I. A.; Kim, J.; Swager, T. M. Mass and Energy Transport in Conjugated Polymer Langmuir−Blodgett Films: Conductivity, Fluorescence, and UV−Vis Studies. *Macromolecules* **2001**, *34*, 2315–2319.

(3) Nesterov, E. E.; Zhu, Z.; Swager, T. M. Conjugation Enhancement of Intramolecular Exciton Migration in Poly(*p* -Phenylene Ethynylene)S. *J. Am. Chem. Soc.* **2005**, *127*, 10083–10088.

(4) Wang, C. F.; White, J. D.; Lim, T. L.; Hsu, J. H.; yang, S. C.; Fann, W. S.; Peng, K. Y.; Chen, S. Illustration of exciton migration in rodlike luminescent conjugated polymers by single-molecule spectroscopy. A. *Phys. Rev. B* **2003**, *67*, 035202

(5) Nguyen, T.; Schwartz, B. J. Conjugated Polymer Aggregates in Solution: Control of Interchain Interactions. *J. Chem. Phys.* **1999**, *110*, 4068-4078

(6) Zhu, M.; Zhou, C.; Zhao, Y.; Li, Y.; Liu, H.; Li, Y. Synthesis of a Fluorescent Polymer Bearing Covalently Linked Thienylene Moieties and Rhodamine for Efficient Sensing. *Macromol. Rapid Commun.* **2009**, *30*, 1339–1344.

(7) Qu, Y.; Zhang, X.; Wu, Y.; Li, F.; Hua, J. Fluorescent Conjugated Polymers Based on Thiocarbonyl Quinacridone for Sensing Mercury Ion and Bioimaging. *Polym Chem* **2014**, *5*, 3396–3403.

(8) McQuade, D. T.; Pullen, A. E.; Swager, T. M. Conjugated Polymer-Based Chemical Sensors. *Chem. Rev.* **2000**, *100*, 2537–2574.

(9) Thomas, S. W.; Joly, G. D.; Swager, T. M. Chemical Sensors Based on Amplifying Fluorescent Conjugated Polymers. *Chem. Rev.* **2007**, *107*, 1339–1386.

(10) Rochat, S.; Swager, T. M. Water-Soluble Cationic Conjugated Polymers: Response to Electron-Rich Bioanalytes. *J. Am. Chem. Soc.* **2013**, *135*, 17703–17706.

(11) Kim, H. N.; Guo, Z.; Zhu, W.; Yoon, J.; Tian, H. Recent Progress on Polymer-Based Fluorescent and Colorimetric Chemosensors. *Chem Soc Rev* **2011**, *40*, 79–93.

(12) Yang, J.-S.; Swager, T. M. Fluorescent Porous Polymer Films as TNT Chemosensors: Electronic and Structural Effects. *J. Am. Chem. Soc.* **1998**, *120*, 11864–11873.

(13) Rose, A.; Zhu, Z.; Madigan, C. F.; Swager, T. M.; Bulović, V. Sensitivity Gains in Chemosensing by Lasing Action in Organic Polymers. *Nature* **2005**, *434*, 876–879.

(14) Li, J.; Kendig, C. E.; Nesterov, E. E. Chemosensory Performance of Molecularly Imprinted Fluorescent Conjugated Polymer Materials. *J. Am. Chem. Soc.* **2007**, *129*, 15911–15918.

(15) Fan, C.; Wang, S.; Hong, J. W.; Bazan, G. C.; Plaxco, K. W.; Heeger, A. J. Beyond Superquenching: Hyper-Efficient Energy Transfer from Conjugated Polymers to Gold Nanoparticles. *Proc. Natl. Acad. Sci.* **2003**, *100*, 6297–6301.

(16) Xie, D.; Parthasarathy, A.; Schanze, K. S. Aggregation-Induced Amplified Quenching in Conjugated Polyelectrolytes with Interrupted Conjugation. *Langmuir* **2011**, *27*, 11732– 11736.

(17) Chen, L.; McBranch, D. W.; Wang, H.-L.; Helgeson, R.; Wudl, F.; Whitten, D. G. Highly Sensitive Biological and Chemical Sensors Based on Reversible Fluorescence Quenching in a Conjugated Polymer. *Proc. Natl. Acad. Sci.* **1999**, *96*, 12287–12292.

(18) Pinto, M. R.; Schanze, K. S. Amplified Fluorescence Sensing of Protease Activity with Conjugated Polyelectrolytes. *Proc. Natl. Acad. Sci.* **2004**, *101*, 7505–7510.

(19) Wosnick, J. H.; Mello, C. M.; Swager, T. M. Synthesis and Application of Poly(Phenylene Ethynylene)s for Bioconjugation: A Conjugated Polymer-Based Fluorogenic Probe for Proteases. *J. Am. Chem. Soc.* **2005**, *127*, 3400–3405.

(20) Gaylord, B. S.; Heeger, A. J.; Bazan, G. C. DNA Detection Using Water-Soluble Conjugated Polymers and Peptide Nucleic Acid Probes. *Proc. Natl. Acad. Sci.* **2002**, *99*, 10954–10957.

(21) Traina, C. A.; Bakus, R. C.; Bazan, G. C. Design and Synthesis of Monofunctionalized, Water-Soluble Conjugated Polymers for Biosensing and Imaging Applications. *J. Am. Chem. Soc.* **2011**, *133*, 12600–12607.

(22) Ho, H. A.; Doré, K.; Boissinot, M.; Bergeron, M. G.; Tanguay, R. M.; Boudreau, D.; Leclerc, M. Direct Molecular Detection of Nucleic Acids by Fluorescence Signal Amplification. *J. Am. Chem. Soc.* **2005**, *127*, 12673–12676.

(23) Kim, T.-H.; Swager, T. M. A Fluorescent Self-Amplifying Wavelength-Responsive Sensory Polymer for Fluoride Ions. *Angew. Chem. Int. Ed.* **2003**, *42*, 4803–4806.

(24) Lupton, J. M. Single-Molecule Spectroscopy for Plastic Electronics: Materials Analysis from the Bottom-Up. *Adv. Mater.* **2010**, *22*, 1689–1721.

(25) Bolinger, J. C.; Traub, M. C.; Brazard, J.; Adachi, T.; Barbara, P. F.; Vanden Bout, D. A. Conformation and Energy Transfer in Single Conjugated Polymers. *Acc. Chem. Res.* **2012**, *45*, 1992–2001.

(26) Pangeni, D.; Nesterov, E. E. “Higher Energy Gap” Control in Fluorescent Conjugated Polymers: Turn-On Amplified Detection of Organophosphorous Agents. *Macromolecules* **2013**, *46*, 7266–7273.

(27) Chiang, C.-H.; Pangeni, D.; Nesterov, E. E. Higher Energy Gap Control of Fluorescence in Conjugated Polymers: *Turn-On* Amplifying Chemosensors For Hydrogen Sulfide. *Macromolecules* **2017**, *50*, 6961-6966.

(28) Lu, S. C. Regulation of Glutathione Synthesis. *Mol. Aspects. Med.* **2009**, *30*, 42–59.

(29) Pham-Huy, L. A.; He, H.; Pham-Huy, C. Free Radicals, Antioxidants in Disease and Health. *Int. J. Biomed. Sci.* **2008**, *4*, 89–96.

(30) Shahrokhian, S. Lead Phthalocyanine as a Selective Carrier for Preparation of a Cysteine-Selective Electrode. *Anal. Chem.* **2001**, *73*, 5972–5978.

(31) Wang, H.; Wang, W.-S.; Zhang, H.-S. Spectrofluorimetic Determination of Cysteine Based on the Fluorescence Inhibition of Cd(II)–8-hydroxyquinoline-5-sulphonic Acid Complex by Cysteine. *Talanta* **2001**, *53*, 1015–1019.

(32) Sato, Y.; Iwata, T.; Tokutomi, S.; Kandori, H. Reactive Cysteine is Protonated in the Triplet Excited State of the LOV2 Domain in Adiantum Phytochrome. *J. Am. Chem. Soc.* **2005**, *127*, 1088–1089.

(33) Vacek, J.; Klejdus, B.; Petrlová, J.; Lojková, L.; Kubáň, V. A Hydrophilic Interaction Chromatography Coupled to a Mass Spectrometry for the Determination of Glutathione in Plant Somatic Embryos. *The Analyst* **2006**, *131*, 1167–1174.

(34) Potesil, D.; Petrlova, J.; Adam, V.; Vacek, J.; Klejdus, B.; Zehnalek, J.; Trnkova, L.; Havel, L.; Kizek, R. Simultaneous Femtomole Determination of Cysteine, Reduced and Oxidized Glutathione, and Phytochelatin in Maize (Zea mays L.) Kernels Using High-Performance Liquid Chromatography with Electrochemical Detection," *Journal of Chromatography A* **2005**, *1084*, 134–144.

(35) Chow, C.-F.; Chiu, B. K. W.; Lam, M. H. W.; Wong, W.-Y. A Trinuclear Heterobimetallic Ru(II)/Pt(II) Complex as a Chemodosimeter Selective for Sulfhydryl-Containing Amino Acids and Peptides. *J. Am. Chem. Soc.* **2003**, *125*, 7802–7803.

(36) Maeda, H.; Matsuno, H.; Ushida, M.; Katayama, K.; Saeki, K.; Itoh, N. 2,4-Dinitrobenzenesulfonyl Fluoresceins as Fluorescent Alternatives to Ellman's Reagent in Thiol-Quantification Enzyme Assays. *Angew. Chem. Int. Ed.* **2005**, *44*, 2922–2925.

(37) Han, M. S.; Lytton-Jean, A. K. R.; Oh, B.-K.; Heo, J.; Mirkin, C. A. Colorimetric Screening of DNA-Binding Molecules with Gold Nanoparticle Probes. *Angew. Chem. Int. Ed.* **2006**, *45*, 1807–1810.

(38) Tang, B.; Yin, L.; Wang, X.; Chen, Z.; Tong, L.; Xu, K. A Fast-Response, Highly Sensitive and Specific Organoselenium Fluorescent Probe for Thiols and Its Application in Bioimaging. *Chem. Commun.* **2009**, *35*, 5293-5295.

(39) Zhu, J.; Dhimitruka, I.; Pei, D. 5-(2-Aminoethyl)Dithio-2-Nitrobenzoate as a More Base-Stable Alternative to Ellman's Reagent. *Org. Lett.* **2004**, *6*, 3809–3812.

(40) Rusin, O.; St. Luce, N. N.; Agbaria, R. A.; Escobedo, J. O.; Jiang, S.; Warner, I. M.; Dawan, F. B.; Lian, K.; Strongin, R. M. Visual Detection of Cysteine and Homocysteine. *J. Am. Chem. Soc.* **2004**, *126*, 438–439.

(41) Lin, W.; Long, L.; Yuan, L.; Cao, Z.; Chen, B.; Tan, W. A Ratiometric Fluorescent Probe for Cysteine and Homocysteine Displaying a Large Emission Shift. *Org. Lett.* **2008**, *10*, 5577– 5580.

(42) Acharya, J. R.; Zhang, H.; Li, X.; Nesterov, E. E. Chemically Controlled Amplified Ratiometric Fluorescence in Surface-Immobilized End-Capped Oligo(*p*-Phenylene Ethynylene)S. *J. Am. Chem. Soc.* **2009**, *131*, 880–881.

(43) Lee, B. H.; Jung, I. H.; Woo, H. Y.; Shim, H.-K.; Kim. G.; Lee, K. Multi-Charged Conjugated Polyelectrolytes as a Versatile Work Function Modifier for Organic Elcetoninc Devices. *Adv. Funct. Mater.* **2014**, *24*, 1100-1108

CHAPTER 4. HYBRID CORE-SHELL NANOPARTICLES CONSISTING OF A SILICA CORE AND TRIBLOCK COPOLYMER SHELLS PREPARED BY SURFACE-INITIATED POLYMERIZATION

4.1. Introduction

Organic/inorganic hybrid nanomaterials possess a unique combination of optical, electronic, magnetic and catalytic properties stemming from the presence of both inorganic and organic components.[1-4] Such materials with controlled size and structural features are particularly suitable for the development of sensory devices,[5-8] photovoltaic,[9,10] optoelectronic,[11,12] and biomedical applications.[13,14] Typical hybrid nanomaterials consist of an inorganic core with an attached polymer shell. Hybrid nanoscale systems provide extensive opportunities for the development of new materials with physical and chemical characteristics unattainable with their single-component counterparts. Among organic materials used in the design of hybrid nanomaterials, conjugated polymers (CPs) are particularly well suited for tuning and modification of the materials' photophysical characteristics.[15,16] CPs are a class of polymers which possess an extensive π-electron delocalization along the polymer backbone and typically display large extinction coefficients for light absorption and, in many cases, show strong fluorescence. In the condensed state, they exhibit complex self-organization driven by entropy and a multitude of weak intermolecular interactions, which often leads to poorly defined mesoscale structure and morphology and complex and not well understood spectroscopic characteristics stemming from intermolecular electronic interactions and chain aggregation. Controlled or directed nano- or mesoscale organization of CPs thus remains a challenge and requires availability of synthetic methods capable of producing hierarchically organized polymer structures.

Recently, our group developed an efficient approach towards preparing structurally well-defined hybrid fluorescent nanoparticles containing SiO_2 cores attached to CP diblock copolymer shells using surface-initiated controlled chain-growth Kumada catalyst-transfer polymerization.[17] These stable, covalently linked and molecularly well-defined fluorescent systems demonstrated remarkable spectroscopic and photophysical characteristics associated with both the effect of nanoscale morphology and specific molecular organization of the polymer chains in the CP shell.[18] Most interesting was the effect of the order of CP chromophores on the intra-particle excitation energy transfer between the constituent polymer chromophores in block copolymer shells showing strong dependence on the "inward" vs. "outward" energy transfer in the nanoscale systems. These findings provide opportunities for fine-tuning of photophysical characteristics of hybrid core-shell nanoparticles, especially for the applications in optoelectronic devices, biomarkers and contrast agents, as well as chemo- and biosensors.

Wu and Bielawski have reported a one-pot controlled chain-growth preparation of P3HT-*b*-poly(alkoxyallene) block copolymers[19-21] using Ni(dppp)Cl_2 as the pre-catalyst which is compatible with the surface initiated controlled chain-growth polymerization we previously developed. The final mesoscopic structure and organization of conjugated block copolymers containing polyallenes have been reported to be highly sensitive to solvent polarity, pH, and reaction temperature during the self-assembly process[22]. Because CP electronic properties are majorly affected by intra- and inter-chain interactions, incorporating polyallenes into CP block-copolymers has the potential to alter the molecular organization and nanoscale morphology of the CP blocks leading to chemically sensitive photoactive materials that display tunable photophysical

characteristics.[23-25] Well-defined poly(alkoxyallene)s are usually prepared through living coordination polymerization on the reactive cumulative double bonds of alkoxyallene monomers with Ni(II) complexes as initiators/catalysts.[26-28]

In this chapter, we will discuss our research on the nanoscale structural characteristics and photophysical properties of hybrid systems based on a silica nanoparticle core and CP/polyallene block copolymer shells. The composition of the polymer shells were chosen in such a way that the two inner blocks were fluorescent CPs poly(*p*-phenylene) (PPP) and poly(3-hexylthiophene) (P3HT), which would be responsible for the observed photophysical properties of the nanoparticles (Figure 4.1), whereas the outer block poly(tetradecyloxyallene) (PTA) provided response to the environment, e.g. solvent. Placing nanoparticles in the environments with different ability to interact with the outer PTA block was expected to result in physical contraction or expansion of the PTA shell, and these solvent-dependent structural changes could be directly monitored by isotopic labeling of the individual polymer layers and quantitative analysis using small-angle neutron scattering (SANS) experiments.

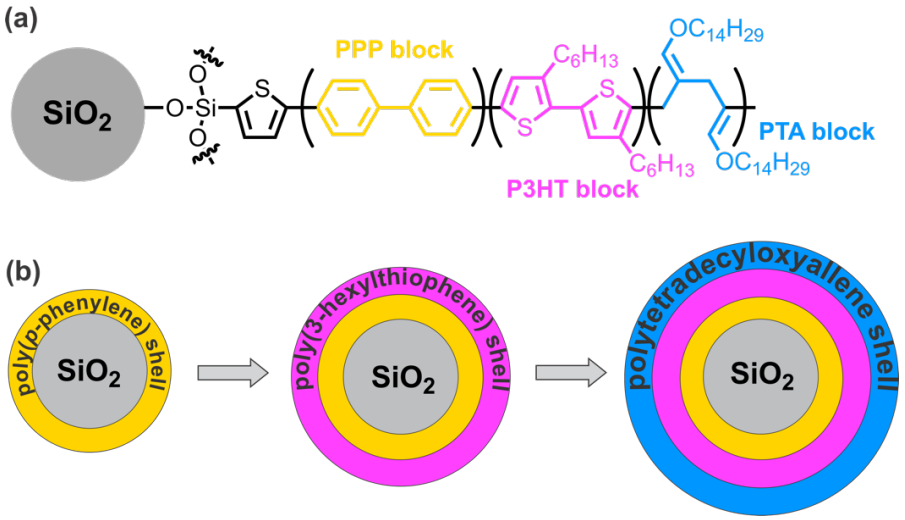

Figure 4.1. (a) Chemical structure of the triblock copolymer shell covalently attached to the SiO_2 core in CP/polyallene hybrid nanoparticles. (b) Schematic representation of the hybrid SiO_2 core – CP/polyallene shell nanoparticles.

Overall, the results of the studies described in this chapter would enable better understanding of the coupled environmental/structural/photophysical phenomena in these novel nanoscale systems. This investigation could also enable deeper fundamental understanding of energy transfer mechanisms in the nanoscale hybrid conjugated polymer nanoparticle systems and can bring about advanced practical applications of these materials in optoelectronic and sensing areas.

4.2. Synthesis and Characterization

Monodispersed SiO_2 nanoparticles were prepared using the Stöber process which is the ammonia-catalyzed hydrolysis of tetraethyl orthosilicate, and subsequent polycondensation into porous network of polysilicate in controlled conditions. The Stöber[29] process is a widely used method but can lead to relatively polydisperse particles using traditional procedures. To overcome this drawback, a reverse microemulsion method developed by Bogush *et al*[30] was used to obtain the more uniformly sized SiO_2 nanoparticles. Maintaining the reaction in basic conditions (pH around 9) minimizes undesirable pathways during SiO_2 particles formation and provides uniform size distribution. We used this modified procedure to obtain SiO_2 nanoparticles with a diameter of 24.3 ± 1.2 nm as measured by transmission electron microscopy (Figure 4.2).

4.2.1 Synthesis of SiO_2@iodothiophene Precursor and Ni(II) Initiator

We utilized the surface-initiated Kumada catalysts-transfer polymerization procedures previously reported by our group to prepare core-shell SiO_2 polymer hybrid nanoparticles containing P3HT, PPP and PTA blocks.[31] First, triethoxysilyl-functionalized iodothiophene was covalently bonded to the SiO_2 surface through a typical immobilization procedure, followed by treatment with an excess of $Ni(dppp)_2$ to generate the surface

immobilized catalytic initiator. The reaction occurs via oxidative addition of $Ni(dppp)_2$ complex to iodothiophene precursor to give efficient conversion of Ni(0) into the active Ni(II) catalysts. This method produces highly active initiator species that have been reported to catalyze formation of defect-free polythiophenes, poly(*p*-phenylenes), and their block copolymers (Figure 4.3).

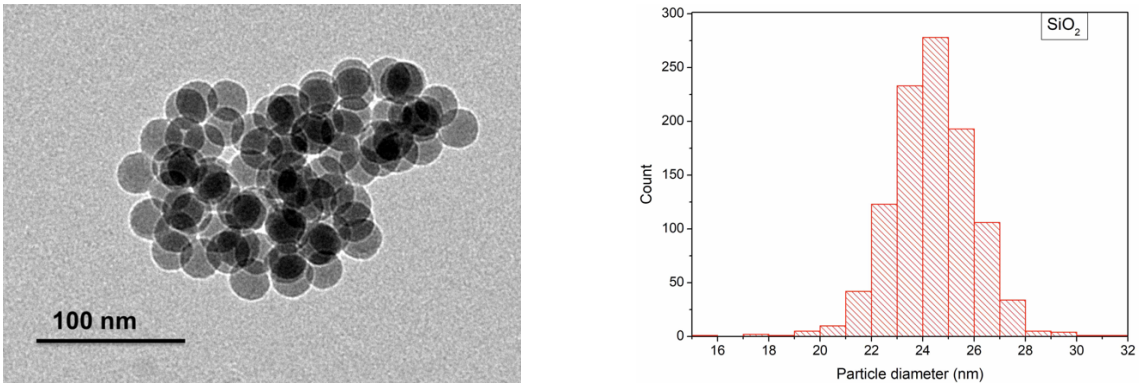

Figure 4.2 Transmission electron micrograph of SiO_2 particles prepared by the Stöber process (left). Statistical size distribution of SiO_2 particles measured by TEM shows an average particle size of 24.3 ± 1.2 nm (right).

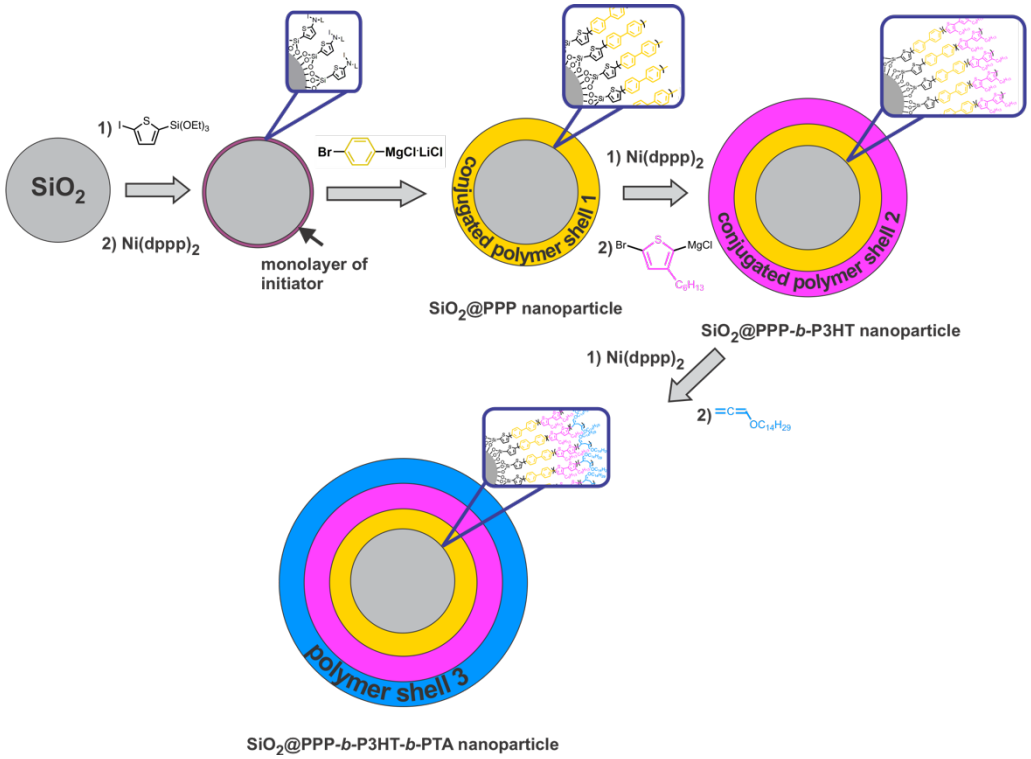

Figure 4.3. Synthesis of homopolymer, diblock copolymer and triblock copolymer shells grafted on silica particles.

4.2.2 XPS Analysis

To determine the conversion efficiency of the surface immobilized iodothiophene precursor to the Ni(II) external initiator, we used high-resolution X-ray photoelectron spectroscopy (XPS). High energy X-ray irradiation that is used in XPS excites electrons from the core of atomic elements existing on the surface of the sample, penetrating only as deep as 5 to 10 nm. The ionization energy of inner electrons from the atomic nucleus is highly sensitive to the valence electron configuration and the effects of chemical bonding on the electronic energy levels.[17]

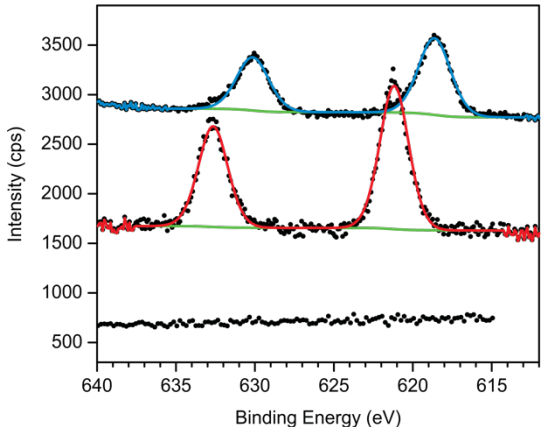

Figure 4.4. Iodine 3*d* region of high-resolution X-ray photoelectron spectroscopy (XPS) data for bare SiO_2 nanoparticles (black trace), SiO_2 nanoparticles surface-functionalized with the iodothiophene precursor (red trace), and surface immobilized Ni(II)iodide external initiator (blue trace). Shirley background (green line) was applied to the top and middle spectra.

The iodothiophene surfaced-modified SiO_2 nanoparticle precursors displayed cleanly resolved signals at 622 and 633 eV corresponding to the Iodine $3d_{5/2}$ and Iodine $3d_{3/2}$ peaks (Figure 4.4, red trace), and these were chosen for analysis. Upon reaction of the iodothiophene-modified nanoparticles with $Ni(dppp)_2$, the XPS signals shifted to a lower binding energy at 618 and 630 eV corresponding to iodide anion in the surface-immobilized Ni(II) initiator (Figure 4.4, blue trace). No observable Iodine 3*d* signals arose from bare precursor which was measured as control. Therefore, the reaction of the

surface-functionalized nanoparticles with $Ni(dppp)_2$ resulted in near-quantitative conversion.

4.2.3 The Synthesis of Hybrid SiO_2 Block Copolymer Nanoparticles

The efficient reaction conversion of surface immobilized aryl iodide to the active Ni(II) catalytic initiator provided an excellent platform for surface initiated living chain-growth polymerization studies. In our previous report, we observed a clear distinction of preparing polythiophenes (PT) as the first block versus using poly-*p*-phenylenes (PPP) as the first polymer block in surface-attached conjugated diblock copolymer nanostructures. The sequence of installing surface bound PT and PPP conjugated block copolymer nanostructures critically affect the formation of nanoscale interfaces that can result in excitation energy transfer (and resulting photophysical properties) being affected by an interfacial exciplex.[18] Installing PPP as the first polymer block from the surface was found to result in a more intense emission, and in this study we used PPP as the first polymer layer. The first conjugated polymer layer was formed upon exposure of surface initiated SiO_2 nanoparticles to a solution of 4-bromophenylmagnesium chloride and lithium chloride (~50 equivalents) to generate a thin film of PPP on top of the SiO_2 core. A deuterated PPP ((*d*)PPP) film on SiO_2 was also synthesized under the same conditions for subsequent studies using small angle neutron scattering (SANS) experiments. After the polymerization, the resulting SiO_2@PPP (or SiO_2@(*d*)PPP) particles were then washed with copious amounts of toluene and THF to remove excess starting materials and free oligomers. The bromo-terminated chain ends of (*d/h*)PPP could then be reacted with additional amount of $Ni(dppp)_2$ to regenerate the surface bound Ni(II) macroinitiators. Formation of each successive layer was done following the same procedure. After

forming the (*d/h*)PPP layer and subsequent regeneration of the catalytic initiator using $Ni(dppp)_2$, a solution of Grignard reagent generated from the reaction of isopropylmagnesium chloride and 2,5-dibromo-3-hexylthiophene was used to form the P3HT block copolymer shell, followed by another solvent washing and catalyst regeneration with $Ni(dppp)_2$. Lastly, adding tetradecyloxyallene monomer resulted in the formation of the final triblock copolymer inorganic/organic hybrid nanoparticles (Figure 4.3). Regenerating the active catalytic chain ends using $Ni(dppp)_2$ increased catalytic initiator surface density versus the one-pot living polymerization because unreactive chain ends or chain-transfer events could leave halogen terminated polymers which would be catalytically unreactive.[17] Condensed forms of conjugated polymer nanomaterials possess an enormous amount of chemical and physical complexity at the length scales ranging from close molecular interactions (energy transfer via Dexter and Förster mechanisms as well as formation of excimer and exciplex states) to the hierarchical packing of polymer nanosystems into macroscopic objects. Because poly-*p*-phenylenes and polythiophenes are two of the most common classes of conjugated polymers that are utilized in variety of applications for electronic and optoelectronic devices, their physical and photophysical properties are well-documented and the abundance of knowledge aids our analysis of the structural and electronic characteristics obtained in our experimental data. Thus, these two polymers were selected to investigate triblock hybrid nanoparticles with CP/polyallene outer shells.

4.2.4 TGA Analysis

To quantify the mass and chain length/degree of polymerization of the constituent blocks of the CP shell, thermogravimetric analysis (TGA) of the bare SiO_2 nanoparticles

containing the iodothiophene surfaced immobilized precursor, single block, diblock and triblock copolymer shells were carried out (Figure 4.5). The particles were subjected to high temperature (800 °C) in air which caused complete combustion of the organic components, leaving behind only the inorganic SiO_2 core. The bare SiO_2 particles were used as baseline reference, and all the hybrid nanoparticles samples were derived from the same starting materials (e.g. all the hybrid n-block particles contained SiO_2 cores generated from the same batch, and each chemically identical polymer layer was grown on from the same reaction batch as well). The TGA of bare silica particles displayed a 7% weight loss that can be attributed to surfactants which were used in the reverse microemulsion modification of Stöber process. The loss of surfactants in these conditions is typical based on other reports in literature and is assumed to occur in all the samples in the experiments containing SiO_2 nanoparticle cores. In addition to the weight loss due to surfactants, an extra 2% weight loss was observed for the nanoparticles with surface immobilized iodothiophene precursor which was consistent with our previous studies on hybrid conjugated nanoparticles.[18] By converting the % mass loss due to combustion to an absolute value which can be associated with the amount of iodothiophene originally bound to the SiO_2 particle surface, TGA experiments allowed for an accurate estimation of the surface grafting density of iodothiophene precursor which was calculated to be 0.5 molecules nm^{-2}. This surface density was also consistent with the value previously reported by Locklin *et al.* for silyl-functionalized aromatic precursors.[32]

TGA analysis revealed the % mass loss of the PPP layer to be 8.1% for the SiO_2@PPP nanoparticles. Using the molecular weight of a phenylene repeating unit, the % mass loss could be converted into moles of phenylene repeating units, and this number

of moles divided by the surface grafting density of the iodothiophene precursor yielded an experimental measurement of the number-average molecular weight M_n of PPP bound to the SiO_2 surface as 1056 Da, corresponding approximately to an average degree of polymerization of 14. Further measurement of the weight loss associated with the P3HT and PTA blocks on SiO_2@PPP-P3HT-PTA particles could also indicate the degree of polymerizations to be 5 and 4 for P3HT and PTA, respectively. A similar analysis of SiO_2@(*d*)PPP nanoparticles estimated a number-average molecular weight of polymer chains M_n of 780 Da, which resulted in approximately 10 (*d*)PPP repeating units per chain. P3HT and PTA layers on SiO_2@(*d*)PPP-P3HT-PTA particles showed 7 and 3 repeating units for P3HT and PTA, respectively.

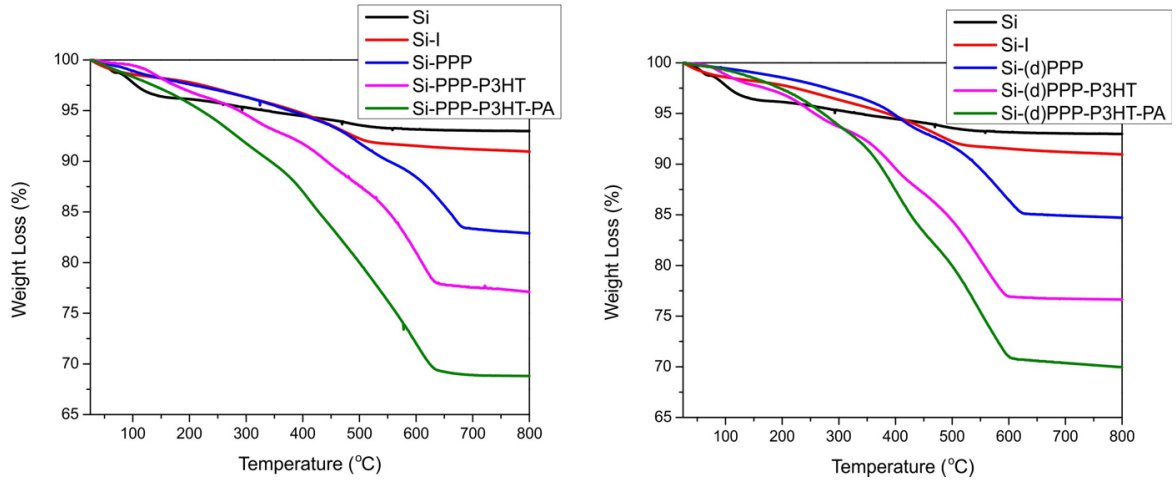

Figure 4.5. Thermogravimetric analysis (TGA) studies of SiO_2 hybrid nanoparticles (in air) and their precursors, the mass loss is attributed to combustion of organic components.

Although electron microscopy images were obtained for SiO_2@triblock copolymer hybrid nanoparticles (Figure 4.6), the aggregation typical of dried drop casted nanoparticles, as well as relatively small thickness of the CP shells made the polymer layer thickness measurements impossible by TEM. Thus, small angle neutron scattering (SANS) was used to analyze the polymer layer thicknesses in solution.

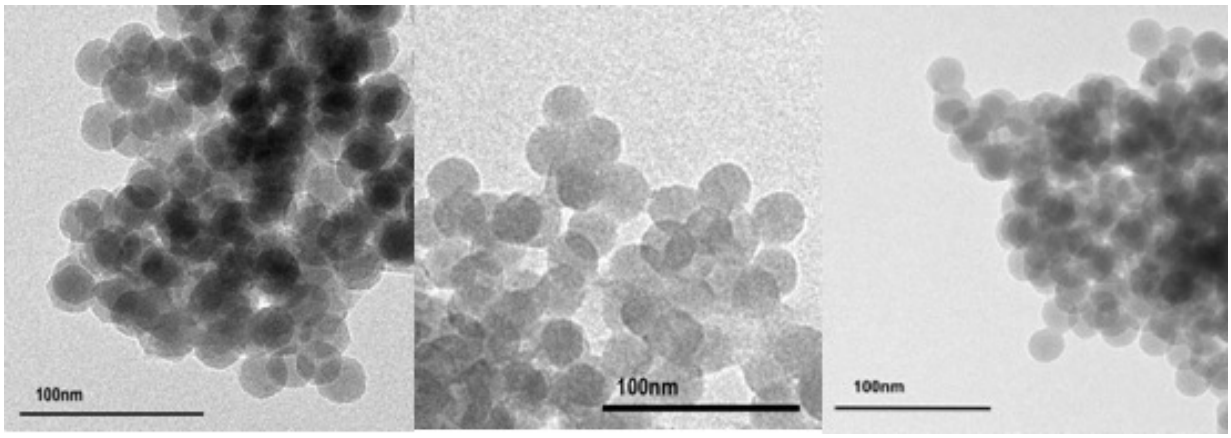

Figure 4.6. TEM images of SiO_2@PPP (left), SiO_2@PPP-P3HT (middle), and SiO_2@PPP-P3HT-PTA (right) hybrid nanoparticles.

4.3. Small Angle Neutron Scattering (SANS) Studies

Neutron scattering is an ideal tool to study the dynamic nature of chemically responsive SiO_2 hybrid nanoparticle structures in solution. Because of the sensitivity of neutron scattering length density (SLD) to both soft matter elemental composition and structural order at the nanometer length scale, measurement of the polymer shell SLD allows for precise measurement of the thickness and density of polymer layers on SiO_2 hybrid nanoparticles and also measurement of changes in molecular packing of the polymer shells in response to changing chemical environments such as solvent polarity. Additionally, by varying %(*d/h*) ratio of the solvent (contrast matching experiment), an accurate measurement of the SiO_2 particle density was obtained through measuring SLD of bare SiO_2. In contrast matching experiments using MeOD/MeOH as the dispersing solvent, we observed the bare SiO_2 particle density of 2.37 g/cm^3 which was consistent with similar commercial SiO_2 nanoparticles produced by the Stöber process. The particle size of the bare SiO_2 core was also measured to be 24.3 nm. The experimentally measured size and density of the SiO_2 cores in addition to degree of polymerization data indirectly obtained by TGA was implemented in physical modeling to quantify the sizes

and effect of solvent polarity on density of each successive polymer building block that was added on. A series of experiments containing single block, diblock, and triblock SiO_2 hybrid nanoparticles were investigated in 1,2-dichlorobenzene-d_4 (1,2-DCB-d_4) which is a "good" solvent for P3HT and PTA, and also in MeOD which is a "bad" solvent for P3HT. The layer thickness and SLD were obtained simultaneously by fitting of the neutron scattering data to a core-shell-shell sphere model in SASView along with inputs obtained from the experimental data (Figure 4.7). In both types of hybrid nanoparticles containing either PPP or (*d*)PPP, the size of the particles in 1,2-DCB-d_4 increased reasonably as P3HT and PTA layers were added with a concomitant decrease in SLD that is appropriate when adding on hydrogen containing polymers onto the nanoparticles (Table 4.1 entry 1-6). The total thickness of the triblock layers was measured to be 1.75 nm for SiO_2@PPP-P3HT-PTA and 1.82 nm for SiO_2-(*d*)PPP-P3HT-PTA which was consistent with observations by TEM.

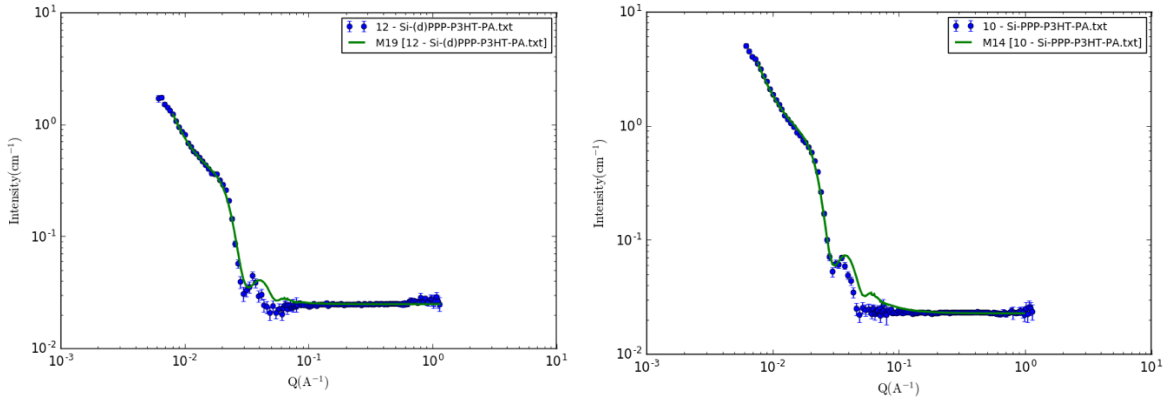

Figure 4.7. SANS data for SiO_2@ triblock copolymer hybrid nanoparticles containing (*d/h*)PPP, P3HT, and PTA blocks.

When changing the solvent from 1,2-DCB-d_4 to MeOD for the SiO_2@PPP-P3HT diblock copolymer system (Table 4.1 entry 2, Table 4.2 entry 7), the SLD increased from 1.81 $Å^{-2}$ in 1,2-DCB-d_4 to 1.94 $Å^{-2}$ in MeOD, corresponding to a physical density of 1.26

g/cm^3 and 1.35g/cm^3, respectively (a 7% increase in density). For SiO_2@(*d*)PPP-P3HT, the change in density was much less significant. A change of SLD of 3.01 Å^{-2} in 1,2-DCB-d_4 (1.21g/cm^3) to 3.02 Å^{-2} (1.21g/cm^3) corresponded to only a 0.4% increase in physical density. Notably for the SiO_2@triblock copolymer hybrid particles, there was a much more significant change in physical density when switching from 1,2-DCB-d_4 to MeOD. From TGA calculations, we estimated the triblock copolymer shell to consist of PPP_{13}-$P3HT_5$-PTA_4 and a change of SLD from 1.53 Å^{-2} (1.49g/cm^3) to 1.94 Å^{-2} (1.88g/cm^3) of a polymer (Table 4.1 entry 3, Table 4.2 entry 8) with this chemical composition corresponds to a change in physical density of 26.2% showing a significant increase in the packing density of the polymer chains, and a clear response to changing solvent polarity when switching from 1,2-DCB-d_4 to MeOD. For SiO_2@(*d*)PPP-P3HT-PTA with the polymer composition (*d*)PPP_{10}-$P3HT_7$-PTA_3 (Table 4.1 entry 6, Table 4.2 entry 10) the change in SLD of 3.02 (1.61g/cm^3) in 1,2-DCB-d_4 to 3.42 (1.82g/cm^3) in MeOD corresponded to the change in physical density of 14.9%. In both cases of using either (*d*)PPP or PPP, SANS experiments showed SiO_2@triblock copolymer hybrid nanoparticles containing PTA generated a significantly higher physical response when changing the solvent from 1,2-DCB-d_4 to MeOD.

Table 4.1. Layer thickness and SLD measurements for SiO_2@n-block copolymer hybrid nanoparticles containing (*d/h*)PPP, P3HT, and PTA as polymer layers in 1,2-DCB-d_4.

entry	first layer	second layer	third layer	layer thickness (Å)	shell SLD (10^{-6} Å^{-2})	Thickness polydispersity (Å)
1	PPP	none	none	7.05	2.04	0.58288
2	PPP	P3HT	none	13.02	1.81	0.051
3	PPP	P3HT	PTA	17.46	1.53	0.3026
4	(*d*)PPP	none	none	5.06	2.90	2.54
5	(*d*)PPP	P3HT	none	13.08	3.01	0.695
6	(*d*)PPP	P3HT	PTA	18.15	3.02	0.00548

Table 4.2. Layer thickness and SLD measurements for SiO_2@n-block copolymer hybrid nanoparticles containing (*d/h*)PPP, P3HT, and PTA as polymer layers in MeOD.

entry	first layer	second layer	third layer	layer thickness (Å)	shell SLD (10^{-6} Å^{-2})	thickness polydispersity (Å)
7	PPP	P3HT	none	10.02	1.91	0.345
8	PPP	P3HT	PTA	7.25	1.94	0.25152
9	(*d*)PPP	P3HT	none	10.46	3.02	1.23
10	(*d*)PPP	P3HT	PTA	7.70	3.42	1.2742

4.4. Spectroscopic Properties of Hybrid SiO_2@CP Nanoparticles

Particles functionalized with mono-, di-, and triblock copolymer, SiO_2@PPP-P3HT-PTA, were suspended in THF for photophysical studies. THF is a good solvent for P3HT and PTA, and thus, overall solvent-polymer interactions were good to stabilize the extended chain conformation of the polymer. The absorption spectra of SiO_2@n-block copolymer hybrid nanoparticles showed broad absorption with fine vibronic bands with maxima at around 380 nm with a shoulder peak at 420 nm which was attributed to the PPP block. Upon incorporating P3HT block, a relatively weak yet broad absorption band was observed between 450nm and 650nm. Broad and featureless P3HT absorption spectra are generally associated with highly disordered electronic states, which can result from spatial confinement and poorly organized chains. Upon addition of the PTA block to the CP shell, a slight but significant decrease in the red-shifted emission of P3HT chromophore was accompanied by an increase in blue emission band of the PPP chromophore. Generally, hypsochromic shifts in UV-Vis absorption spectra are indicative of shorter conjugation path length, which may occur due to twisting of the conjugated polymer backbone, bending, and other types of spatial confinement and defects which reduce the planarity of the □-conjugated backbone. (Figure 4.8). This would indicate that the PTA block was slightly less solubilized or nearly equally solubilized as the P3HT block.

Single step energy transfer between conjugated polymers can take place via intermolecular (through-space or “Förster” energy transfer) or intramolecular energy transfer (occurring by both through-space and through-bond or “Dexter” energy transfer mechanisms) processes from an excited donor molecule to an acceptor molecule. The emission spectra of SiO_2@triblock copolymer hybrid nanoparticles clearly showed efficient energy transfer from poly(*p*-phenylene) chromophore to P3HT chromophore – the process which is thermodynamically favorable. The efficiency of the through-space (Förster-type) process is proportional to the Coulombic interactions between transition dipoles, and the energy transfer rate (k_{ET}) increases with an efficient spectral overlap of the donor emission with acceptor absorption. Even though P3HT in the hybrid systems had a relatively weak absorption, its absorption region around 450 – 650 directly overlapped with the emission of PPP. Because of the favorable overlap integral between PPP and P3HT and their inherent thermodynamics, efficient energy transfer was expected to be spontaneous at a close packing range. The rate of Förster energy transfer is inversely proportional to the distance between acceptors and donors where $k_{ET} \sim 1/R^6$. (R is distance, k_{ET} is the rate of energy transfer) (Equation 4.1).

$$k_{ET}(\text{Coulombic}) \rightarrow E^2 \sim \left(\frac{\mu_D \mu_A}{{R_{DA}}^3}\right)^2 = \frac{\mu_D^2 \mu_A^2}{{R_{DA}}^6} \qquad (4.1)$$

Assuming that P3HT and PTA polymer blocks were solubilized and extended out into solution in good solvents such as THF, the large difference between the solvability of unsubstituted PPP (PPP is generally insoluble at long chain lengths and is not expected to extend outward from the surface of SiO_2 nanoparticle) affords a mechanism for sensing conditions that dramatically affect the organization of the conjugated polymer blocks

packing on the SiO_2 surface (mainly spatially and orientation dependent energy transfer rates can be exploited).

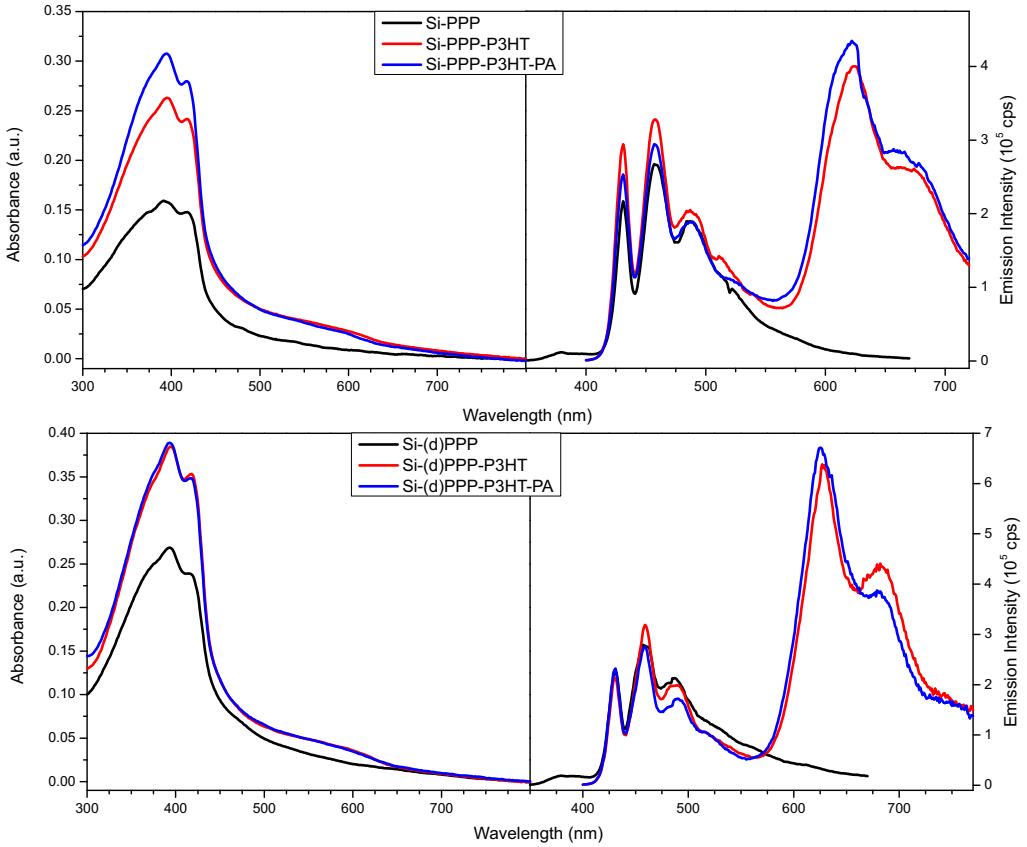

Figure 4.8. UV/vis absorption (left) and fluorescent emission (right) spectra of hybrid SiO_2@CP block copolymer nanoparticles.

Emission spectra of the diblock and triblock copolymer shells can be divided into two regions: one from 400-550 nm and the other from 550-750 nm. The first region (400-550 nm) originated from the contribution of the poly(*p*-phenylene) chromophore, and the other region (from 550-750 nm) could be attributed to P3HT chromophore (Figure 4.8). Comparison of the two sequences of SiO_2@block copolymer systems indicated that the emission band from P3HT in SiO_2@(*d*)PPP-P3HT-PTA was more intense than in the SiO_2@PPP-P3HT-PTA system, mainly due to a higher thiophene to phenylene ratio of in the SiO_2@(*d*)PPP-P3HT-PTA particles resulting in higher energy transfer efficiency.

4.5. Conclusion

We have developed a series of solvent responsive hybrid materials consisting of SiO_2 nanoparticles functionalized with fluorescent PPP and P3HT conjugated block copolymers and a solvent sensing PTA block prepared via surface-initiated controlled chain-growth Kumada catalyst-transfer polymerization. The hybrid nanoparticles were characterized using electron microscopy, small angle neutron scattering and thermal analysis which allowed to evidence controlled formation of the polymer shells. The environmentally (solvent) responsive behavior which demonstrated by the contraction of polymer layers in changing solvents was primarily investigated and confirmed by neutron scattering. This physical conformation changing phenomenon which could be attributed to the change of environment to which the PTA outer block was exposed to resulted in change in fluorescent characteristics of the hybrid conjugated polymer nanoparticles. This interesting novel phenomenon may provide an opportunity for the design interesting chemo- or biosensing applications based on this nanoscale hybrid systems.

4.6. References

(1) Jung, J. H.; Yoon, M. J.; Lim, J. W.; Lee, Y. H.; Lee, K. E.; Kim, D. H.; Oh, J. H. High-performance UV-vis-NIR phototransistors based on single-crystalline organic semiconductor gold hybrid nanomaterials. *Adv. Funct. Mater.* **2017**, *27*, 1604528.

(2) Chen, Y.; Shi, J. Chemistry of mesoporous organosilica in nanotechnology: molecularly organic-inorganic hybridization into frameworks. *Adv. Mater.* **2016**, *28*, 3235-3272.

(3) Zhang, Q.; Wang, C.-F.; Ling, L.-T.; Chen, S. Fluorescent nanomaterial-derived white light-emitting diodes: what's going on? *J. Mater. Chem. C* **2014**, *2*, 4358-4373.

(4) Su, X.; Zhang, J.; Sun, L.; Koo, T.-W.; Chan, S.; Sundararajan, N.; Yamakawa, M.; Berlin, A. A. Composite organic- inorganic nanoparticles (COINs) with chemically encoded optical signatures. *Nano Lett.* **2005**, *5*, 49-54.

(5) Wang, J. Nanomaterial-based electrochemical biosensors. *Analyst* **2005**, *130*, 421-426.

(6) Darbha, G. K.; Ray, A.; Ray, P. C. Gold nanoparticle-based miniaturized nanomaterial surface energy transfer probe for rapid and ultrasensitive detection of mercury in soil, water, and fish. *ACS Nano* **2007**, *1*, 208-214.

(7) Shi, J.; Zhu, Y.; Zhang, X.; Baeyens, W. R. G.; García-Campaña, A. M. Recent developments in nanomaterial optical sensors. *TrAC, Tends Anal. Chem.* **2004**, *23*, 351-360.

(8) Rowland, C. E.; Brown III, C. W.; Delehanty, J. B.; Medintz, I. L. Nanomaterial-based sensors for the detection of biological threat agents. *Mater. Today* **2016**, *19*, 464-477.

(9) Landi, B. J.; Castro, S. L.; Ruf, H. J.; Evans, C. M.; Bailey, S. G.; Raffaelle, R. P. CdSe quantum dot-single wall carbon nanotube complexes for polymeric solar cells. *Sol. Energy Mater. Sol. Cells* **2005**, *87*, 733-746.

(10) Hammer, N. I.; Emrick, T.; Barnes, M. D. Quantum dots coordinated with conjugated organic ligands: new nanomaterials with novel photophysics. *Nanoscale Res. Lett.* **2007**, *2*, 282-290.

(11) Jariwala, D.; Sangwan, V. K.; Lauhon, L. J.; Marks, T. J.; Hersam, M. C. Carbon nanomaterials for electronics, optoelectronics, photovoltaics, and sensing. *Chem. Soc. Rev.* **2013**, *42*, 2824-2860.

(12) Pramanik, M.; Patra, A. K.; Bhaumik, A. Self-assembled titanium phosphonate nanomaterial having a mesoscopic void space and its optoelectronic application. *Dalton Trans.* **2013**, *42*, 5140-5149.

(13) Ray, P. C.; Khan, S. A.; Singh, A. K.; Senapati, D.; Fan, Z. Nanomaterials for targeted detection and photothermal killing of bacteria. *Chem. Soc. Rev.* **2012**, *41*, 3193-3209.

(14) Bartelmess, J.; Quinn, S. J.; Giordani, S. Carbon nanomaterials: multi-functional agents for biomedical fluorescence and Raman imaging. *Chem. Soc. Rev.* **2015**, *44*, 4672-4698.

(15) Bajaj, A.; Miranda, O. R.; Kim, I.-B.; Phillips, R. L.; Jerry, D. J.; Bunz, U. H. F.; Rotello, V. M. Detection and differentiation of normal, cancerous, and metastatic cells using nanoparticle-polymer sensor array. *Proc. Natl. Acad. Sci. U. S. A.* **2009**, *106*, 10912-10916.

(16) Islam, M. A.; Purkait, T. K.; Mobarok, M. H.; Hoehlein, I. M. D.; Sinelnikov, R.; Iqbal, M.; Azulay, D.; Balberg, I.; Millo, O.; Rieger, B.; Veinot, J. G. C. Grafting poly(3-hexylthiophene) from silicon nanocrystal surfaces: synthesis and properties of a functional hybrid material with direct interfacial contact. *Angew. Chem. Int. Ed.* **2016**, *55*, 7393-7397.

(17) Youm, S. G.; Hwang, E.; Chavez, C. A.; Li, X.; Chatterjee, S.; Lusker, K. L.; Lu, L.; Strzalka, J.; Ankner, J. F.; Losovyj, Y.; Garno, J. C.; Nesterov, E. E. Polythiophene thin films by surface-initiated polymerization: mechanistic and structural studies. *Chem. Mater.* **2016**, *28*, 4787-4804.

(18) Chatterjee, S.; Karam, T. E.; Rosu, C.; Wang, C.-H.; Youm, S.-G.; Li, X.; Do, C.; Losovyj, Y.; Russo, P. S.; Haber, L. H.; Nesterov, E. E. Silica – conjugated polymer hybrid fluorescent nanoparticles: preparation by surface-initiated polymerization and spectroscopic studies. *J. Phys. Chem. C.* **2018**, *122*, 6963-6975.

(19) Wu, Z.-Q.; Ono, R. J.; Chen, Z.; Bielawski, C. W., Synthesis of Poly(3-alkylthiophene)- block-poly(arylisocyanide): Two Sequential, Mechanistically Distinct Polymerizations Using a Single Catalyst. *J. Am. Chem. Soc.* **2010**, *132*, 14000-14001.

(20) Wu, Z.-Q.; Radcliffe, J. D.; Ono, R. J.; Chen, Z.; Li, Z.; Bielawski, C. W., Synthesis of conjugated diblock copolymers: two mechanistically distinct, sequential living polymerizations using a single catalyst. *Polym. Chem.* **2012**, *3*, 874-881.

(21) Wu, Z.-Q.; Chen, Y.; Wang, Y.; He, X.-Y.; Ding, Y.-S.; Liu, N., One pot synthesis of poly(3-hexylthiophene)-block-poly(hexadecyloxylallene) by sequential monomer addition. *Chem. Commun.* **2013**, *49*, 8069-8071.

(22) Ding, A. P.; Lu, G.; Guo, H.; Huang, X., ATPR Synthesis of Polyallene-based Amphiphilic Triblock Copolymer. *Polym. Chem.* **2017**, *8*, 6997-7008.

(23) Yu, Z.-P.; Ma, C.-H.; Wang, Q.; Liu, N.; Yin, J.; Wu, Z.-Q., Polyallene-block-polythiophene-block-polyallene Copolymers: OnePot Synthesis, Helical Assembly, and Multiresponsiveness. *Macromolecules* **2016**, *49*, 1180−1190.

(24) Mochizuki, K.; Tomita, I., π-Allylnickel-catalyzed living coordination polymerization of allene having homochiral phenylcarbamoyloxy-substituted binaphthyl function. *Macromolecules* **2006**, *39*, 6336-6340.

(25) Zhang, X.; Shen, Z.; Feng, C.; Yang, D.; Li, Y.; Hu, J.; Lu, G.; Huang, X., PMHDO-g- PEG Double-Bond-Based Amphiphilic Graft Copolymer: Synthesis and Diverse Self- Assembled Nanostructures. *Macromolecules* **2009**, *42*, 4249-4256.

(26) Endo, T.; Tomita, I., Novel polymerization methods for allene derivatives. *Prog. Polym. Sci.* **1997**, *22*, 565-600.

(27) Taguchi, M.; Tomita, I.; Endo, T., Living coordination polymerization of allene derivatives bearing hydroxy groups by π-allylnickel catalyst. *Angew. Chem., Int. Ed.* **2000**, *39*, 3667-3669.

(28) Kino, T.; Taguchi, M.; Tazawa, A.; Tomita, I., Living Coordination Polymerization of Allene Derivatives in Protic Solvents: Remarkable Acceleration of Polymerization and Increase of 1,2-Polymerization Selectivity. *Macromolecules* **2006**, *39*, 7474-7478.

(29) Stoeber, W.; Fink, A.; Bohn, E., Controlled growth of monodisperse silica spheres in the micron size range. *J. Colloid Interface Sci.* **1968**, *26*, 62-9.

(30) Bogush, G. H.; Tracy, M. A.; Zukoski, C. F. I., Preparation of monodisperse silica particles: control of size and mass fraction. *J. Non-Cryst. Solids* **1988**, *104*, 95-106.

(31) Chavez, C. A.; Choi, J.; Nesterov, E. E., One-Step Simple Preparation of Catalytic Initiators for Catalyst-Transfer Kumada Polymerization: Synthesis of Defect-Free Polythiophenes. *Macromolecules* **2014**, *47*, 506-516.

(32) Sontag, S. K.; Sheppard, G. R.; Usselman, N. M.; Marshall, N.; Locklin, J. Surface-confined nickel mediated cross-coupling reactions: characterization of initiator environment in Kumada catalyst-transfer polycondensation. *Langmuir* **2011**, *27*, 12033−12041.

CHAPTER 5. EXPERIMENTAL SECTION

5.1 General Procedures

All the reactions were performed under an atmosphere of dry nitrogen (unless mentioned otherwise). Column chromatography was performed on silica gel (Sorbent Technologies, 60 Å, 40-63 μm) slurry packed into glass columns. Tetrahydrofuran (THF), ether, toluene, and hexane were dried by passing through activated alumina, and *N,N*-dimethylformamide (DMF) was dried by passing through molecular sieves, using a PS-400 Solvent Purification System from Innovative Technology, Inc. The water content of the solvents was periodically controlled by Karl Fischer titration (using a DL32 coulometric titrator from Mettler Toledo). High purity $Pd(PPh_3)_4$ was obtained from Stem while all other reagents and solvents were obtained from Aldrich and Alfa Aesar and used without further purification. Isopropylmagnesium chloride (2.0 M solution in THF) was purchased from Acros Organic, organometallic reagents were titrated with salicylaldehyde phenylhydrazone prior to use.[1] UV/vis absorption spectra were recorded on a Varian Cary 50 UV-Vis spectrometer. Fluorescence studies were carried out using a PTI QuantaMaster4/2006SE spectrofluorimeter. ^{1}H NMR spectra were recorded at 300 MHz, 400 MHz, and 500 MHz and are reported in ppm downfield from tetramethylsilane. High-resolution mass spectra (HRMS) was obtained at the Louisiana State University Mass Spectrometry Facility using an Agilent 6210 instrument. GPC analysis of polymers was performed with an Agilent 1100 chromatograph equipped with two PLgel 5 μm MIXED-C and one PLgel 5 μm 1000 Å columns connected in series, using THF as a mobile phase, and calibrated against polystyrene standards. Dialysis purification was carried out using Spectrum Laboratories, Inc. Spectra/Por® dialysis tubing with MWCO 8kDa. DFT and *ab*

initio computations were carried out using *Gaussian 16* computational package running on a Windows-based computer.[2]

5.2 Small-angle neutron scattering (SANS)

Experiments were carried out at the extended *Q*- range small-angle neutron scattering diffractometer (EQ-SANS) beamline (BL-6) at the Spallation Neutron Source (SNS) located at Oak Ridge National Laboratory (ORNL). Sample-to-detector distances of 1.3, 4 and 8 m were used with minimum wavelengths, λ, of 4, 10, and 12 Å, respectively at 60 Hz operation frequency, covering a q range of 0.002 Å^{-1} < q < 1 Å^{-1} where $q = (4\pi/\lambda)\sin(\theta/2)$ is the magnitude of the scattering vector, and θ is the scattering angle.[3,4] The measured scattering intensity was corrected according to standard procedures with *Mantid Plot*.[5] Reduced scattering intensities were azimuthally averaged into $I(q)$ vs q and placed on an absolute scale using a calibrated standard porous silica, which is known to have a scattering intensity 450 cm^{-1} at very small q. Samples with concentration of 10 mg ml^{-1} in deuterated 1,2-dichlorobenzene were stirred overnight before experiments. Titanium sample cells with quartz windows and a 1 mm path length were used.

5.3 X-ray Photoelectron Spectroscopy (XPS)

XPS samples were prepared by drop-casting colloidal solutions of the nanoparticles in toluene on Al foil substrate with subsequent vacuum drying. The XPS experiments were carried out using PHI *VersaProbe II* instrument equipped with a monochromatic Al K(alpha) source. Instrument base pressure was ca. 8×10^{-10} Torr. The X-ray power of 50 W at 15 kV was used for all experiments with 200 micron beam size at the X-ray incidence and take off angles of 45°. The instrument work function was calibrated to give a binding energy (BE) of 84.0 eV for Au 4$f_{7/2}$ line for metallic gold and the spectrometer dispersion

was adjusted to give a BE's of 284.8 eV, 932.7 eV and of 368.3 eV for the C 1*s* line of adventitious (aliphatic) carbon presented on the non-sputtered samples, Cu $2p_{3/2}$ and Ag $3d_{5/2}$ photoemission lines, respectively. dual charge neutralization system was used on all samples. The high resolution I 3*d* and Ni 2*p* spectra were taken with a minimum of 10-60 s scans using 0.1 eV steps and 23.5 eV pass energy. All XPS spectra were recorded using PHI software *SmartSoft -XPS* v2.0 and processed using *MultiPack* v9.0 PHI and/or *CasaXPS* v.2.3.15. Peaks were fitted using GL line shapes a combination of Gaussians and Lorentzians. A given sample was examined at 5-6 different spots on the mounted specimen to assure that consistent, reproducible results were obtained.

5.4 Supporting Information Associated to Chapter 2

Photoirradiation Experiments

Rose Bengal modified polystyrene beads (10 mg) were added to a solution of compound **2-P1** or **2-M1** in DMSO in a 1 cm path rectangular quartz cuvette. The mixture was stirred under flow of O_2 (50 ml/min) and irradiated for specified time periods using a 500 W tungsten-halogen lamp placed at a distance of 0.3 m from the sample.

5.5 Supporting Information Associated to Chapter 4

Table 5.1. Fitting parameters for I 3*d* high-resolution XPS spectra in Figure 4.4.

Trace/ Sample	Transitions	Position, eV	Position separation, eV	FWHM, eV	% Gauss	% Area	Chi Squared
Blue trace	I 3*d*5/2	618.63	0.0	2.45	100	57.5	2.32
	I 3*d*3/2	630.26	11.62	2.54	100	42.5	
Red trace	I 3*d*5/2	621.16	0.00	2.2	100	57.0	2.69
	I 3*d*3/2	632.74	11.57	2.2	93	43.0	

5.6 Synthesis Details

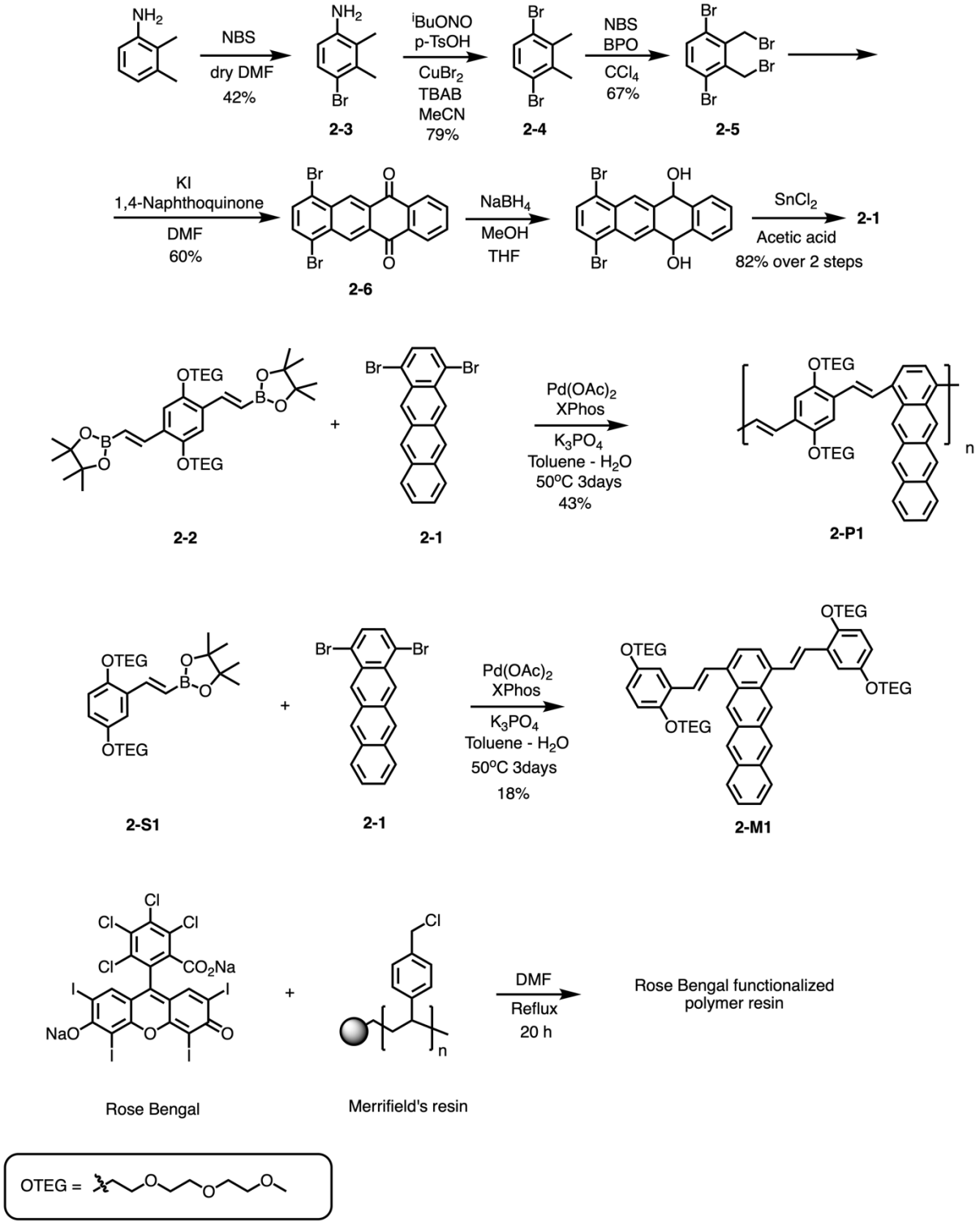

Scheme 5.1. Synthesis of 1,4-dibromotetracene **2-1**, polymer sensors **2-P1**, small-molecule sensor **2-M1**, and Rose Bengal functionalized polymer resin.

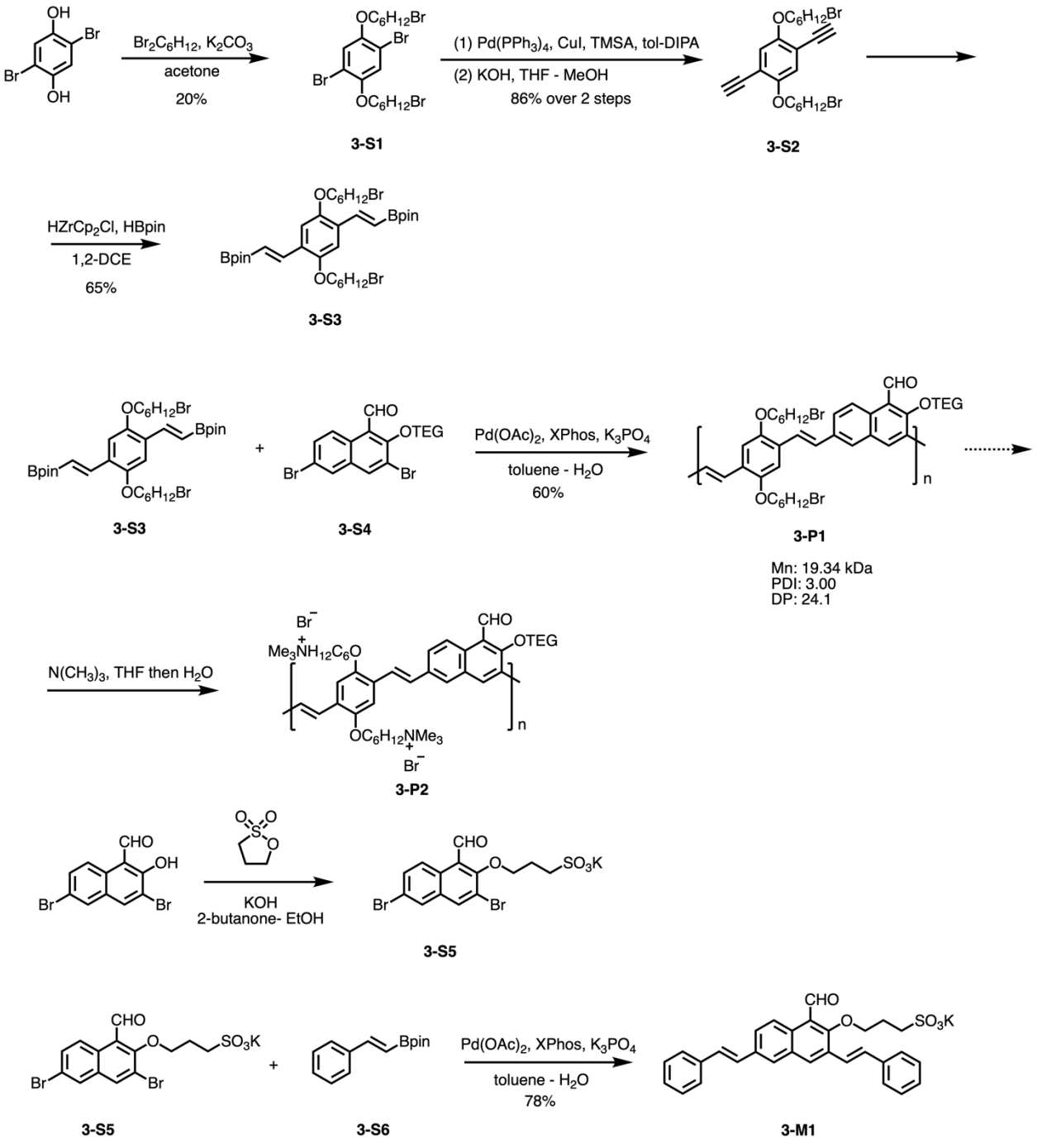

Scheme 5.2. Synthesis of polymer sensors **3-P2**, and small-molecule sensor **3-M1**

1,4-bis(2-(2-(2-Methoxyethoxy)ethoxy)ethoxy)-2,5-bis((4,4,5,5-tetramethyl)-1,3,2-dioxaborolan-1-yl)benzene (2-2) and **1,4-bis(2-(2-(2-Methoxyethoxy)ethoxy)ethoxy)-2-((4,4,5,5-tetramethyl)-1,3,2-dioxaborolan-1-yl)benzene (2-S1)** were prepared following previous literature procedures.[6]

4-Bromo-2,3-dimethylaniline (2-3). A solution of *N*-bromosuccinimide (44.06 g, 248 mmol) in 100 ml of dry DMF was added dropwise to a solution of 2,3-dimethylaniline (30 g, 248 mmol) in 50 ml of dry DMF, and the resulting mixture was stirred at room temperature for 24 h. The mixture was then poured into water and extracted with dichloromethane. The organic layer was dried over Na_2SO_4 and concentrated *in vacuo*. The crude mixture was purified by column chromatography on silica gel (eluent hexanes: CH_2Cl_2 1:1) to yield 33.94 g (42 %) of **2-3** as a viscous purple oil, R_f 0.2. ^{1}H NMR ($CDCl_3$, 400 MHz) δ 7.20 (d, J = 4.0 Hz, 1H), 6.44 (d, J = 6.4 Hz, 1H), 3.56 (br s, 2H), 2.38 (s, 3H), 2.13 (s, 3H).

1,4-Dibromo-2,3-dimethylbenzene (2-4). A solution of isobutyl nitrite (3.17 g, 30.8 mmol) and *p*-TsOH (5.84 g, 30.8 mmol) in 20 ml of dry acetonitrile was added dropwise to a solution of compound **2-3** (5.13 g, 25.6 mmol) in 50 ml of dry acetonitrile and the mixture was stirred at room temperature for 10 min. This was followed by addition of tetra-*n*-butylammonium bromide (TBAB, 16.5 g, 51.2 mmol) and catalytic amount of copper(II) bromide (57.2 mg, 0.26 mmol), and the reaction mixture was stirred at room temperature for 50 min. After completion of the reaction (as confirmed by TLC) the reaction mixture was concentrated *in vacuo*. The solid was washed with water and extracted with dichloromethane. The organic solution was dried over anhydrous Na_2SO_4 and concentrated *in vacuo*. The crude product was purified by column chromatography

on silica gel (eluent hexane) to yield 5.33 g (79 %) of compound **2-4** as a white solid, R_f 0.55, mp. 44 °C. ^{1}H NMR ($CDCl_3$, 400 MHz) δ 7.25 (s, 2H), 2.45 (s, 6H).

1,4-dibromo-2,3-bis(dibromomethyl)benzene (2-5).[7] A mixture of 1,4-dibromo-2,3-dimethylbenzene **2-4** (2.66 g, 10.1 mmol), NBS (4.31 g, 24.2 mmol) and benzoyl peroxide (244 mg, 1.01 mmol) was refluxed in CCl_4 overnight. After cooling to room temperature, water (100 ml) was added and the mixture was extracted with dichloromethane (3 × 75 ml). The organic layers were combined, dried over Na_2SO_4, and concentrated *in vacuo*. Recrystallization from EtOH yielded 2.87 g (67 %) of compound **2-5** as a pale yellow crystalline solid, mp. 108 °C. ^{1}H NMR ($CDCl_3$, 400 MHz) δ 7.43 (s, 2H), 4.82 (s, 4H).

1,4-Dibromo-6,11-tetracenequinone (2-6). A solution of compound **2-5** (2.0 g, 4.74 mmol), 1,4-naphthoquinone (749 mg, 4.74 mmol) and potassium iodide (3.15 g, 19.0 mmol) in 150 ml of dry DMF was stirred at 110 °C for 18 h. After cooling to room temperature, the resulting mixture was poured into 500 ml of 4:1 methanol: water mixture. The solid was collected on a Büchner funnel, washed successively with methanol, water and small amount of dichloromethane to yield 1.18 g (60%) of compound **2-6** as a yellow solid, mp. 321 °C. ^{1}H NMR ($CDCl_3$, 400 MHz) δ 9.27 (s, 2H), 8.44 - 8.42 (m, 2H), 7.88 - 7.86 (m, 2H), 7.83 (s, 2H).

1,4-Dibromotetracene (2-1). A mixture of compound **2-6** (963 mg, 2.32 mmol), sodium borohydride (192 mg, 5.10 mmol) and 60 ml of dry THF and 60 ml of dry MeOH was stirred at room temperature for 1 h. The resulting mixture was then poured into 300 ml of water and a white solid precipitated and was collected without further purification. A mixture of the obtained solid (890 mg), $SnCl_2$ (1.05 g, 4.66 mmol) and acetic acid (150

ml) was refluxed for 4 hours. After cooling down to room temperature, the mixture was poured into 400 ml of water to yield an orange solid. This orange solid was collected and further purified by column chromatography on silica gel (eluent hexane: CH_2Cl_2 5:1) to yield 667 mg (82 %) of compound **2-1** as an orange solid, R_f 0.6, mp. 212 °C. ^{1}H NMR ($CDCl_3$, 400 MHz) δ 9.09 (s, 2H), 8.80 (s, 2H), 8.07 - 8.04 (m, 2H), 7.57 (s, 2H), 7.49-7.46 (m, 2H). HRMS *m/e* 383.9149 M^+ (calcd for $C_{18}H_{10}Br_2$ 383.9143).

Small-molecule sensor 2-M1. A mixture of compound **2-S1** (75.6 mg, 0.136 mmol), 1,4-dibromotetracene **2-1** (24.2 mg, 62 μmol), $Pd(OAc)_2$ (0.7 mg, 3.1 μmol), XPhos (2.95 mg, 6.2 μmol), K_3PO_4 (105 mg, 0.50 mmol) in 10 ml of toluene and 2 ml of ultrapure water was stirred in a sealed air-free flask at 50 °C for 72 h. After allowing to cool down to room temperature, the reaction mixture was filtered through a glass filter, and the filtrate was concentrated *in vacuo*. The crude product was purified by column chromatography on silica gel (eluent ethyl acetate: MeOH 50:1) to afford 12 mg (18%) of **2-M1** as a red solid, R_f 0.2. ^{1}H NMR (CD_2Cl_2, 400 MHz) δ 9.12 (s, 2H), 8.77 (s, 2H), 8.17 (d, *J* = 16 Hz, 2H), 8.03 (m, 2H), 7.77 (s, 2H), 7.62 (d, *J* = 16 Hz, 2H), 7.42 (m, 4H), 6.97 (d, *J* = 8 Hz, 4H), 4.22 (m, 8H), 3.93-3.87 (m, 8H), 3.73-3.61 (m, 16H), 3.56-3.46 (m, 16H), 3.33 (d, *J* = 8 Hz, 12H). HRMS *m/e* 1079.5355 $[M–2+H]^+$ (calcd for $C_{62}H_{80}O_{16}$ 1079.5323).

Conjugated Polymer 2-P1. A mixture of monomer **2** (81.2 mg, 0.109 mmol), 1,4-dibromotetracene **2-1** (42.7 mg, 0.109 mmol), $Pd(OAc)_2$ (1.23 mg, 5.4 μmol), XPhos (5.20 mg, 10.9 μmol), K_3PO_4 (185 mg, 0.87 mmol) in 10 ml of toluene and 2 ml of ultrapure water was stirred in a sealed air-free flask at 50 °C for 72 h. After cooling down to room temperature, the reaction mixture was added dropwise to acetone (100 ml), and the precipitate was collected by centrifugation and dried *in vacuo* to yield 32 mg (43%) of

polymer **2-P1** as a dark red solid. GPC (THF vs. polystyrene standard): M_n 11.8 kDa, PDI 1.64. ^{1}H NMR (CD_2Cl_2, 400 MHz) δ 9.30-9.12 (broad m, 2H), 8.80-8.51 (broad m, 2H), 8.16-7.94 (broad m, 4H), 7.58-7.20 (broad m, 8H), 4.50-3.00 (broad m, 30H).

Rose Bengal functionalized polystyrene beads.[8] A mixture of 1.0 g (1.05 mmol) of Rose Bengal and 1 g of chloromethylated styrene-divinylbenzene copolymer beads (2.0-3.5 mmol/g Cl, 50-100 mesh) in 60 ml of dimethylformamide was refluxed for 20 h. After cooling down to room temperature, the polymer solid (now dark red) was filtered and washed successively with 150 ml portions of benzene, ethanol, ethanol-water (1:1), water, methanol-water (1:1), and methanol. Upon completing the washing, the final filtrate was colorless. The polymer beads were dried in a vacuum oven to a final weight of 1.1 g.

3,6-Dibromo-2-(2-(2-methoxyethoxy)ethoxy)ethoxy)-1-naphthaldehyde (3-S4) and (*E*)-4,4,5,5-tetramethyl-2-styryl-1,3,2-dioxaborolane (3-S6) were prepared following previous literature procedures.[6]

1,4-dibromo-2,5-bis(6-bromohexyloxy)benzene (3-S1). 11.4 g (46.65 mmol) of 1,6-dibromohexane in 50 mL of acetone was added dropwise into a mixture of 5 g (18.66 mmol) of 2,5-dibromohydroquinone, 11.6 g (83.99 mmol) of potassium carbonate in 110 mL of acetone under reflux. After heating for 24 h, the mixture was cooled down to rt and filtered. The resulting filtrate was concentrated *in vacuo* and purified by recrystallized from MeOH - $CHCl_3$ (10:1) to give 2 g (20%) of **3-S1** as a white solid. ^{1}H NMR($CDCl_3$, 400 MHz) δ 7.08 (s, 2H), 3.96 (t, J = 6.4 Hz, 4H), 3.43 (t, J = 6.8 Hz, 4H), 1.90 (quintet, J = 6.8, 7.0, 6.8, 7.0 Hz, 4H), 1.82 (quintet, J = 6.8, 7.0, 6.8, 7.0 Hz, 4H), 1.54-1.52 (m, 8H).

1,4-Bis(6-bromohexyloxy)-2,5-diethynylbenzene (3-S2). A mixture of 992 mg (3 mmol) of (trimethylsilyl)acetylene, 2.0 g (3.37 mmol) of **3-S1**, 117 mg (3 mol%) of

$Pd(PPh_3)_4$ and 19 mg (3 mol%) of CuI in 150 mL of toluene - *i*-Pr_2NH (7:3) solvent was stirred at 75 °C in a sealed air-free flask for 72 h. After cooling down to room temperature, the mixture was concentrated *in vacuo*, and the crude product was used without further purification. 297 mg (5.3 mmol) of potassium hydroxide in 20 mL of MeOH was added into a mixture of the crude product in 40 mL of THF. After stirred at room temperature for 1h. The mixture was washed with 100 mL of H_2O (3X) and extracted with 150 mL of ethyl acetate (3X). The combined organic fraction was washed with brine, dried over Na_2SO_4, and concentrated *in vacuo*. The crude product was purified by column chromatography on silica gel eluted with CH_2Cl_2: hexane (1:1) to afford 1.4 g (86%) of **3-S2** as a white solid, R_f 0.35 ^{1}H NMR($CDCl_3$, 400 MHz) δ 6.95 (s, 2H), 3.98 (t, *J* = 6.4 Hz, 4H), 3.42 (t, *J* = 6.8 Hz, 4H). 3.34 (s, 2H), 1.89 (quintet, *J* = 6.8, 7.0, 6.8, 7.0 Hz, 4H), 1.82 (quintet, *J* = 6.8, 7.0, 6.8, 7.0 Hz, 4H), 1.54-1.50 (m, 8H).

1,4-Bis(6-bromohexyloxy)-2,5-bis(4,4,5,5-tetramethyl-1,3,2-dioxaborolan-1-yl)benzene (3-S3). A mixture of 815 mg (1.68 mmol) of **3-S2**, 538 mg (4.21 mmol) of pinacolborane, and 38 mg (0.17 mmol) of $ZrCp_2HCl$ in 20 ml of 1,2-dichloroethane was stirred in a sealed Schlenk flask at 65 °C for 72 h. After cooling down to room temperature, the reaction mixture was poured into water, extracted with dichloromethane, washed with water, and dried over Na_2SO_4. Concentration in vacuo afforded crude product that was further purified by column chromatography on silica gel (eluent hexane:DCM 1:2) to afford 810 mg of **3-S3** as a yellow sticky liquid (65%). ^{1}H NMR($CDCl_3$, 400 MHz) δ 7.70 (d, *J* = 18.4 Hz, 2H), 7.05 (s, 2H), 6.12 (d, *J* = 18.4 Hz, 2H), 3.96 (t, *J* = 6.4 Hz, 4H), 3.44 (t, *J* = 6.8 Hz, 4H). 1.92 (quintet, *J* = 6.8, 7.0, 6.8, 7.0 Hz, 4H), 1.83 (quintet, *J* = 6.8, 7.0, 6.8, 7.0 Hz, 4H), 1.54-1.50 (m, 8H). 1.3 (s, 24H).

Potassium 3-(3,6-dibromo-1-formylnaphthalen-2-yloxy)propane-1-sulfonate (3-S5). A mixture of 26 mg (0.46 mmol) KOH in 1 mL of ethanol was added into a solution of 100 mg (0.3 mmol) of 9 in 3 mL of methyl ethyl ketone at 70 °C. A solution of 56 mg (0.46 mmol) 43 of 1,3-propanesultone in 1 mL of methyl ethyl ketone was added into the reaction mixture and stirred for overnight. After cooling down to rt, the reaction mixture was poured into acetone and white solid was precipitated. The white solid was collected after centrifuge and recrystallized from hot water to afford 77 mg (56%) of 10 as a white solid. ^{1}H NMR (*d6*-DMSO, 400 MHz): δ 10.61 (s, 1H), 8.96 (d, 1H), 8.70 (s, 1H), 8.29 (s, 1H), 7.85 (d, 1H), 4.23 (t, 2H), 2.65 (t, 2H), 2.17 (m, 2H).

Conjugated Polymer 3-P1. A solution of 178 mg (0.84 mmol) of K_3PO_4 in 1 ml of water was added into a solution of 77 mg (0.11 mmol) of **3-S3**, 50 mg (0.11 mmol) of **3-S4**, 0.5 mg (2.1 μmol) of $Pd(OAc)_2$ and 3 mg (5.3 μmol) of XPhos in 5 ml of toluene and 1 ml of H_2O, and the resulting solution was stirred at 65 ºC for 96 h. After cooling down to rt, the reaction mixture was purified by precipitation from acetone, the solid was then dissolved in $CHCl_3$ and precipitated in ether resulting in 50 mg of **3-P1** as a yellow sticky solid (60%), M_n 19.3 kDa, PDI 3.00 (GPC, vs. polystyrene). ^{1}H NMR(CD_2Cl_2, 400 MHz) δ 10.91 (s, 1H), 9.17 (s, 1H), 8.37 (s, 1H), 7.94-7.91 (m, 2H), 7.74-7.57 (m, 3H), 7.39-7.26 (m, 3H), 4.29-4.27 (m, 2H), 4.17-4.12 (m, 3H), 3.88-3.87 (m, 2H). 3.70-3.42 (m, 13H), 3.30 (s, 3H), 2.01-1.86 (m, 8H). 1.67-1.58 (m, 8H).

Conjugated Polymer 3-P2.[9] 3mL of condensed trimethylamine was added dropwise to a solution of **3-P1**(50mg) in 5ml of THF. The mixture was stirred in room temperature for 24 hrs. The precipitate was re-dissolved by addition of excess water and additional 2 ml trimethylamine. The resulting mixture was further stirred for 48 hrs at room

temperature. The reaction mixture was precipitated in acetone following by dialysis from nanopure water for 3 days (with an 8 kDa cutoff membrane) to yield 39 mg of **3-P2** (66%). ^{1}H NMR(DMSO, 300 MHz) δ 10.82 (s, 1H), 9.08 (br d, 1H), 8.58 (s, 1H), 8.14-8.00 (m, 3H), 7.71-7.31 (m, 5H), 4.27-4.10 (m, 6H), 3.84-3.25 (m, 13H), 3.05 (s, 18H), 1.90-1.43 (m, 8H). 1.23 (s, 8H).

Small-molecule sensor 3-M1. A solution of 70 mg (0.33 mmol) of K_3PO_4 in 2 mL of H_2O was added into a solution of 25 mg (0.06 mmol) of **3-S5**, 38 mg (0.17 mmol) of **3-S6**, 0.6 mg (2.8 μmol) of $Pd(OAc)_2$ and 3 mg (5.5 μmol) of XPhos in 5 ml of toluene and 1ml of H_2O, and the resulting solution was stirred in a sealed Airfree flask at 70 °C for 72 h. After allowing to cool down to room temperature, the reaction mixture was poured into acetone to form solid crude product. The solid was then vigorously washing with CH_2Cl_2 and THF to afford 22 mg (83%) of **3-M1** as a light greenish solid. ^{1}H NMR (*d6*-DMSO, 400 MHz) δ 10.72 (s, 1H), 9.04 (d, *J* = 8.0 Hz, 1H), 8.67 (s,1H), 8.12 (s, 1H), 8.15 (d, *J* = 12.0 Hz, 1H), 7.73-7.67 (m, 4H), 7.65 (d, *J* = 12.0 Hz, 1H), 7.46-7.40 (m, 6H), 7.36-7.31 (m, 3H), 4.18 (t, *J* = 8.0 Hz, 2H), 2.68 (t, *J* = 8.0 Hz, 2H), 2.17 (t, *J* = 8.0 Hz, 2H). HR-ESI-MS (m/z calc.: 497.1423; found: 497.1427).

Silica nanoparticles,[10] Triethoxy(5-iodothiophen-2-yl)silane,[11] Bis[1,3-bis(diphenylphosphino)propane]nickel(0),[12] and mono-, di-, and triblock copolymer silica nanoparticles[13] were prepared following previous literature procedures.

5.7 References

(1) Love, B. E.; Jones, E. G. The Use of Salicylaldehyde Phenylhydrazone as an Indicator for the Titration of Organometallic Reagents. *J. Org. Chem.* **1999**, *64*, 3755–3756.

(2) Gaussian 16, Revision A.03, Frisch, M. J.; Trucks, G. W.; Schlegel, H. B.; Scuseria, G. E.; Robb, M. A.; Cheeseman, J. R.; Scalmani, G.; Barone, V.; Petersson, G. A.; Nakatsuji, H.; Li, X.; Caricato, M.; Marenich, A. V.; Bloino, J.; Janesko, B. G.; Gomperts, R.; Mennucci, B.; Hratchian, H. P.; Ortiz, J. V.; Izmaylov, A. F.; Sonnenberg, J. L.; Williams-Young, D.; Ding, F.; Lipparini, F.; Egidi, F.; Goings, J.; Peng, B.; Petrone, A.; Henderson, T.; Ranasinghe, D.; Zakrzewski, V. G.; Gao, J.; Rega, N.; Zheng, G.; Liang, W.; Hada, M.; Ehara, M.; Toyota, K.; Fukuda, R.; Hasegawa, J.; Ishida, M.; Nakajima, T.; Honda, Y.; Kitao, O.; Nakai, H.; Vreven, T.; Throssell, K.; Montgomery, J. A., Jr.; Peralta, J. E.; Ogliaro, F.; Bearpark, M. J.; Heyd, J. J.; Brothers, E. N.; Kudin, K. N.; Staroverov, V. N.; Keith, T. A.; Kobayashi, R.; Normand, J.; Raghavachari, K.; Rendell, A. P.; Burant, J. C.; Iyengar, S. S.; Tomasi, J.; Cossi, M.; Millam, J. M.; Klene, M.; Adamo, C.; Cammi, R.; Ochterski, J. W.; Martin, R. L.; Morokuma, K.; Farkas, O.; Foresman, J. B.; Fox, D. J. Gaussian, Inc., Wallingford CT, 2016.

(3) Zhao, J. K.; Gao, C. Y.; Liu, D. The extended *Q*-range small-angle neutron scattering diffractometer at the SNS. *J. Appl. Cryst.* **2010**, *43*, 1068-1077.

(4) Wignall, G. D.; Bates, F. S. Absolute calibration of small-angle neutron scattering data. *J. Appl. Cryst.* **1987**, 20, 28-40.

(5) Arnold O.; Bilheux, J. C.; Borreguero, J. M.; Buts, A.: Campbell, S. I.; Chapon, L.; Doucet, M.; Draper, N.; Leal, R. F.; Gigg, M. A.; Lynch, V. E.; Markvardsen, A.; Mikkelson, D. J.; Mikkelson, R. L.; Miller, R.; Palmen, K.; Parker, P.; Passos, G.; Perring, T. G.; Peterson, P. F. *et al.* Mantid – Data analysis and visualization package for neutron scattering and μ SR experiments. *Nucl. Instrum. Methods Phys. Res., Sect. A* **2014**, *764*, 156-166.

(6) Chiang, C.-H.; Pangeni, D.; Nesterov, E. E. Higher Energy Gap Control of Fluorescence in Conjugated Polymers: *Turn-On* Amplifying Chemosensors For Hydrogen Sulfide. *Macromolecules* **2017**, *50*, 6961-6966

(7) Plunkett, K. N.; Godula, K.; Nuckolls, C.; Tremblay, N.; Whalley, A. C.; Xiao, S. Expeditious Synthesis of Contorted Hexabenzocoronenes *Org. Lett.,* **2009**, *11*, 2225-2228.

(8) Taylor, R. P.; Vatz, J. B. Polymer-based sensitizers for photooxidations. *J. Am. Chem. Soc.* **1973**, *95*, 5820-5822.

(9) Lee, B. H.; Jung, I. H.; Woo, H. Y.; Shim, H.-K.; Kim, G.; Lee, K. Multi-Charged Conjugated Polyelectrolytes as a Versatile Work Function Modifier for Organic Electronic Devices. *Adv. Funct. Mater.* **2014**, *24*, 1100-1108.

(10) Bogush, G. H.; Tracy, M. A.; Zukoski, C. F. I., Preparation of monodisperse silica particles: control of size and mass fraction. *J. Non-Cryst. Solids* **1988**, *104*, 95-106.

(11) Youm, S. G.; Hwang, E.; Chavez, C. A.; Li, X.; Chatterjee, S.; Lusker, K. L.; Lu, L.; Strzalka, J.; Ankner, J. F.; Losovyj, Y.; Garno, J. C.; Nesterov, E. E. Polythiophene thin films by surface-initiated polymerization: mechanistic and structural studies. *Chem. Mater.* **2016**, *28*, 4787-4804.

(12) Chavez, C. A.; Choi, J.; Nesterov, E. E., One-Step Simple Preparation of Catalytic Initiators for Catalyst-Transfer Kumada Polymerization: Synthesis of Defect-Free Polythiophenes. *Macromolecules* **2014**, *47*, 506-516.

(13) Chatterjee, S.; Karam, T. E.; Rosu, C.; Wang, C.-H.; Youm, S.-G.; Li, X.; Do, C.; Losovyj, Y.; Russo, P. S.; Haber, L. H.; Nesterov, E. E. Silica – conjugated polymer hybrid fluorescent nanoparticles: preparation by surface-initiated polymerization and spectroscopic studies. *J. Phys. Chem. C.* **2018**, *122*, 6963-6975.

APPENDIX A. PERMISSIONS

Title: Excitation energy migration assisted processes in conjugated polymers
Author: Emil J.W List,Günther Leising
Publication: Synthetic Metals
Publisher: Elsevier
Date: 18 March 2004

Logged in as:
Chun-Han Wang
Account #:
3001467058
LOGOUT

Order Completed

Thank you for your order.

This Agreement between Chun-Han Wang ("You") and Elsevier ("Elsevier") consists of your order details and the terms and conditions provided by Elsevier and Copyright Clearance Center.

License number	Reference confirmation email for license number
License date	Jun, 13 2019
Licensed Content Publisher	Elsevier
Licensed Content Publication	Synthetic Metals
Licensed Content Title	Excitation energy migration assisted processes in conjugated polymers
Licensed Content Author	Emil J.W List,Günther Leising
Licensed Content Date	18 March 2004
Licensed Content Volume	141
Licensed Content Issue	1-2
Licensed Content Pages	8
Type of Use	reuse in a thesis/dissertation
Portion	figures/tables/illustrations
Number of figures/tables/illustrations	1
Format	both print and electronic
Are you the author of this Elsevier article?	No
Will you be translating?	No
Original figure numbers	Figure 3
Title of your thesis/dissertation	CHEMOSENSORS BASED ON HIGHER ENERGY GAP CONTROL OF FLUORESCENCE IN CONJUGATED POLYMERS
Expected completion date	Aug 2019
Estimated size (number of pages)	100
Requestor Location	Mr. Chun-Han Wang 894 Regent Dr APT 5

	DEKALB, IL 60115 United States Attn: Mr. Chun-Han Wang
Publisher Tax ID	98-0397604
Billing Type	Invoice
Billing address	Mr. Chun-Han Wang 232 Choppin Hall BATON ROUGE, LA 70803 United States Attn: Mr. Chun-Han Wang
Total	0.00 USD

CLOSE WINDOW

THE AMERICAN ASSOCIATION FOR THE ADVANCEMENT OF SCIENCE LICENSE TERMS AND CONDITIONS

Jun 10, 2019

This Agreement between Mr. Chun-Han Wang ("You") and The American Association for the Advancement of Science ("The American Association for the Advancement of Science") consists of your license details and the terms and conditions provided by The American Association for the Advancement of Science and Copyright Clearance Center.

License Number	4605520124799
License date	Jun 10, 2019
Licensed Content Publisher	The American Association for the Advancement of Science
Licensed Content Publication	Science
Licensed Content Title	Coherent Intrachain Energy Migration in a Conjugated Polymer at Room Temperature
Licensed Content Author	Elisabetta Collini,Gregory D. Scholes
Licensed Content Date	Jan 16, 2009
Licensed Content Volume	323
Licensed Content Issue	5912
Volume number	323
Issue number	5912
Type of Use	Thesis / Dissertation
Requestor type	Scientist/individual at a research institution
Format	Print and electronic
Portion	Figure
Number of figures/tables	1
Order reference number	
Title of your thesis / dissertation	CHEMOSENSORS BASED ON HIGHER ENERGY GAP CONTROL OF FLUORESCENCE IN CONJUGATED POLYMERS
Expected completion date	Aug 2019
Estimated size(pages)	100
Requestor Location	Mr. Chun-Han Wang 894 Regent Dr APT 5 DEKALB, IL 60115 United States Attn: Mr. Chun-Han Wang
Total	**0.00 USD**

Terms and Conditions

American Association for the Advancement of Science TERMS AND CONDITIONS

Regarding your request, we are pleased to grant you non-exclusive, non-transferable permission, to republish the AAAS material

Title: Conjugation Enhancement of Intramolecular Exciton Migration in Poly(p-phenylene ethynylene)s

Author: Evgueni E. Nesterov, Zhengguo Zhu, Timothy M. Swager

Publication: Journal of the American Chemical Society

Publisher: American Chemical Society

Date: Jul 1, 2005

Logged in as:
Chun-Han Wang
LOGOUT

PERMISSION/LICENSE IS GRANTED FOR YOUR ORDER AT NO CHARGE

This type of permission/license, instead of the standard Terms & Conditions, is sent to you because no fee is being charged for your order. Please note the following:

- Permission is granted for your request in both print and electronic formats, and translations.
- If figures and/or tables were requested, they may be adapted or used in part.
- Please print this page for your records and send a copy of it to your publisher/graduate school.
- Appropriate credit for the requested material should be given as follows: "Reprinted (adapted) with permission from (COMPLETE REFERENCE CITATION). Copyright (YEAR) American Chemical Society." Insert appropriate information in place of the capitalized words.
- One-time permission is granted only for the use specified in your request. No additional uses are granted (such as derivative works or other editions). For any other uses, please submit a new request.

If credit is given to another source for the material you requested, permission must be obtained from that source.

BACK CLOSE WINDOW

Title: Fluorescent Chemosensors Based on Energy Migration in Conjugated Polymers: The Molecular Wire Approach to Increased Sensitivity

Author: Qin Zhou, Timothy M. Swager

Publication: Journal of the American Chemical Society

Publisher: American Chemical Society

Date: Dec 1, 1995

Logged in as:
Chun-Han Wang
LOGOUT

PERMISSION/LICENSE IS GRANTED FOR YOUR ORDER AT NO CHARGE

This type of permission/license, instead of the standard Terms & Conditions, is sent to you because no fee is being charged for your order. Please note the following:

- Permission is granted for your request in both print and electronic formats, and translations.
- If figures and/or tables were requested, they may be adapted or used in part.
- Please print this page for your records and send a copy of it to your publisher/graduate school.
- Appropriate credit for the requested material should be given as follows: "Reprinted (adapted) with permission from (COMPLETE REFERENCE CITATION). Copyright (YEAR) American Chemical Society." Insert appropriate information in place of the capitalized words.
- One-time permission is granted only for the use specified in your request. No additional uses are granted (such as derivative works or other editions). For any other uses, please submit a new request.

If credit is given to another source for the material you requested, permission must be obtained from that source.

BACK CLOSE WINDOW

Title: Chemical Sensors Based on Amplifying Fluorescent Conjugated Polymers

Author: Samuel W. Thomas, Guy D. Joly, Timothy M. Swager

Publication: Chemical Reviews

Publisher: American Chemical Society

Date: Apr 1, 2007

Logged in as:
Chun-Han Wang
LOGOUT

PERMISSION/LICENSE IS GRANTED FOR YOUR ORDER AT NO CHARGE

This type of permission/license, instead of the standard Terms & Conditions, is sent to you because no fee is being charged for your order. Please note the following:

- Permission is granted for your request in both print and electronic formats, and translations.
- If figures and/or tables were requested, they may be adapted or used in part.
- Please print this page for your records and send a copy of it to your publisher/graduate school.
- Appropriate credit for the requested material should be given as follows: "Reprinted (adapted) with permission from (COMPLETE REFERENCE CITATION). Copyright (YEAR) American Chemical Society." Insert appropriate information in place of the capitalized words.
- One-time permission is granted only for the use specified in your request. No additional uses are granted (such as derivative works or other editions). For any other uses, please submit a new request.

If credit is given to another source for the material you requested, permission must be obtained from that source.

BACK CLOSE WINDOW

Title: Fluorescent Porous Polymer Films as TNT Chemosensors: Electronic and Structural Effects

Author: Jye-Shane Yang, Timothy M. Swager

Publication: Journal of the American Chemical Society

Publisher: American Chemical Society

Date: Nov 1, 1998

PERMISSION/LICENSE IS GRANTED FOR YOUR ORDER AT NO CHARGE

This type of permission/license, instead of the standard Terms & Conditions, is sent to you because no fee is being charged for your order. Please note the following:

- Permission is granted for your request in both print and electronic formats, and translations.
- If figures and/or tables were requested, they may be adapted or used in part.
- Please print this page for your records and send a copy of it to your publisher/graduate school.
- Appropriate credit for the requested material should be given as follows: "Reprinted (adapted) with permission from (COMPLETE REFERENCE CITATION). Copyright (YEAR) American Chemical Society." Insert appropriate information in place of the capitalized words.
- One-time permission is granted only for the use specified in your request. No additional uses are granted (such as derivative works or other editions). For any other uses, please submit a new request.

If credit is given to another source for the material you requested, permission must be obtained from that source.

BACK CLOSE WINDOW

Title: Chemosensory Performance of Molecularly Imprinted Fluorescent Conjugated Polymer Materials

Author: Jiahui Li, Claire E. Kendig, Evgueni E. Nesterov

Publication: Journal of the American Chemical Society

Publisher: American Chemical Society

Date: Dec 1, 2007

Logged in as:
Chun-Han Wang
LOGOUT

PERMISSION/LICENSE IS GRANTED FOR YOUR ORDER AT NO CHARGE

This type of permission/license, instead of the standard Terms & Conditions, is sent to you because no fee is being charged for your order. Please note the following:

- Permission is granted for your request in both print and electronic formats, and translations.
- If figures and/or tables were requested, they may be adapted or used in part.
- Please print this page for your records and send a copy of it to your publisher/graduate school.
- Appropriate credit for the requested material should be given as follows: "Reprinted (adapted) with permission from (COMPLETE REFERENCE CITATION). Copyright (YEAR) American Chemical Society." Insert appropriate information in place of the capitalized words.
- One-time permission is granted only for the use specified in your request. No additional uses are granted (such as derivative works or other editions). For any other uses, please submit a new request.

If credit is given to another source for the material you requested, permission must be obtained from that source.

BACK CLOSE WINDOW

JOHN WILEY AND SONS LICENSE TERMS AND CONDITIONS

Jun 10, 2019

This Agreement between Chun-Han Wang ("You") and John Wiley and Sons ("John Wiley and Sons") consists of your license details and the terms and conditions provided by John Wiley and Sons and Copyright Clearance Center.

License Number	4605530138364
License date	Jun 10, 2019
Licensed Content Publisher	John Wiley and Sons
Licensed Content Publication	Angewandte Chemie International Edition
Licensed Content Title	A Fluorescent Self-Amplifying Wavelength-Responsive Sensory Polymer for Fluoride Ions
Licensed Content Author	Tae-Hyun Kim,Timothy M. Swager
Licensed Content Date	Sep 23, 2003
Licensed Content Pages	4
Type of Use	Dissertation/Thesis
Requestor type	University/Academic
Format	Print and electronic
Portion	Figure/table
Number of figures/tables	1
Original Wiley figure/table number(s)	Figure 2
Will you be translating?	No
Title of your thesis / dissertation	CHEMOSENSORS BASED ON HIGHER ENERGY GAP CONTROL OF FLUORESCENCE IN CONJUGATED POLYMERS
Expected completion date	Aug 2019
Expected size (number of pages)	100
Requestor Location	Mr. Chun-Han Wang 894 Regent Dr APT 5 DEKALB, IL 60115 United States Attn: Mr. Chun-Han Wang
Publisher Tax ID	EU826007151
Total	**0.00 USD**
Terms and Conditions	

TERMS AND CONDITIONS

This copyrighted material is owned by or exclusively licensed to John Wiley & Sons, Inc. or one of its group companies (each a"Wiley Company") or handled on behalf of a society with which a Wiley Company has exclusive publishing rights in relation to a

Title: "Higher Energy Gap" Control in Fluorescent Conjugated Polymers: Turn-On Amplified Detection of Organophosphorous Agents

Author: Deepa Pangeni, Evgueni E. Nesterov

Publication: Macromolecules

Publisher: American Chemical Society

Date: Sep 1, 2013

PERMISSION/LICENSE IS GRANTED FOR YOUR ORDER AT NO CHARGE

This type of permission/license, instead of the standard Terms & Conditions, is sent to you because no fee is being charged for your order. Please note the following:

- Permission is granted for your request in both print and electronic formats, and translations.
- If figures and/or tables were requested, they may be adapted or used in part.
- Please print this page for your records and send a copy of it to your publisher/graduate school.
- Appropriate credit for the requested material should be given as follows: "Reprinted (adapted) with permission from (COMPLETE REFERENCE CITATION). Copyright (YEAR) American Chemical Society." Insert appropriate information in place of the capitalized words.
- One-time permission is granted only for the use specified in your request. No additional uses are granted (such as derivative works or other editions). For any other uses, please submit a new request.

If credit is given to another source for the material you requested, permission must be obtained from that source.

BACK CLOSE WINDOW

Title: Higher Energy Gap Control of Fluorescence in Conjugated Polymers: Turn-On Amplifying Chemosensor for Hydrogen Sulfide

Author: Chien-Hung Chiang, Deepa Pangeni, Evgueni E. Nesterov

Publication: Macromolecules

Publisher: American Chemical Society

Date: Sep 1, 2017

Logged in as:
Chun-Han Wang
LOGOUT

PERMISSION/LICENSE IS GRANTED FOR YOUR ORDER AT NO CHARGE

This type of permission/license, instead of the standard Terms & Conditions, is sent to you because no fee is being charged for your order. Please note the following:

- Permission is granted for your request in both print and electronic formats, and translations.
- If figures and/or tables were requested, they may be adapted or used in part.
- Please print this page for your records and send a copy of it to your publisher/graduate school.
- Appropriate credit for the requested material should be given as follows: "Reprinted (adapted) with permission from (COMPLETE REFERENCE CITATION). Copyright (YEAR) American Chemical Society." Insert appropriate information in place of the capitalized words.
- One-time permission is granted only for the use specified in your request. No additional uses are granted (such as derivative works or other editions). For any other uses, please submit a new request.

If credit is given to another source for the material you requested, permission must be obtained from that source.

BACK CLOSE WINDOW

APPENDIX B. ^{1}H NMR SPECTRA OF THE KEY COMPOUNDS

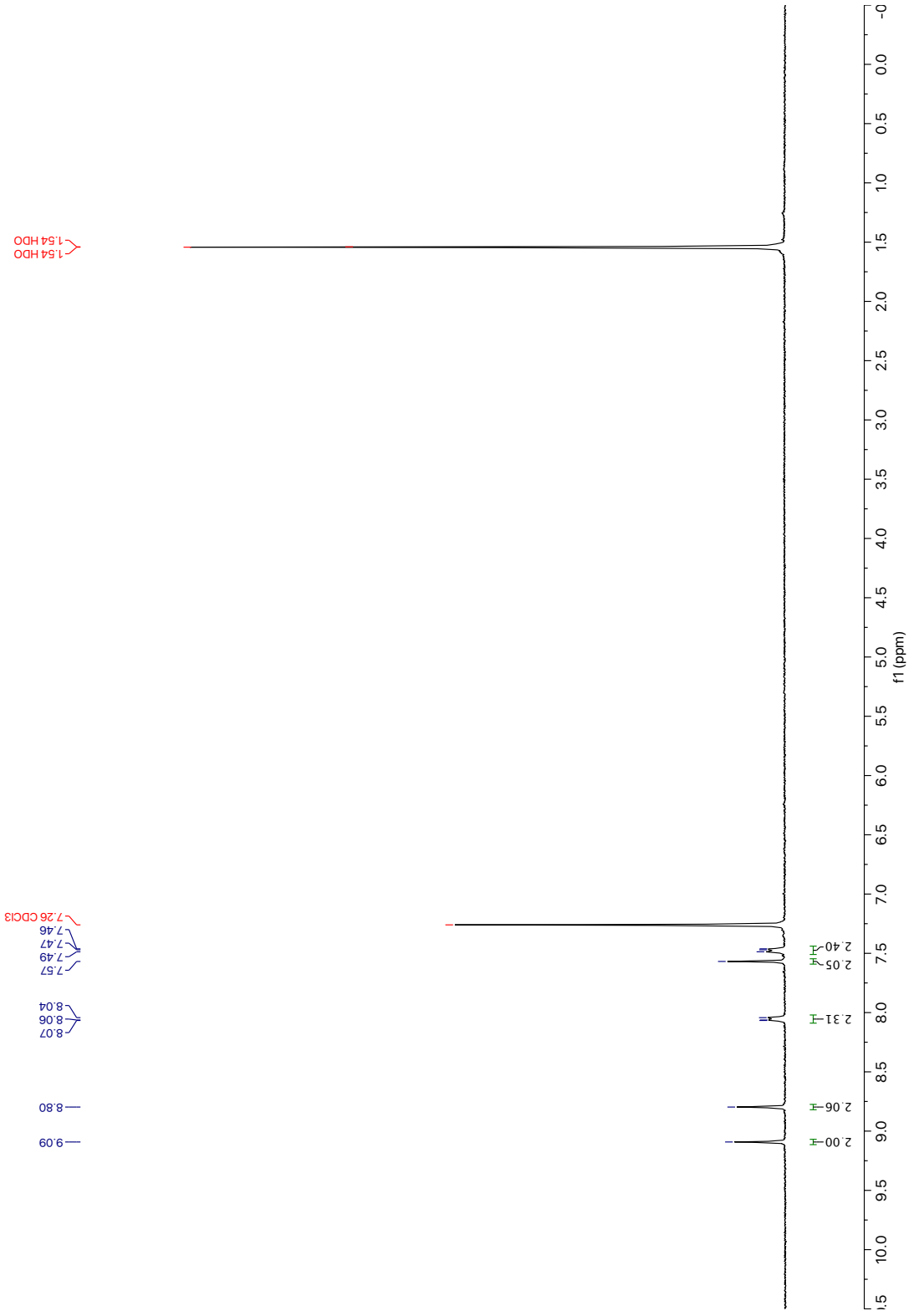

Figure Appendix B.1. ^{1}H NMR spectrum of compound **2-1** ($CDCl_3$, 400 MHz).

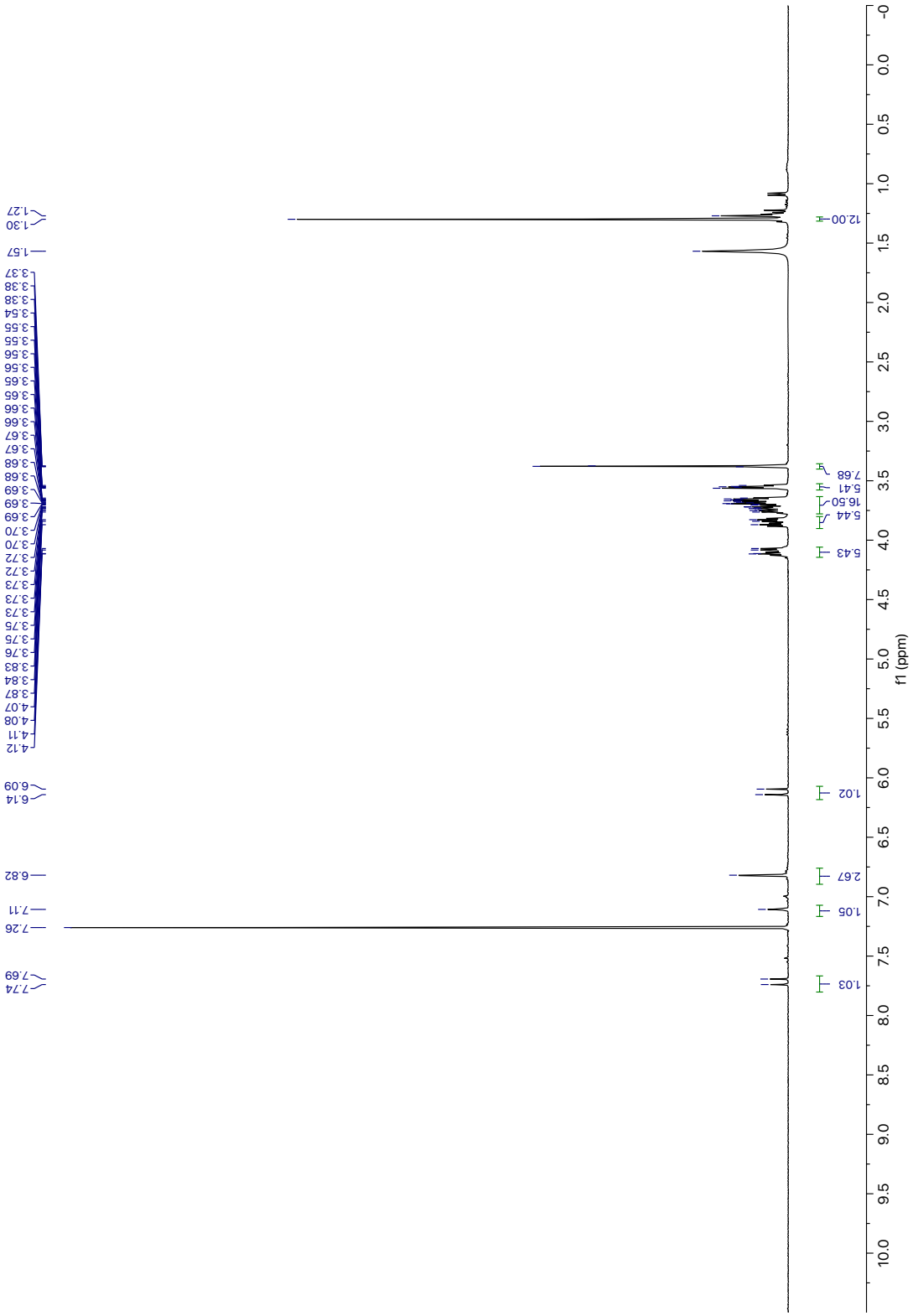

Figure Appendix B.2. ^{1}H NMR spectrum of compound **2-2** ($CDCl_3$, 400 MHz).

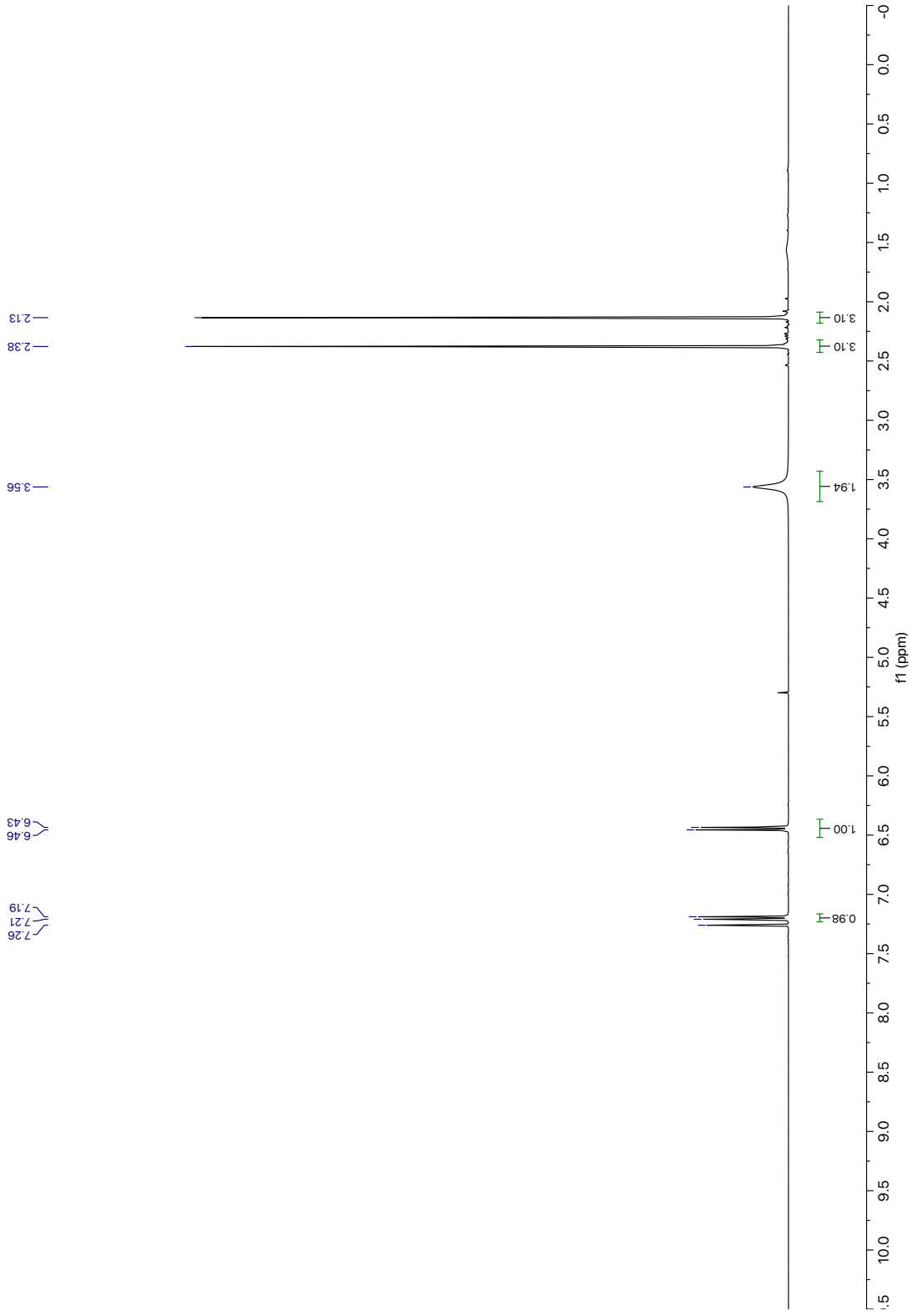

Figure Appendix B.3. ^{1}H NMR spectrum of compound **2-3** ($CDCl_3$, 400 MHz).

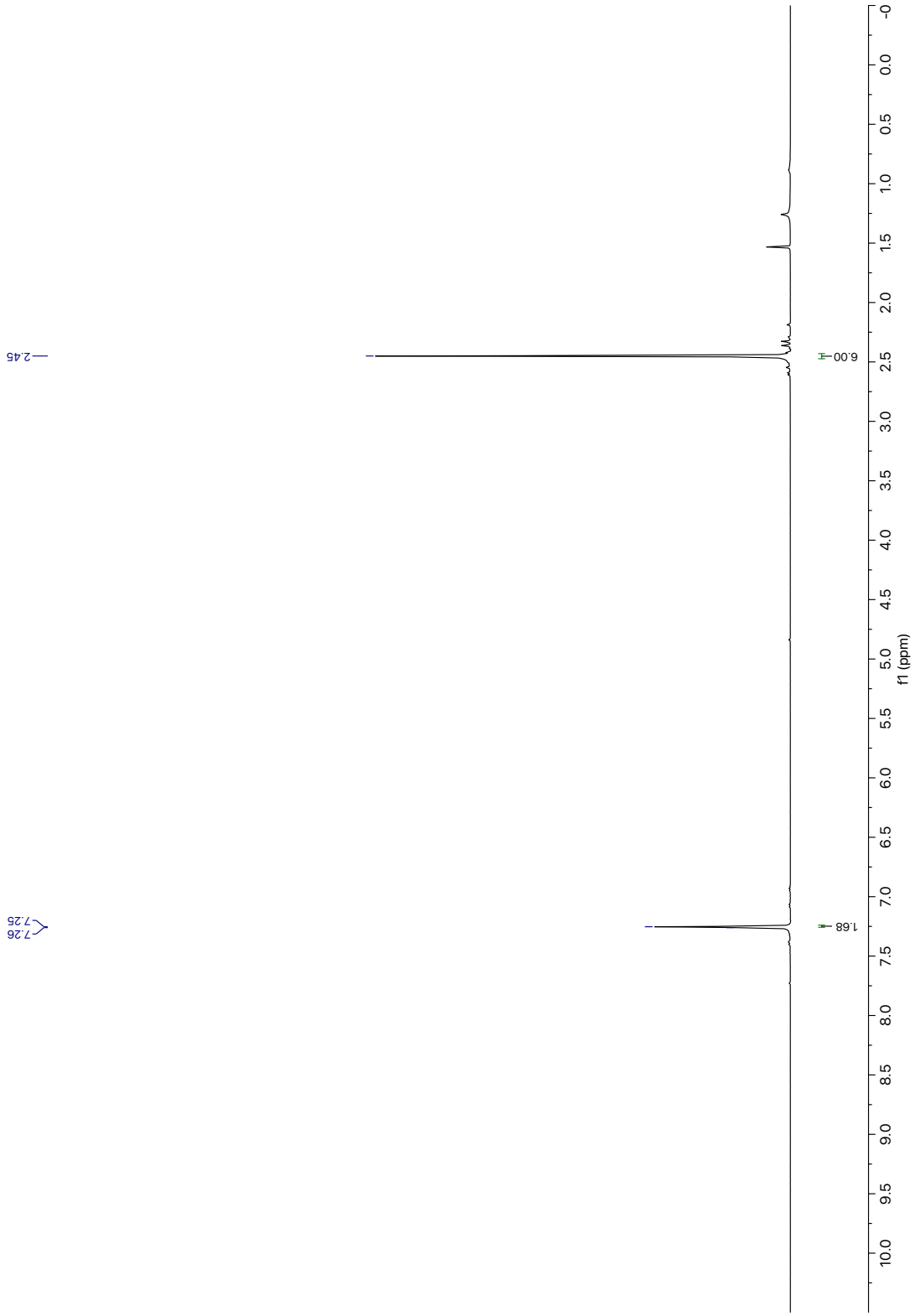

Figure Appendix B.4. ^{1}H NMR spectrum of compound **2-4** ($CDCl_3$, 400 MHz).

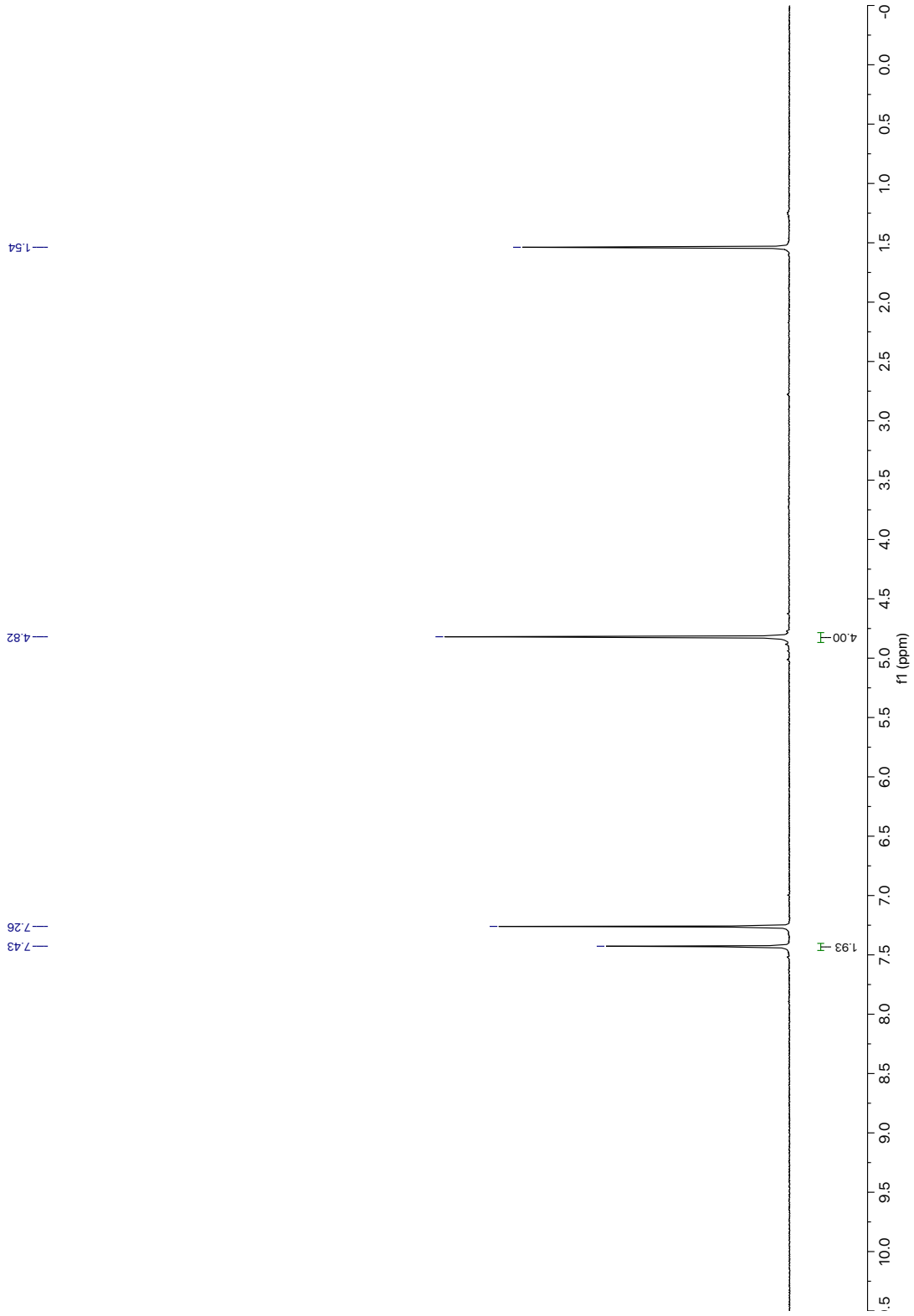

Figure Appendix B.5. ^{1}H NMR spectrum of compound **2-5** ($CDCl_3$, 400 MHz).

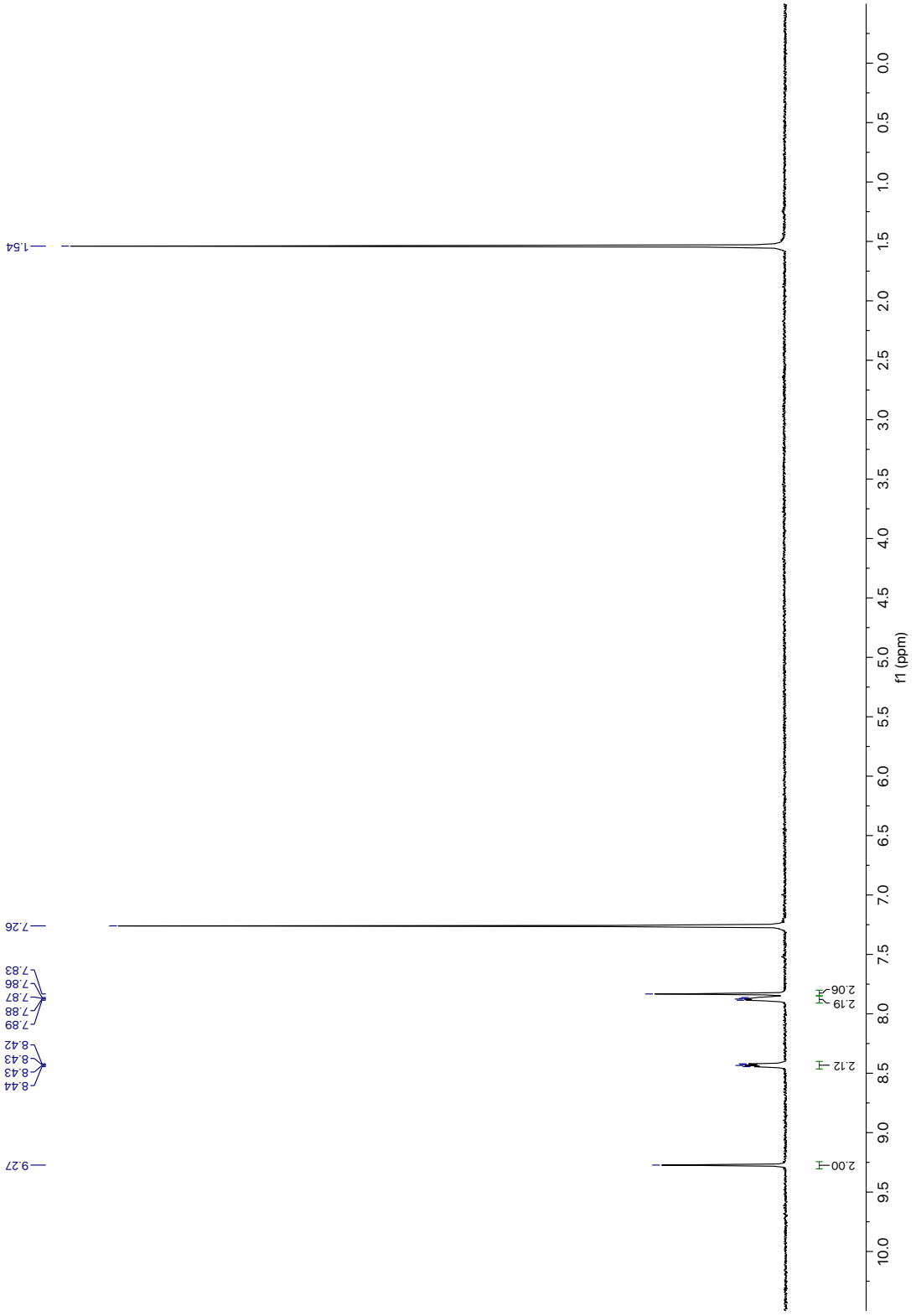

Figure Appendix B.6. ^{1}H NMR spectrum of compound **2-6** ($CDCl_3$, 400 MHz).

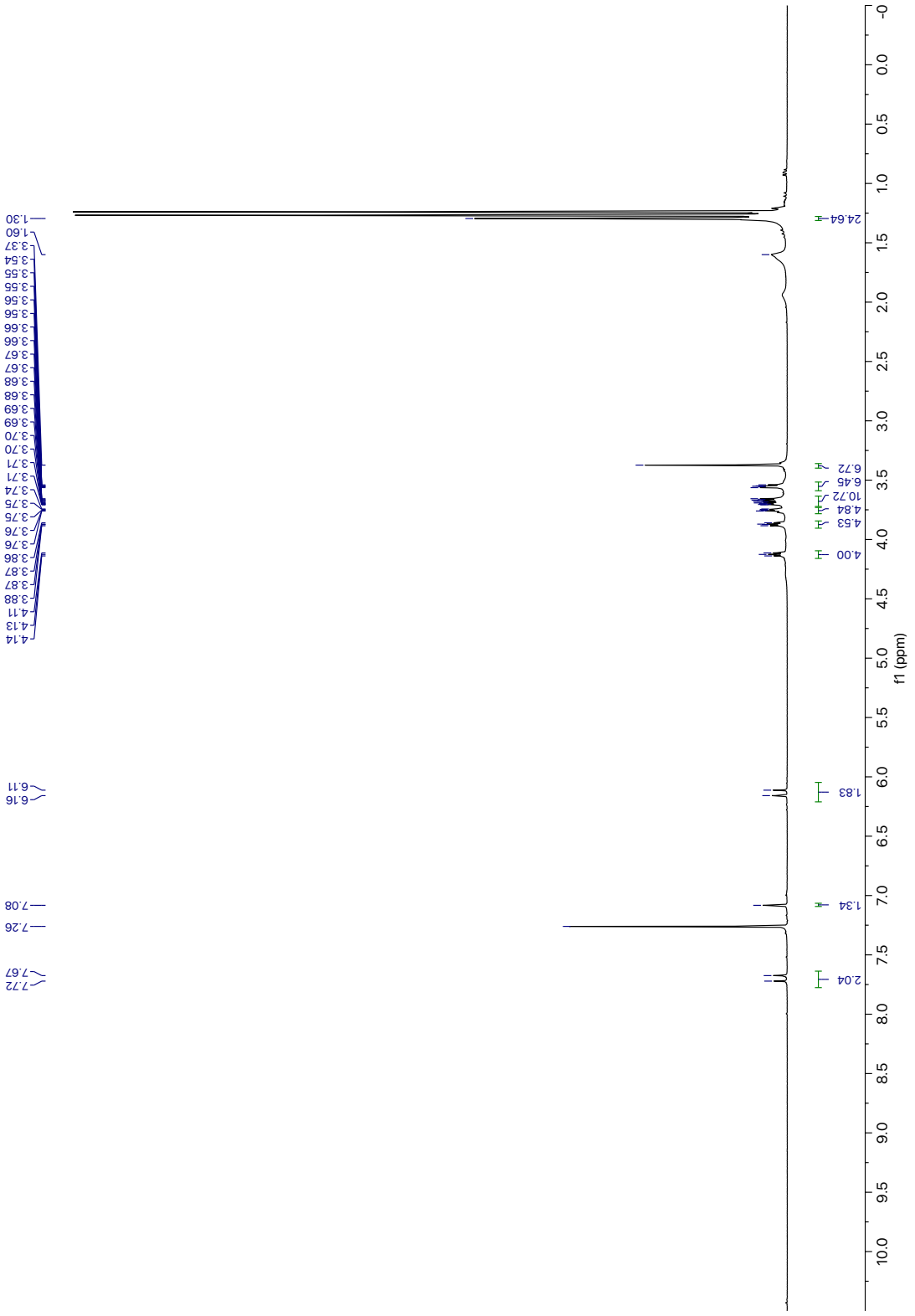

Figure Appendix B.7. ^{1}H NMR spectrum of compound **2-S1** ($CDCl_3$, 400 MHz).

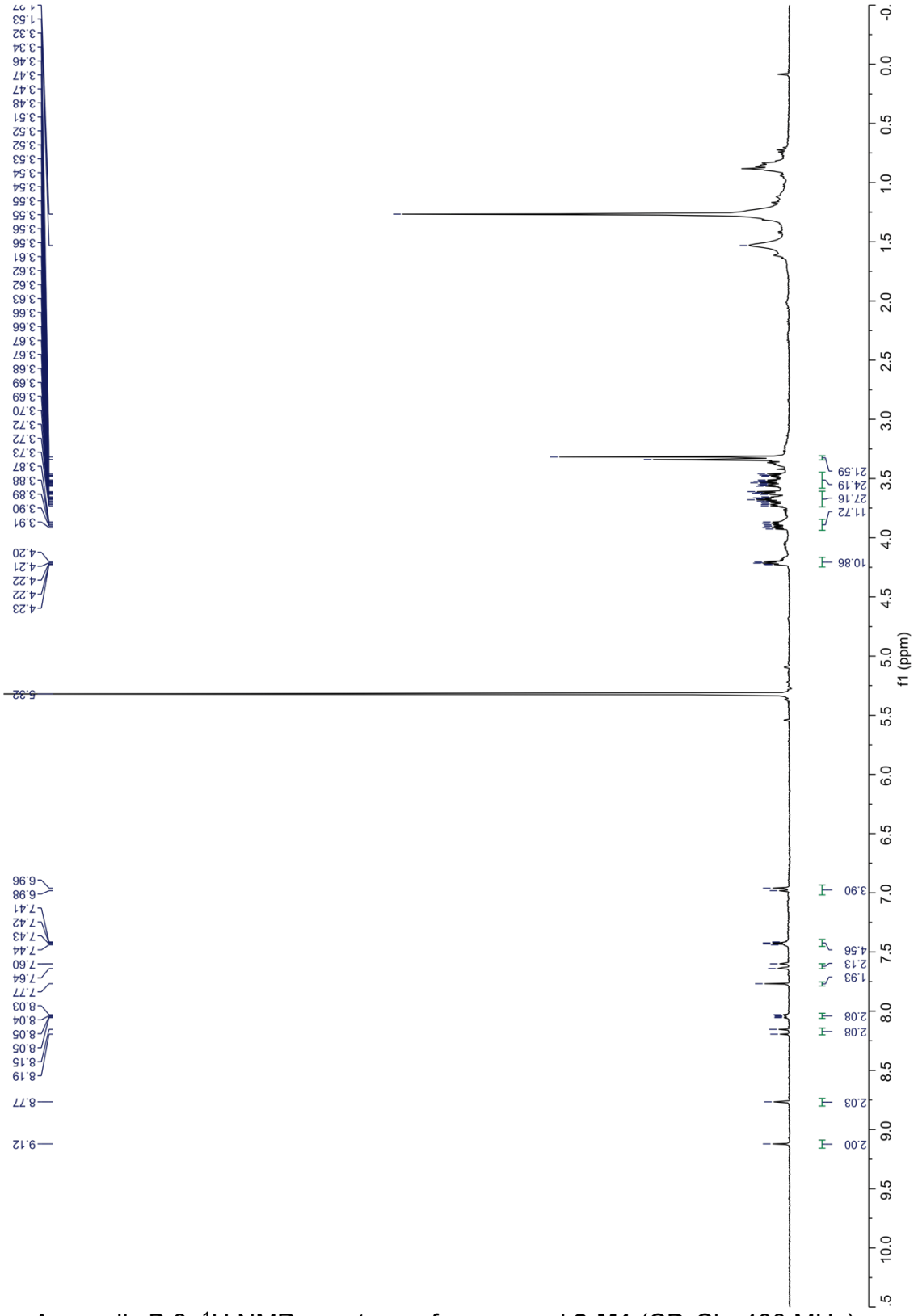

Figure Appendix B.8. ^{1}H NMR spectrum of compound **2-M1** (CD_2Cl_2, 400 MHz).

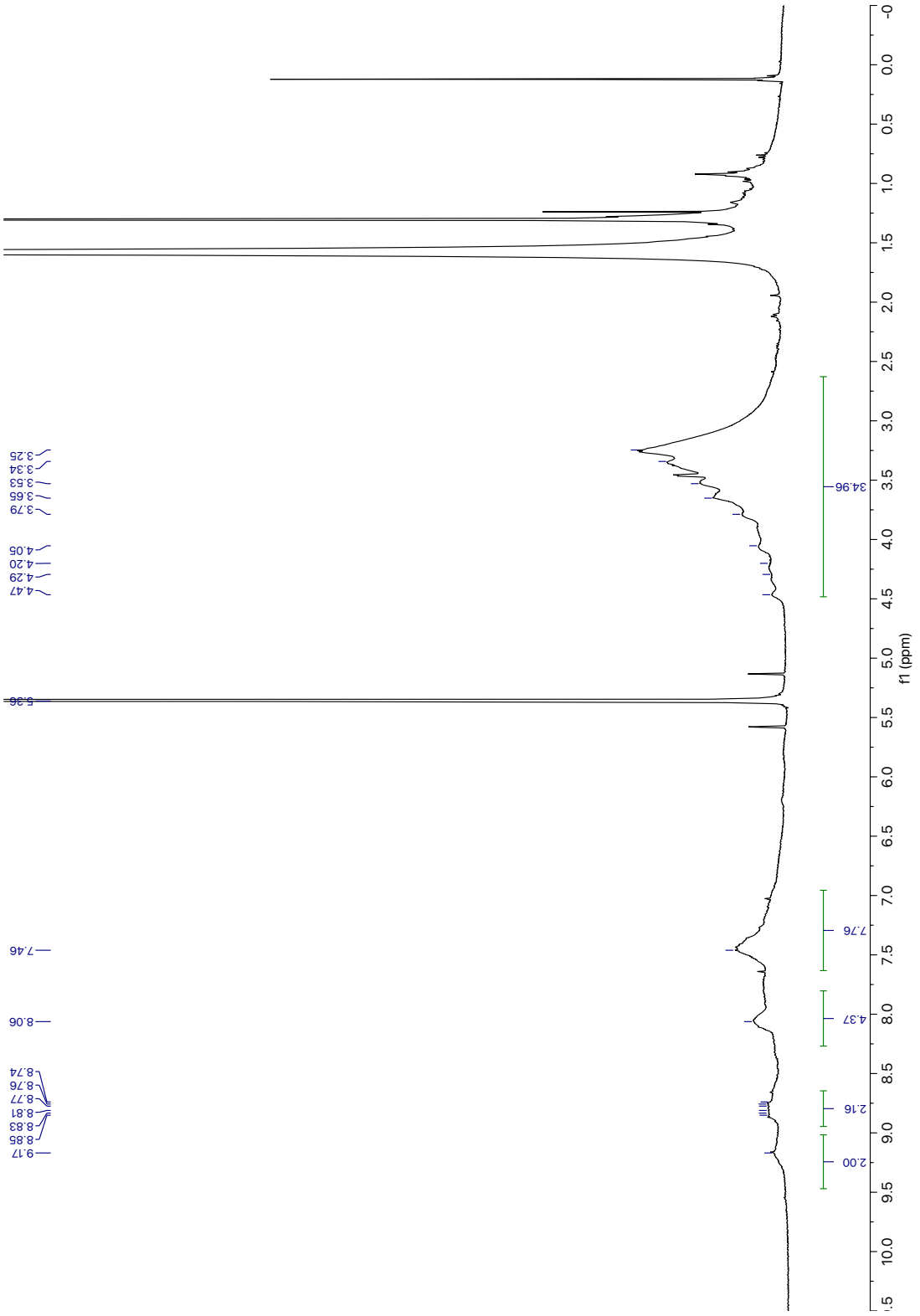

Figure Appendix B.9. ^{1}H NMR spectrum of compound **2-P1** (CD_2Cl_2, 400 MHz).

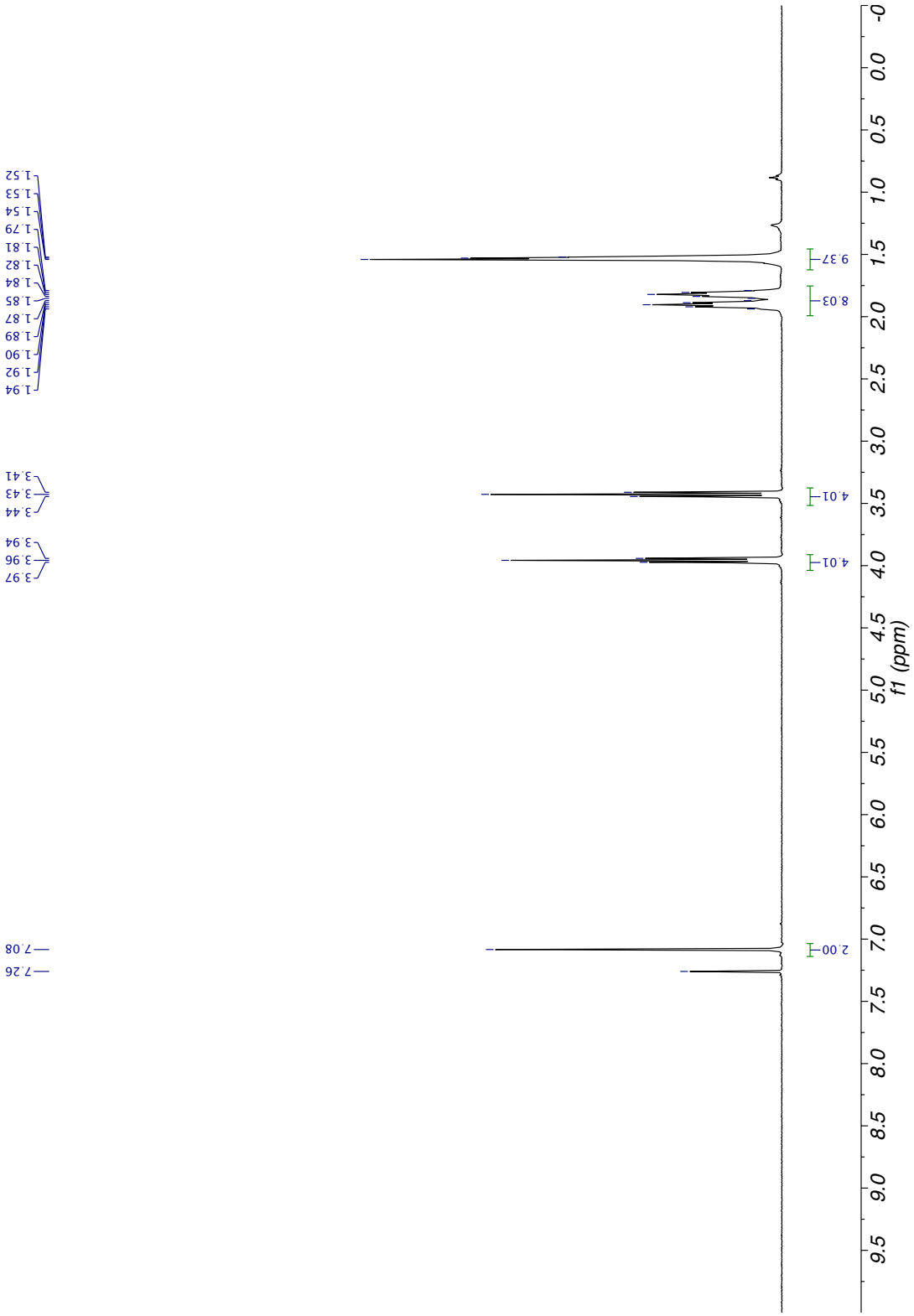

Figure Appendix B.10. ^{1}H NMR spectrum of compound **3-S1** ($CDCl_3$, 400 MHz).

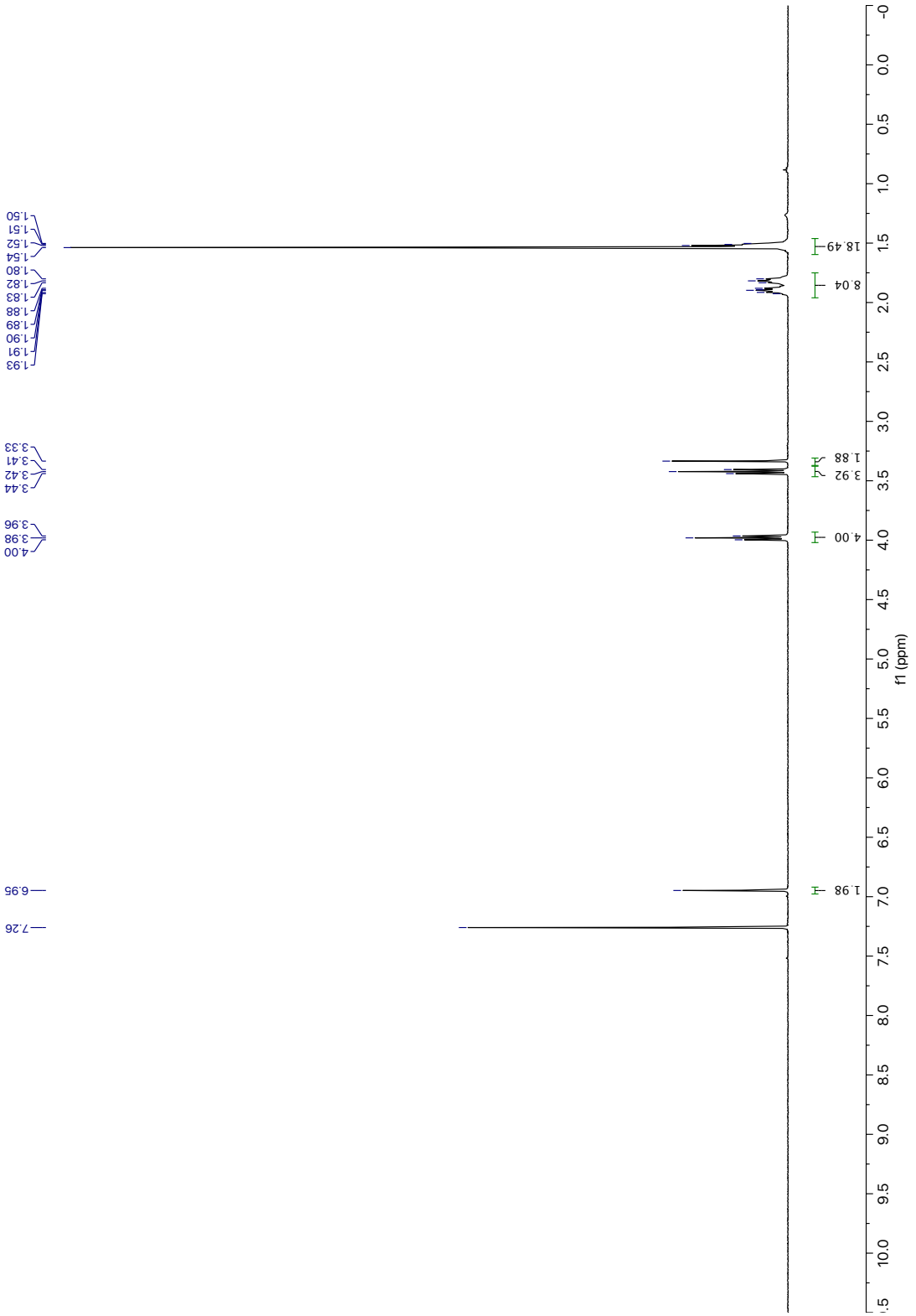

Figure Appendix B.11. ^{1}H NMR spectrum of compound **3-S2** ($CDCl_3$, 400 MHz).

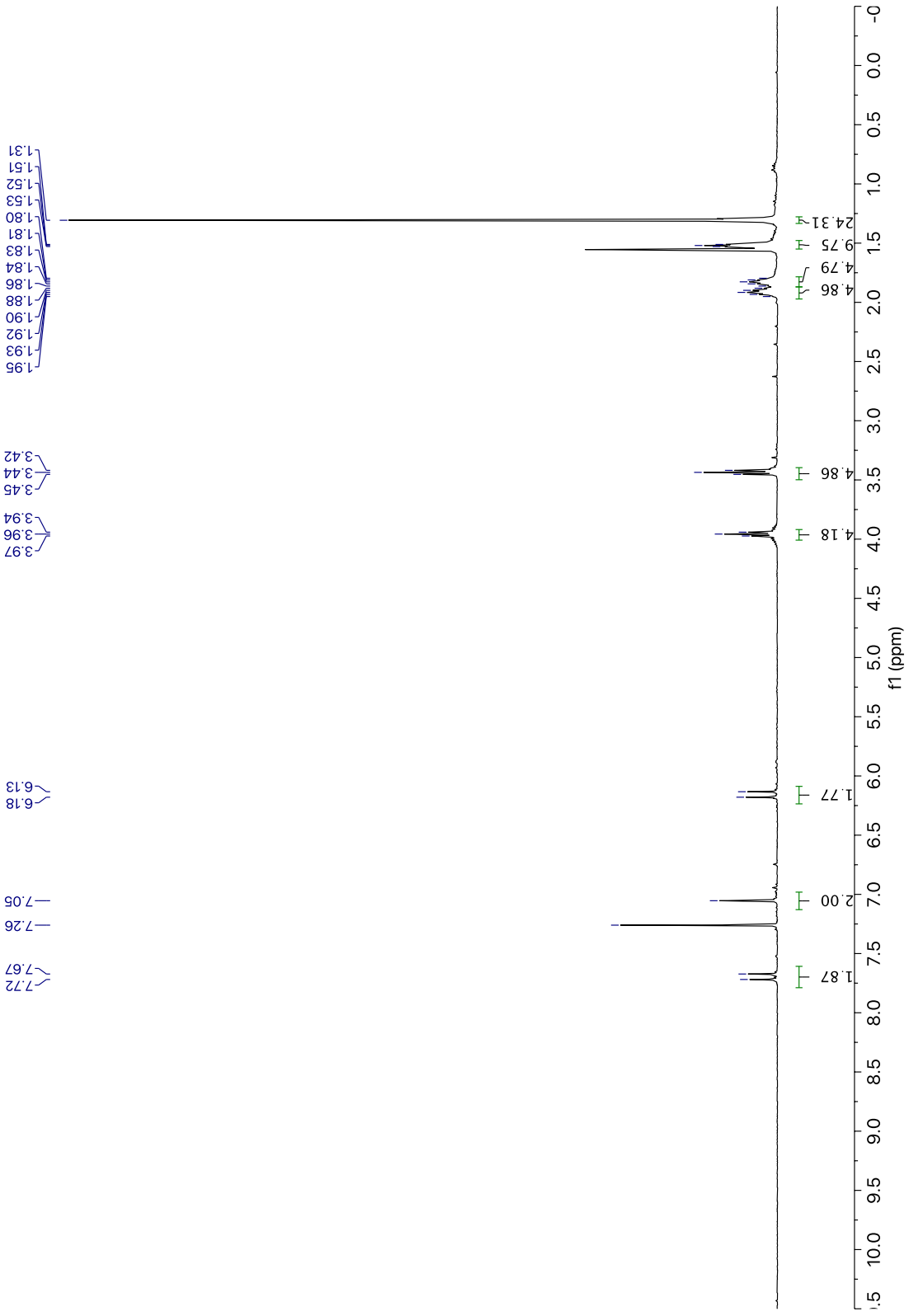

Figure Appendix B.12. ^{1}H NMR spectrum of compound **3-S3** ($CDCl_3$, 400 MHz).

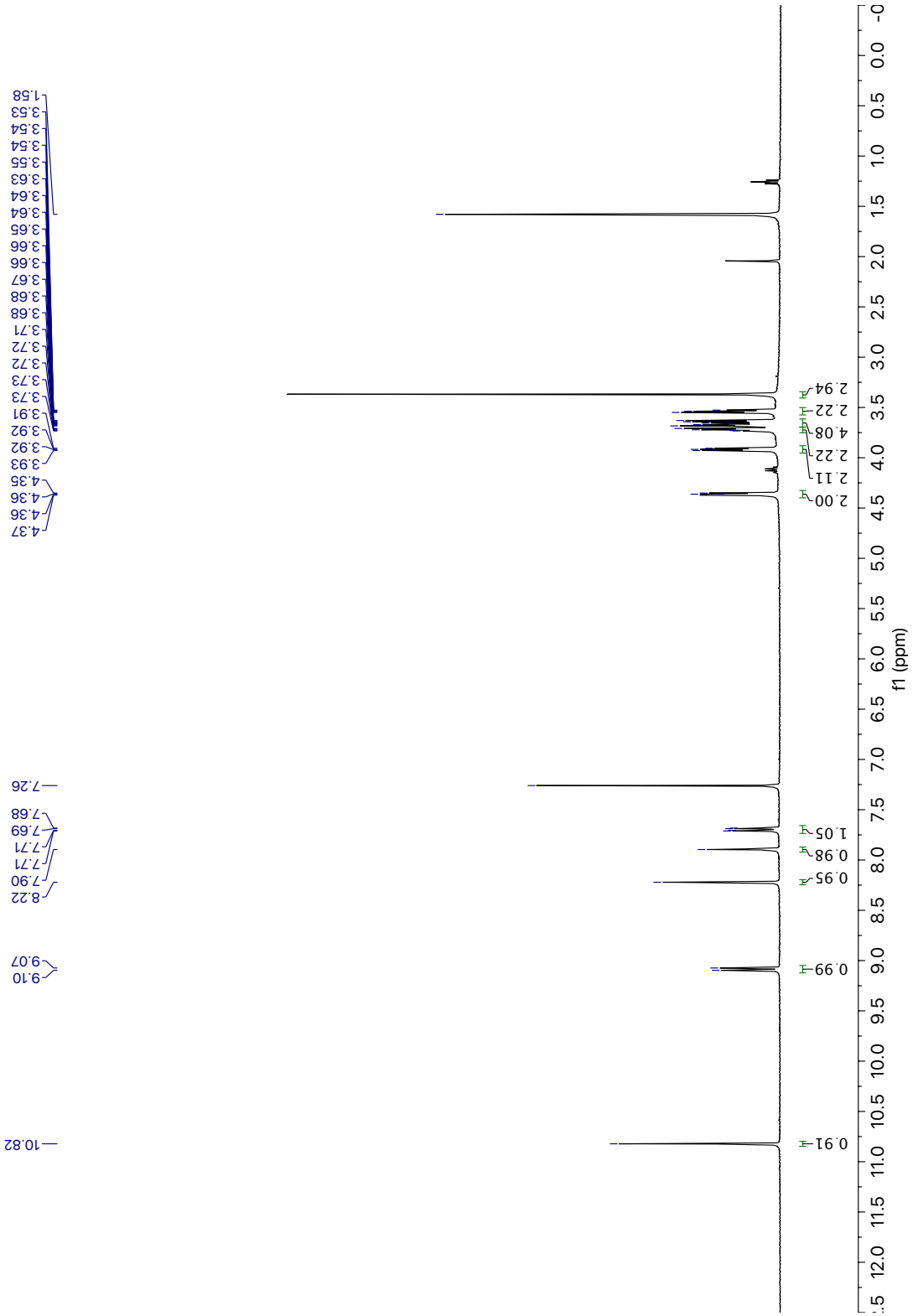

Figure Appendix B.13. ^{1}H NMR spectrum of compound **3-S4** ($CDCl_3$, 400 MHz).

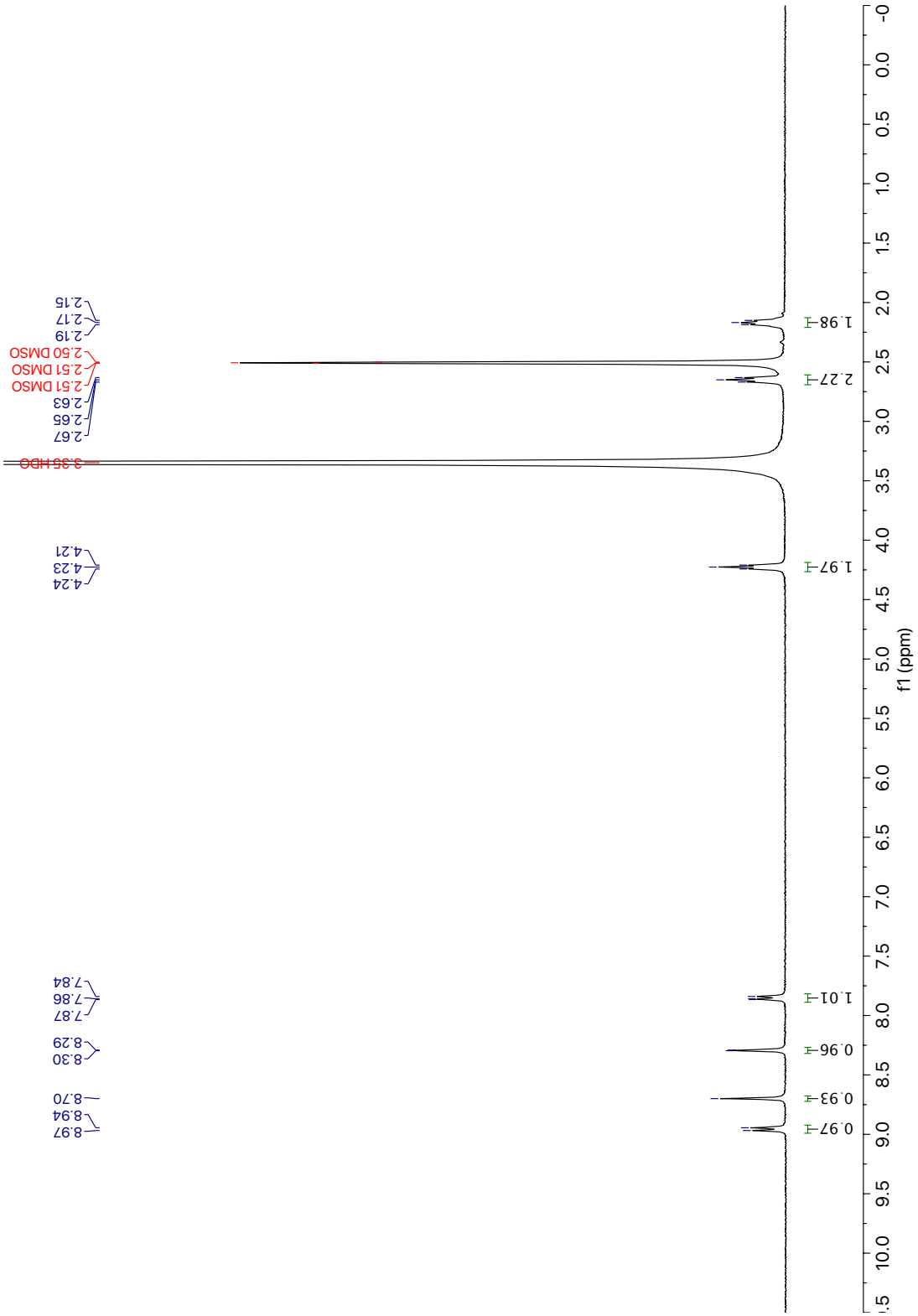

Figure Appendix B.14. ^{1}H NMR spectrum of compound **3-S5** (DMSO-d6, 400 MHz).

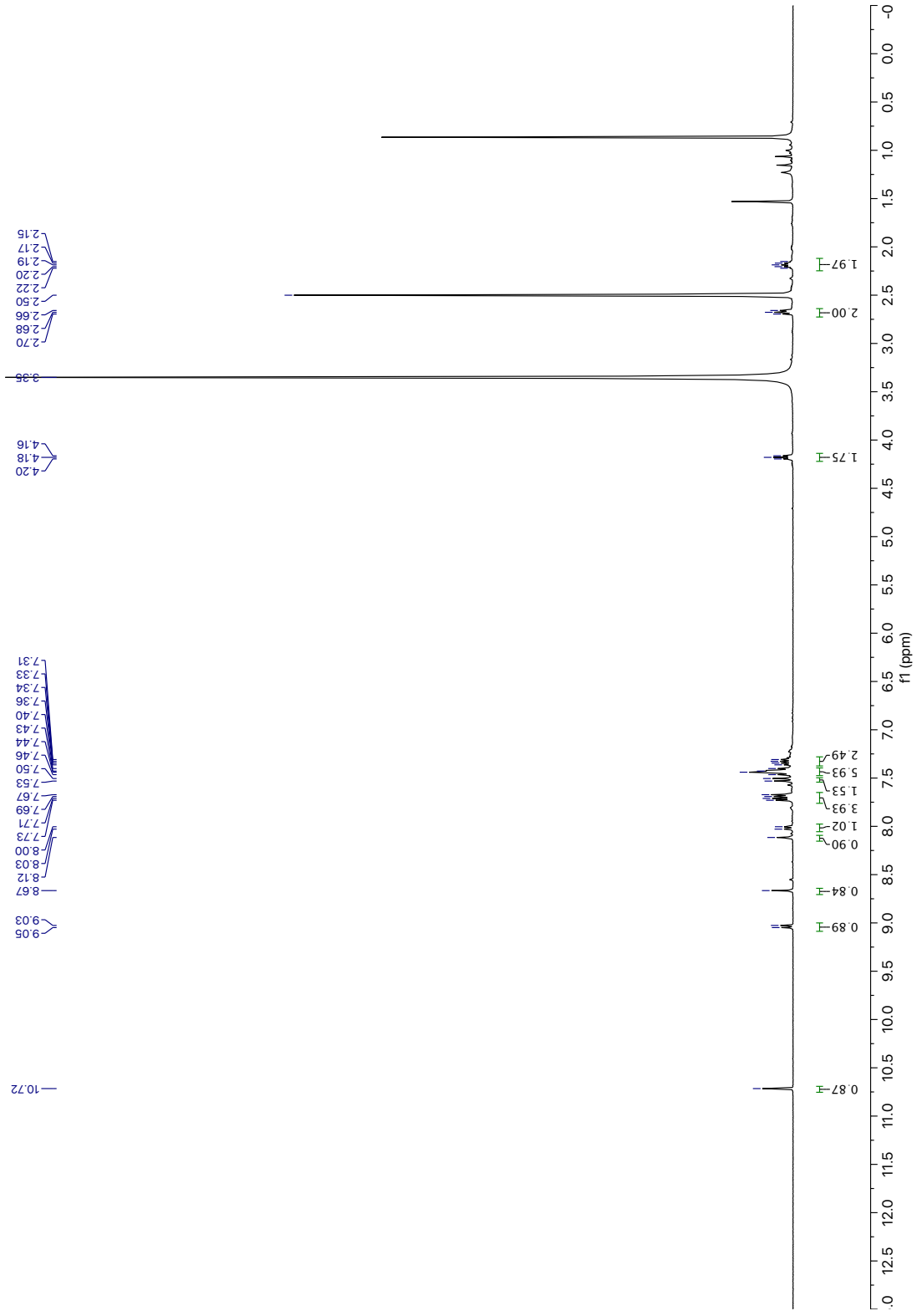

Figure Appendix B.15. ^{1}H NMR spectrum of compound **3-M1** (DMSO-d6, 400 MHz).

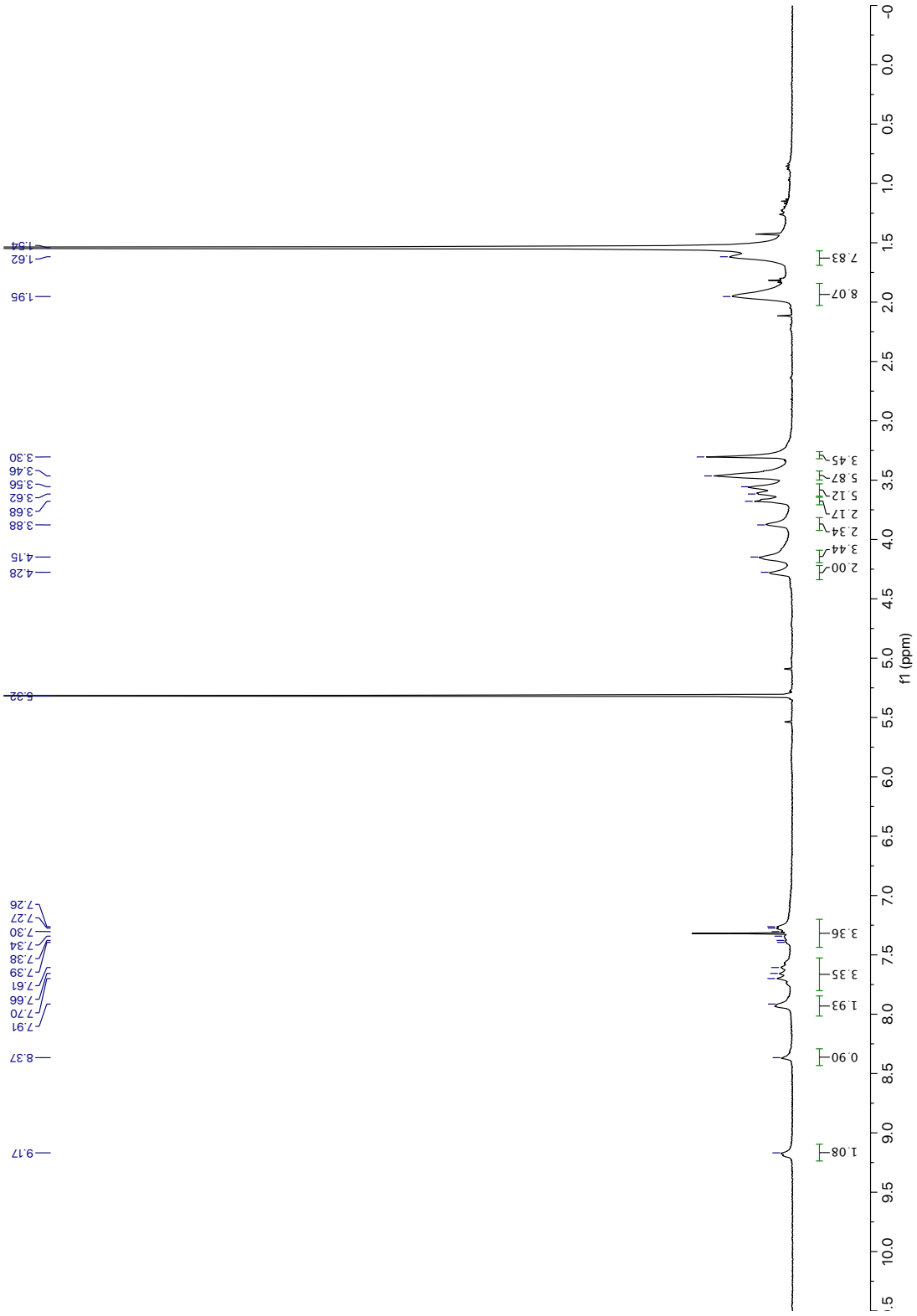

Figure Appendix B.16. ^{1}H NMR spectrum of compound **3-P1** (CD_2Cl_2, 400 MHz).

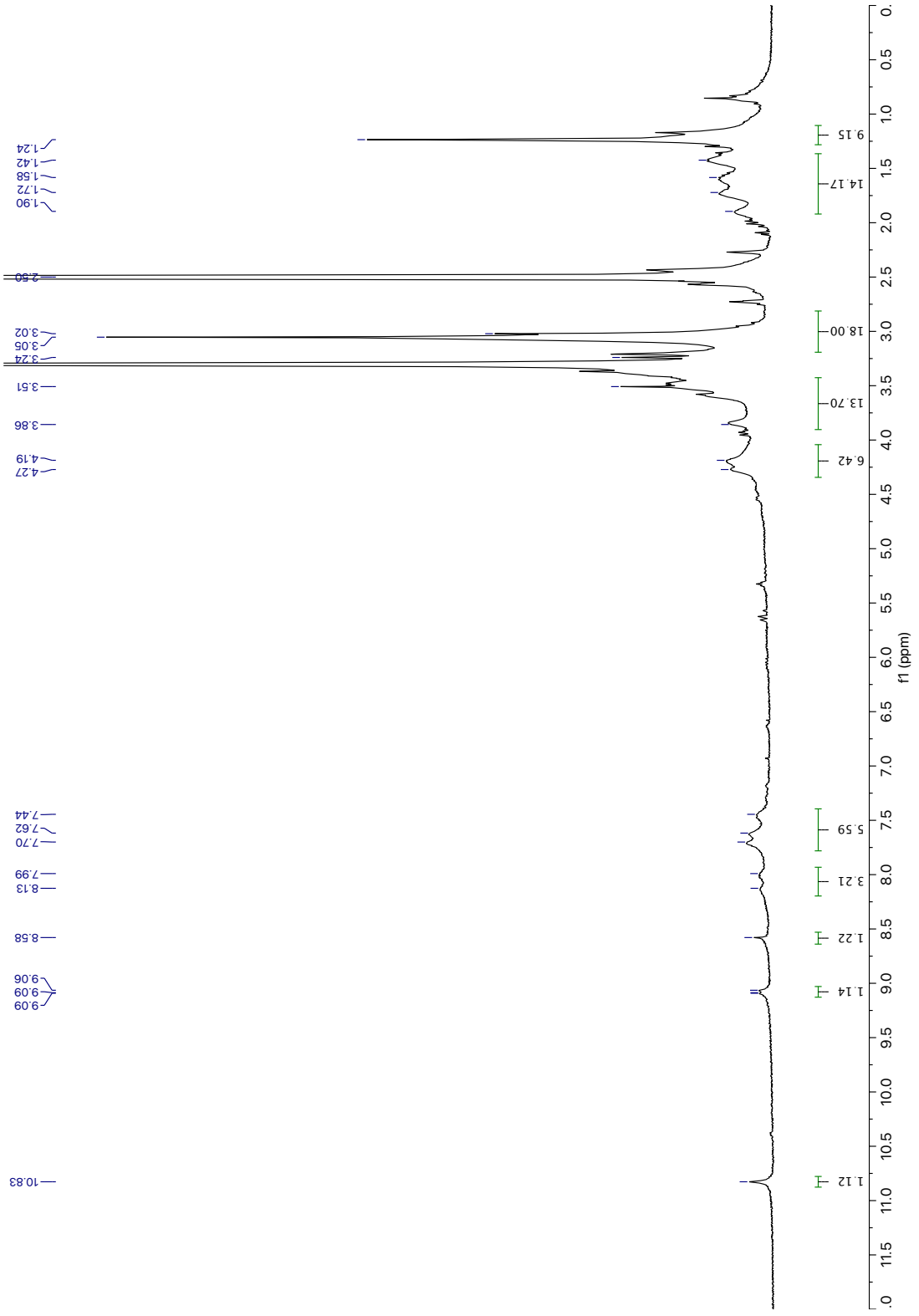

Figure Appendix B.17. ^{1}H NMR spectrum of compound **3-P2** (DMSO-d6, 300 MHz).

VITA

Chun-Han Wang was born in 1984 in Taipei, Taiwan. He received his Bachelor of Science degree in chemistry in June 2006 from National Sun Yat-Sen University in Kaohsiung, Taiwan. He began his research career in the lab of Professor Tiow-Gan Ong at Academia Sinica in Taipei, Taiwan. In June 2009, he graduated with a Master of Science degree in chemistry with the thesis titled “Synthesis and Structure of Anionic Covalent Linked Nitrogen-Heterocyclic Carbene and The Reactivity of Its Aluminum Adduct” from National Taiwan Normal University in Taipei, Taiwan. After serving for the R.O.C Army, he then worked at Lam Research Corp. as a process engineer in the DRAM microchip manufacturing foundry. In August 2013, Chun-Han moved to Louisiana State University in Baton Rouge, Louisiana where he joined the laboratory of Professor Evgueni E. Nesterov. Chun-Han researched the development of fluorescent conjugated polymer sensors based on higher energy gap control and its application in sensing singlet oxygen and cysteine. Chun-Han also studied the solvent responsive fluorescence properties of SiO_2, conjugated polymer hybrid nanoparticle systems. Chun-Han received the degree of Doctor of Philosophy in Organic Chemistry in August 2019. His dissertation is titled “Chemosensors Based on Higher Energy Gap Control of Fluorescence in Conjugated Polymers”.